LEO High Voltage Solar Array Arcing Response Model
Interim Report
NAG 3-576 Continuation V - April, 1989

Roger N. Metz
Dept. of Physics and Astronomy
Colby College
Waterville, Maine 04901

LEO High Voltage Solar Array Arcing Response Model
Interim Report
NAG 3-576 Continuation V - April, 1989

Roger N. Metz
Dept. of Physics and Astronomy
Colby College
Waterville, Maine 04901

I. Introduction

Mathematical modeling of the interactions of large, high-voltage solar arrays with the space plasma in Low Earth Orbit (LEO) has been conducted by the P.I. since 1984. An early series of models sought to identify the main features of the electrical response of a model solar array/power system to arcing at points of negative bias on the array relative to the plasma potential (refs. 1-4). In addition to characterizing array responses to various arcs, this early work suggested that a description of the electrically floating state of an array prior to an arc requires a correct description of the plasma sheath that surrounds the array.

One approach to the treatment of the plasma sheath near a solar array is contained in the two-fluid, warm plasma model (ref. 5). If magnetic fields are ignored, the plasma equations in this model are the equations of continuity and of motion for the electrons and the ions and Poisson's Equation connecting the electron and ion charge densities with the electrostatic potential. In three dimensions, for irrotational flows, these comprise five partial differential equations in five scalar fields: the electron and ion charge densities, the electron and ion velocity potentials and the electrostatic potential.

An active solar array has a distribution of voltage bias relative to plasma ground over its surface. Solar cell layouts designed to minimize $\mathbf{v}\times\mathbf{B}$ forces necessitate that some points of sharp voltage discontinuity will be present on the array. Points of shape discontinuity, such as edges and corners, also occur. Proper description of the sheath near such discontinuities can be expected

to require that the sheath equations be solved in their multi-dimensional form. Approximations based on one-dimensional assumptions embedded in a sheath model are potential sources of error.

In the limiting cases when surface bias voltages are either low or high as compared with the electron and ion thermal energies divided by the electron charge, the equations of the two-fluid, warm plasma model yield the Debye (low bias) or Child-Langmuir (high bias) approximations, respectively. A fully three-dimensional treatment of the sheath equations for arbitrarily shaped and biased objects is desirable but is difficult to achieve. However, some insight to sheath structure can be gained by less ambitious calculations. Herein we present calculations in two dimensions, for special geometries and in the limiting, Debye and Child-Langmuir approximations.

II. Previous Work

In the summer of 1987 the P.I. began a study of the electron sheath near surfaces of a model high-voltage solar array (ref. 6). An evaluation was conducted of the NASCAP/LEO computer model. This is a three-dimensional model designed to calculate electrostatic potential distributions, particle fluxes and floating conditions near objects of chosen shape, composition and voltage biasing in LEO (refs. 7-8). The model gives an extensive picture of the plasma sheaths near voltage-biased structures.

Calculational features, possibly designed to make a three dimensional model tractable, limit NASCAP LEO's descriptive power somewhat. For some kinds of objects the model has rather low resolution in crucial places. The biased object under study is confined to a 17x17x33 pt. inner grid. The next outer grid has half the resolution of the inner grid. Thus, to obtain the highest resolution available for the sheath immediately above object surfaces, the object must be kept well within the inner grid volume. Few grid points can be deployed near fine surface features of the object.

NASCAP/LEO contains an essentially one-dimensional treatment of the relation between the electrostatic potential, velocity and charge density. This permits the electrostatic potential to be calculated from Poisson's Equation directly, which is a great convenience. Particle fluxes are calculated using particle-tracking once the electrostatic potential has been calculated. This treatment is likely to be deficient near multi-dimensional features such as discontinuities and does not take particle-particle interactions into account in the particle flux calculations.

A plasma fluid model should be free of the above limitations provided that it's equations are solved in their true multi-dimensional form and symmetries are imposed that permit use of a higher resolution grid. To test this, four plasma sheath problems were defined for study by the P.I. in 1987. In each of two geometries (Fig. 1), an equipotential, rectangular bar and a sheet of alternating-bias strips, and in each of the two limiting approximations, Debye and Child-Langmuir, the equations of the warm plasma model were developed and programmed for computer solution in two dimensions. During the summer of 1988 preliminary solutions of the Debye equations were obtained (ref. 9). During the summer of 1989 final Debye solutions were obtained, comparisons to NASCAP/LEO results made and work on the Child-Langmuir cases begun.

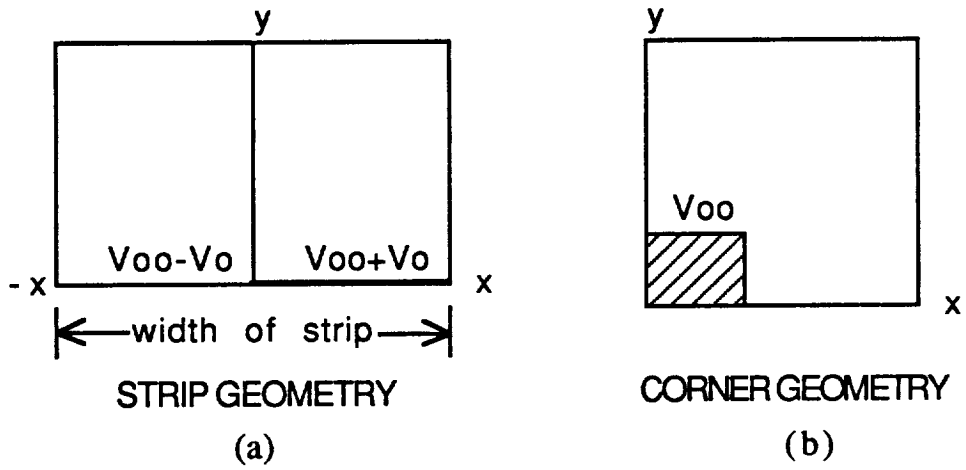

Fig. 1

GEOMETRIES: Fig. 1.a is a cross-section taken perpendicular to a plane containing strips of voltages alternately V_o volts above and

below V_{oo}. The strips run from plus to minus infinity in the z direction and, side by side, to plus and minus infinity in the x direction. Shown is a region half a strip wide on either side of the origin. Fig. 1.b shows one quadrant of a cross-section through a rectangular bar at voltage V_{oo}. The bar extends to plus and minus infinity in the z direction.

III. Work Conducted in 1989 under NAG 3-576

A. Debye Approximation

1) Sheath Equations

Of the two limiting approximations of the fluid model, the Debye Approximation contains the simpler field equations. The Equation of Motion can be integrated exactly and yields scalar, exponential relations between the particle densities and the electrostatic potential. These relations are then used in Poisson's Equation to produce a single equation for the electrostatic potential. Once Poisson's Equation is solved, the particle densities can be used in the Equation of Continuity to determine the velocity field of the fluid flow.

The field equations of the Debye Approximation ($e\Phi<<kT$) as derived in the warm plasma model (ref. 9) are as follows:

$$\nabla^2\Phi - \Phi/(\lambda_d)^2 = 0 \qquad \text{(Poisson's Equation)}$$

$$\nabla\cdot(NV) = 0 \qquad \text{(Equation of Continuity)} \qquad (1)$$

$$\nabla N/N = -q\nabla\Phi\,/kT \qquad \text{(Equation of Motion)}$$

where Φ is the electrostatic potential, λ_d is the Debye Length, N is the number density of a species (electrons or ions), q is the charge of the species particles and V is the velocity field associated with a species. The solution of the third of these equations is $N_{ion} = N_o\exp(-e\Phi/kT)$ and $N_{electron} = N_o\exp(e\Phi/kT)$, where e is the magnitude of the charge on the electron. Using $e\Phi/kT<<1$, for the electrons and $N_{ion} = N_o$ for the ions, the above form of Poisson's Equation results. For the ions, the assumed zero velocity field

trivially solves the Equation of Continuity. For the electrons, with the assumption of irrotational flow, i.e., $\nabla x V = 0$, the Equation of Continuity becomes: $\nabla^2 F + \nabla(e\Phi/kT)\cdot\nabla F = 0$ where $\nabla F = V$.

These results may be put in dimensionless form with the substitutions: $\lambda_d \nabla = \nabla'$, $e\Phi/kT = \Phi'$ and $n = N/N_o$, where N_o is the species density in the ambient plasma. The velocity units are arbitrary and the velocity V' is derived from $\nabla' F' = V'$. With these definitions the field equations become:

$$(\nabla')^2\Phi' = \Phi' \qquad \text{(Poisson's Equation)}$$

$$\nabla'^2 F' + \nabla'\Phi'\cdot\nabla' F' = 0 \qquad \text{(Equation of Continuity for Electrons)} \qquad (2)$$

$$n = \exp(\Phi') \qquad \text{(Relative Electron Density)}$$

2) Numerical Solutions

A two-dimensional, numerical model achieving solutions of these equations using Central-Difference methods was developed in the summers of 1987 and 1988. Electrostatic potential distributions and electron flow fields have been modeled for both the edge and the strip geometries. In the case of the strip geometry, an analytical solution to Poisson's Equation was obtained. During the summer of 1989 these solutions were fully implemented and compared with output from NASCAP/LEO.

To accomplish this comparison, NASCAP/LEO was run using three-dimensional objects spanning the full length of the 33 point axis of the inner grid. The objects were a long rectangular bar and a set of adjacent, plane rectangles. Cross-sections through the centers of these objects provided two-dimensional data against which runs of our model were compared.

A computer program written by a student assistant, Bishwa Basnet, was used to read the NASCAP/LEO output files and put them in a form suitable for contour plotting with S, which is the graphics package we use to plot the output from the fluid model. Thus, contour plots of our output and the NASCAP/LEO output were

made directly comparable. Results of the NASCAP/LEO electrostatic potential calculations were generally in agreement with fluid model results except in regions of the sheaths near the corner of the edge in the edge geometry or near the surface voltage discontinuity in the strip geometry. In such regions, our calculations were able to yield somewhat more detail than those of NASCAP/LEO.

3) NASCAP/LEO Code Comparisons

Figures 2-5 show comparisons in the Debye Approximation between NASCAP/LEO electrostatic potentials and electrostatic potentials calculated using the fluid model. In these figures voltages have been normalized to kT. Plasma parameters used to calculate these results are as follows:

Electron Temperature = 0.1 e.v.
Electron Density = 10^6/cc
Debye Length = 0.00235 meters

Fig. 2 is a plot of NASCAP/LEO output based on a cross section through the center of a rectangular bar of dimensions $4\lambda_D$ x $2\lambda_D$ x $11\lambda_D$. The width of the bar spans 12 of the available 16 grid units in the inner grid of the NASCAP/LEO, the height spans 6 grid units and the length spans all 32 of the available units. Thus the upper surface of the corner shown in Fig. 2 is spanned by 7 grid points and the right side is spanned by 4 grid points. The solution has been set to zero on the boundary of the first outer grid.

Fig. 3 shows a solution of the NASCAP/LEO-type Poisson's Equation (eq. 9) using the fluid model. Our calculations reflect a grid of 21 x 21 points and $3\lambda_D$ = one grid space. Thus our grid is identical to that used by NASCAP/LEO in Fig. 2. One can see that, except for the placement of the zero boundary (our zero is on the upper and right hand extreme boundaries), the equipotential lines in the two figures fall almost exactly on top of each other. There is excellent agreement between our calculations and NASCAP/LEO's in these figures.

Fig. 4 is a plot of NASCAP/LEO output based on four strips occupying the median plane of the inner grid. Each strip is 8 grid

spaces wide and 16 grid spaces long. The voltages of the strips alternate, beginning with a low voltage strip and ending with a high voltage strip. The arrangement is shown below in Fig. 6. Fig. 4 shows a vertical cross-section centered on the discontinuity between the first low-voltage strip and the first high-voltage strip and perpendicular to the line of discontinuity. Only 9 grid points span the x axis of the calculation space, which is shown by the box.

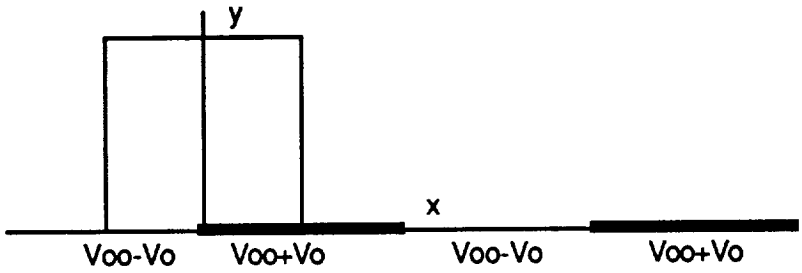

Fig. 6

Fig. 5 shows a calculation based on the same grid adopted in Fig. 4 but using the analytical solution of Poisson's Equation for the electrostatic potential in the strip geometry (ref. 6). The two contour plots are similar. They differ in the placement of the potential zero, which is at a numerically determined distance above the surface in Fig. 4 and is at infinity for the calculation shown in Fig. 5. This artificially compresses the equipotentials toward the surface in Fig. 4 relative to those in Fig.5.

The lack of good resolution in both figures leads to some differences near the voltage discontinuity. Poor resolution is forced by the the need to have four adjacent strips in the inner grid of NASCAP/LEO's calculation space. We were unable to achieve convergent runs of NASCAP/LEO using only two strips. Even using the longest available dimension of the inner grid, only 8 grid units per strip could be accommodated. The analytical solution shown in Fig.5 is, in principle, exact but was calculated and plotted on the sparse grid of NASCAP/LEO for comparison purposes. Thus, Fig. 5 has the same lack of resolution as does Fig. 4.

The results plotted in Figures 2-5 suggest that, in the Debye Approximation, our numerical approach replicates that of

NASCAP/LEO within the precision of that model and for the geometries we have chosen to analyze. Where resolution is sufficient in both approaches, agreement is good. Where differences occur, poor resolution prohibits taking the differences too seriously.

4) Fluid Model Runs

Calculations in both the strip geometry and in the edge geometry using the fluid model were fully reported in our March, 1989 Interim Report (ref. 9).

B. Child-Langmuir Approximation

1) Sheath Equations

The Child-Langmuir Approximation describes sheath regions where $e\Phi >> kT$. Since $kT << 1$ e.v. in LEO this approximation is the appropriate one for modeling high-voltage solar arrays deployed there. Although the Equation of Motion (eqs. 2) can be integrated exactly, as in the Debye Approximation, the result is a quadratic relationship between the magnitude of the fluid velocity and the electrostatic potential. This is the relationship used in NASCAP/LEO. However, no scalar relationship between the electrostatic potential and the charge density arises in more than one dimension, as is assumed in NASCAP/LEO. Thus, in the fluid model, Poisson's Equation does not separate from the other equations as an equation for the electrostatic potential alone. The equations of motion and continuity remain coupled to Poisson's Equation and must be solved simultaneously with Poisson's Equation.

If attention is focused mainly on that part of the sheath nearest the high voltage surfaces, where ions are excluded, the ion contribution to the sheath equations can be ignored and the sheath becomes an electron sheath. The field equations for the electron sheath in the Child-Langmuir Approximation, as derived in the warm plasma model (ref. 6) and assuming irrotational flows, are as follows:

$$\nabla^2\Phi - eN/\varepsilon_0 = 0 \qquad \text{(Poisson's Equation)}$$

$$\nabla\cdot(NV) = 0 \qquad \text{(Equation of Continuity)} \qquad (3)$$

$$mV^2/2 - e\Phi = 0 \qquad \text{(Equation of Motion - Energy Eq.)}$$

where N is the electron density, **V** is the electron velocity field and Φ is the electrostatic potential. The ion density differs from zero only on the outer boundary region of the sheath where the charge density term in Poisson's Equation must reflect the presence of the ions. Notice that the Equation of Motion also expresses conservation of energy for single particles.

The appropriate scale length in the high-voltage sheath is the Child-Langmuir length, D_{CL}, given by:

$$D_{CL}^2 = (4\varepsilon_0/9)(4\pi/ekT)^{1/2}\Phi_0^{3/2}/N_0 \qquad (4.a)$$

In comparison to the Debye length, λ_D:

$$D_{CL}^2/\lambda_D^2 = (4/9)(4\pi)^{1/2}(e\Phi_0/kT)^{3/2} \qquad (4.b)$$

where Φ_0 is the surface potential, i.e., the value of the voltage on the surface of the edge or the average voltage of the alternating strips. One can see that, if $e\Phi_0 >> kT$, the Child-Langmuir length greatly exceeds the Debye length. Thus, because the typical high-voltage sheath must be calculated out from the surfaces at least one Child-Langmuir length and only a finite number of calculational grid points can be deployed in such a calculation, features of the sheath or the surface having the scale of the Debye length are unlikely to be resolved. A sheath thickness of the order of D_{CL} is suggested by the result that D_{CL} is the thickness of the one-dimensional sheath above a uniformly biased, plane surface.

As in the Debye Approximation, dimensionless forms of the sheath equations can be found. However, the appropriate norm voltage is not kT/e but Φ_0 and the appropriate length scale is not λ_D but D_{CL}. The transformation to dimensionless units is accomplished

by making the substitutions: $D_{CL}\nabla = \nabla'$, $\Phi' = \Phi/\Phi_o$, $V' = V/V_o$ and $n = N/N_o$, where $V_o = (2e\Phi_o/m)$, m is the mass of an electron and V' is derived from $V' = \nabla'F'$. With these definitions, and using eq.(4.b), the field equations become:

$$(\nabla')^2\Phi' - (4/9\gamma)(kT/e\Phi_o)n = 0 \qquad \text{(Poisson's Equation)}$$

$$n\nabla'^2F' + \nabla'n\cdot\nabla'F' = 0 \qquad \text{(Equation of Continuity)} \qquad (5)$$

$$(V')^2 = \Phi' \qquad \text{(Equation of Motion - Energy Eq.)}$$

where $\gamma \equiv (kT/e\Phi_o)^{3/2}/(4\pi)^{1/2} = 4\lambda_D^2/9D_{CL}^2$ (6)

{Note: A numerically more useful form of the Equation of Continuity is $\nabla^2(gF') + (g-2)\nabla'g\cdot\nabla'F' - F'\nabla'^2g = 0$, where $g \equiv \ln(n)$.}

2) Numerical Solutions

In the summer of 1989, computer programs were written to solve the Child-Langmuir equations in two dimensions in the edge and strip geometries. A self-consistent field calculation for the electron density, electrostatic potential and electron velocity field of the electron sheath was planned.

In the self-consistent approach a trial electrostatic potential is chosen. The relative electron density is then deduced from Poisson's Equation and used in the Equation of Continuity to produce the electron velocity potential. The magnitude of the velocity is calculated throughout the grid from the velocity potential and the Energy Equation is used to produce a new electrostatic potential. The new electrostatic potential and the trial electrostatic potential are compared. If sufficiently different, they are mixed and introduced as a new trial potential beginning a new calculation cycle.

To produce a trial electrostatic potential, we have chosen to solve the non-linear Poisson's Equation that arises using NASCAP/LEO's relation connecting the charge density, velocity field

and the electrostatic potential in the sheath (ref. 8) . As given by Katz, Mandell and Cooke in unnormalized units, this relationship is:

$$\rho = -(\varepsilon_0\Phi/\lambda_D^2)[1 + (4\pi)^{1/2}(e\Phi/kT)^{3/2}]^{-1} \qquad (7)$$

When $e\Phi/kT << kT$, this expression reduces to the correct form of the net charge density in the Debye Approximation, namely, $\rho = -N_0e^2\Phi/kT$. When $e\Phi/kT >> kT$, the expression gives the electron charge density in the one-dimensional, Child-Langmuir Approximation, namely, $\rho = -N_0e/(4\pi e\Phi/kT)^{1/2}$.

Whereas the Debye limit of eq.(7) can easily be shown to be correct in more than one dimension, this is not true of the Child-Langmuir limit. As pointed out above, there is no reason to expect that a scalar relationship between ρ and Φ exists in more than one dimension for this limit. Thus, while we shall use the NASCAP/LEO relationship to develop the trial potentials in our Child-Langmuir analysis, we expect that the self-consistent procedure will produce different final potentials. Differences should be most evident near intrinsically multi-dimensional regions of the sheath such as surface shape and voltage discontinuities.

If eq.(7) is written in the dimensionless units adopted in eqs.(5), the result is an expression for the relative electron density:

$$n = \gamma\Phi'(e\Phi_0/kT)/[\gamma + (\Phi')^{3/2}] \qquad (8)$$

Using this result, Poisson's Equation becomes:

$$(\nabla')^2\Phi' = (4\Phi'/9)/[\gamma + \Phi'^{3/2}] \qquad (9)$$

To solve this equation numerically, we linearize the right-hand side, viz:

$$f(u) \equiv u/[\gamma+u^{3/2}] \approx 3u_0^{5/2}/2(\gamma+u_0^{3/2})^2 + \{(\gamma-u_0^{3/2}/2)/(\gamma+u_0^{3/2})^2\}u \qquad (10)$$

Using this expansion, we solve $(\nabla')^2\Phi' = (4/9)f(\Phi')$ iteratively.

Initially the function Φ'_0 is the solution of Laplace's Equation

(f = 0) using the chosen boundary conditions. After one iteration the solution, Φ', is compared with the starting function, Φ'_0. If sufficiently different they are mixed and the mixture introduced as Φ'_0 in a new iteration. This process continues until agreement between Φ' and Φ'_0 is obtained to within a chosen precision.

As Katz, et al, have found (ref. 7), to achieve numerical stability it is necessary to replace the value of γ in eq.(9) with a larger value. Since $\gamma = 4\lambda_D^2/9D_{CL}^2$, this has the effect of replacing λ_D as the intrinsic scale length of the sheath in regions where $e\Phi << kT$. Thus, in such regions the model becomes unable to resolve features on the scale of λ_D. As Katz, et al, point out, however, the grid spacing for a sheath surrounding a high voltage object is typically chosen to be many times larger than a Debye length and there is little point in trying to model features smaller than a grid spacing .

A second potential instability arises when the coefficient of u in the second term on the right-hand side of eq.(10) is positive. Katz, et al, deal with this instability by setting this term to zero at any point at which this occurs. We deal with it by choosing the potential on the outer boundary so that the maximum electron relative density obtains on the outer boundary of the calculation space. This guarantees that the coefficient, which is the derivative of the relative electron density, is negative everywhere.

Numerical solutions to eqs.(5) have been found in both the edge and strip geometries starting with NASCAP/LEO-type electrostatic potential solutions resulting from eq.(9) and producing the fields, n, F' and Φ' through one iteration cycle. Solutions of eq.(9) have been compared with output of the NASCAP/LEO code for the electrostatic potential. As expected, the electrostatic potentials are quite comparable in regions that are not sensitively multi-dimensional. Near the corner in the edge geometry and near the voltage discontinuity in the strip geometry, however, differences are readily seen.

3) Boundary Conditions

Symmetry permits the solutions on the boundaries perpendicular to the biased surfaces to be "mirrored", e.g., equipotential lines cross these boundaries perpendicularly. Such boundaries include the two side boundaries in the strip geometry and the x and y axes in the edge geometry.

For solutions of Poisson's Equation, the normalized electrostatic potential is equal to one on the corner surface in the edge geometry (Fig. 1.b). The normalized outer boundary potential is 0.01, initially. This means that, on a 100 Volt corner, the outer boundary would be at 1 Volt. Similarly, the average potential of the strip surface (Fig. 1.a) is also set to one and the upper boundary to 0.01, initially.

With the outer boundary potential value set initially to 0.01, a minimum value of γ is found that produces convergence of eq.(9). The potential on the outer boundary is then set equal to $\Phi_b' \equiv (2\gamma)^{2/3}$. This guarantees that $(\gamma - \Phi'^{3/2}/2) \leq 0$ everywhere. Solutions are then recalculated using this value of Φ_b'.

The above process results in an outer boundary potential of 2-4 Volts for a 100 Volt surface. Thus, since both the ion and electron thermal kinetic energies in the ambient plasma are much less than 2 e.v., the sheaths modeled in this way are fully Child-Langmuir in character and the ions are effectively excluded from the sheath. There are no regions in the sheath where $e\Phi << kT$ since the electrostatic potential rises monotonically as one proceeds inward from the outer sheath to the biased surfaces.

The boundary conditions on the velocity potential, F', are similar to those on the electrostatic potential. The same translation and reflection symmetries obtain for F' as for Φ' and so the boundaries perpendicular to the biased surfaces are, again, "mirrored". However, although definite values of Φ' are imposed on the biased surfaces and the outer boundary, the values of F' on these surfaces are not known a-priori. What is known is the magnitude of the gradient of F' derived from the Energy Equation,

$(\nabla' F')^2 = \Phi'$. To deal with these boundary conditions, the value of F' on the outer boundary is set to zero in our calculations and the equation for F' iterated until the Energy Equation is satisfied everywhere on the biased surfaces. This requires a delicate numerical approach and much computer time.

4) The Self-Consistent Cycle

Once F' is found using the density function, n, calculated by taking the Laplacian of the NASCAP/LEO-type electrostatic potential, a new electrostatic potential is calculated from $(\nabla' F')^2 = \Phi'$. This potential is compared with the NASCAP/LEO-type potential at every point in the calculation space. Further processing of the self-consistent cycle should consist of testing the agreement of these two potentials to some precision and, if they are sufficiently different, mixing the potentials, taking the Laplacian of the result so as to produce a new relative electron density, n, solving the Equation of Continuity for a new velocity potential, F', and finding yet another electrostatic potential via the Energy Equation.

Even after experience with only one processing cycle, it is clear that the self-consistent process is fraught with numerical instabilities. Solving the Equation of Continuity to high precision is especially important. For calculations on a 41x41 point grid, a single flow solution can consume many minutes on our VAX 8200 computer. For this reason, self-consistent solution cycles beyond the first cycle have not yet been seriously attempted. However, over one cycle it has been found that the input and output electrostatic potentials differ significantly near the voltage discontinuity in the strip geometry for high-modulation cases and almost everywhere in the edge geometry. This means that the NASCAP/LEO-type electrostatic potentials are not good solutions of the fluid model equations, as suspected.

5) Comparisons With NASCAP/LEO

Figures 7&8 show comparisons in the edge geometry between an electrostatic potential calculated using NASCAP/LEO and an electrostatic potential calculated using the fluid model. We have replotted the NASCAP/LEO code output using S. In these figures,

the surface voltages have been normalized to one. Plasma parameters used to calculate these results are as follows:

Electron Temperature = 0.1 e.v.
Electron Density = 10^6/cc
Debye Length = 0.00235 meters
Surface Voltage = 100 Volts
Child-Langmuir Length = 0.525 meters

As in the Debye Approximation plots (Figs. 2-5), the NASCAP/LEO plot of Fig. 7 has a zero on the surface of the 1st outer grid. The zero in Fig.8 is beyond the calculation space, the boundary value of the potential having been chosen to maximize the electron density on the boundary. One sees that the equipotentials in Figs. 7&8 are nearly coincident although the NASCAP equipotentials are somewhat compressed toward the surface in the outer sheath, no doubt due to the position of the zero surface.

Comparisons of the fluid model and NASCAP/LEO are not reported for the strip geometry because of our inability to obtain numerically stable runs of NASCAP/LEO using the object shown in Fig. 6 with V_{oo} = 100 Volts.

6) Fluid Model Runs

a) Strip Geometry

Calculations for the strip geometry have been made using the plasma parameters given above. Adjacent strips have voltages, V_{oo} plus or minus a percentage modulation. With V_{oo} = 100 Volts a 10% modulation means that the higher voltage strips are at 110 Volts and the lower voltage strips are at 90 Volts. All calculations have been done on a 41x41 point grid and, as in the Debye case, voltages have been normalized through division by V_{oo}.

Calculations for modulations of 0%, 10%, 20%, 30%, 40%, 50%, 60%, 70% and 90% have been made. Figures 9-38 show the results of calculations having 0%, 10%, 30%, 50%, 70% and 90% modulations. The figures are arranged in groups of five. The first figure in each

group shows the solution of Laplace's Equation. This solution is used as the initial electrostatic potential in the iteration of the NASCAP/LEO-type, non-linear Poisson's Equation (eq. 9), the solution of which is shown in the next figure.

The third figure shows the normalized electron charge density, $n = N/N_0$, derived by taking the Laplacian of the Poisson solution and multiplying it by the appropriate factor (see eqs. 5).

The fourth figure is the solution of the Equation of Continuity for the velocity potential, F'. Fluxes over the outer boundaries and onto the biased surfaces have been calculated for these solutions and used to check particle conservation. These results are summarized in Table I.

The fifth and last figure in each group shows the output electrostatic potential derived from the Energy Equation (also denoted as derived from the Velocity Potential). This solution is to be compared to the NASCAP/LEO-type, Poisson potential. If these potentials are essentially the same, one can conclude that the NASCAP/LEO-type potential is a solution of the two-dimensional sheath equations presented here. Significant differences between these solutions would suggest that the NASCAP/LEO-type potential is not a solution of the equations presented. If differences occur most prominently near the surface voltage or shape discontinuities, one may infer that the one-dimensional charge-potential relation assumed in NASCAP/LEO is asserting its presence.

Figures 9-13 show strip-geometry solutions having no modulation. Thus, this case is one-dimensional. Fig. 9 shows a Laplace solution that falls-off linearly with distance above the uniformly charged surface. This is to be expected since the solution of Laplace's Equation in one dimension is a straight line. Fig. 10 shows the NASCAP/LEO-type potential. One can see that space charge pulls the equipotential surfaces toward the biased surface somewhat.

Fig. 11 shows the relative electron density. Because the relative electron density is proportional to the Laplacian of the electrostatic potential, here it is proportional to the second

derivative of the potential with respect to y. One can see that the second derivative is near zero just above the surface and increases as one goes toward increasing y values.

Fig. 12 shows the velocity potential, F', derived from the Equation of Continuity. The velocity field is the gradient of this potential. One can see that the velocities are larger near the surface than in the outer sheath. This agrees with the behavior of the analytical solution of the Equation of Continuity in one dimension, namely, nV = const. Where n is small V will be large and where n is large V will be small.

Fig. 13 shows the output electrostatic potential derived from the velocity potential. Superposition of Figures 10 and 13 shows almost exact agreement between the NASCAP/LEO-type electrostatic potential and the new electrostatic potential. Were we interested merely in the one-dimensional sheath above a biased surface, the self-consistent field process could be considered to have converged after only one cycle. This result is to be expected since the NASCAP/LEO-type solution should be correct in one dimension.

Figures 14-18 show solutions for a 100 Volt surface with a 10% modulation. In these figures one can begin to see the effects of the differing biases of the strips. Notice that the NASCAP/LEO-type Poisson solution is not very different from the Laplace solution. The electron densities in the sheath appear so small that, for rough purposes, the electrostatic potential may be approximated by the Laplace solution. Notice also that the velocity potential shows a particle flow only slightly skewed toward the higher voltage strip. Apparently, 10% modulation does not change the downward flow of electrons appreciably. Finally, notice that the NASCAP/LEO-type potential (Fig. 15) and the new electrostatic potential (Fig. 18) remain very close.

Figures 19-38 show results in the strip geometry for a 100 Volt surface having modulations of 30%, 50%, 70% or 90%. These figures show, as expected, that increasing modulation causes increased skewing of the potentials toward the higher voltage strip. This is also true of the particle fluxes, although the effect is much

less than would be expected by looking at the velocity potential plots and the electron density plots separately. Because flux is the product of velocity and density, the high velocities shown over the higher voltage strip are almost completely compensated by the low densities there. Table I summarizes the associated particle flux calculations. Notice in Table I that overall particle loss is extremely small in all cases. This means that the Equation of Continuity is being solved quite well in these runs.

Comparisons of the Laplace and the Poisson solutions at each value of modulation show that the Laplace solutions are increasingly poor approximations to the electrostatic potential in the sheath as the modulation is increased. Further, comparison of the NASCAP/LEO-type potentials with the potentials derived from the velocity potentials shows increasing disagreement as the modulation is increased. The assumption presented here is that this is due to the breakdown of the one-dimensional charge density-electrostatic potential relationship (eq.7) embedded in the NASCAP/LEO-type solutions.

It should be pointed out that, because they differ significantly after one cycle of the self-consistent process, neither the NASCAP/LEO-type potentials nor the potentials calculated subsequently from the velocity potential can be correct solutions of the fluid model equations. Correct solutions require convergence of the self-consistent field process over, perhaps, many cycles. Achieving this awaits a better computing environment.

b) Edge Geometry

Figures 39-63 show results of runs made using the edge geometry. In all cases the electrostatic potentials are normalized to the potential on the surface of the edge, 100 Volts. The voltage on the outer boundary is set initially at 1 Volt but is adjusted upward to as much as 4 volts for calculational stability. The plasma parameters are the same as given in part (B.5) above.

The figures are arranged in groups of five as above: Laplace solution, NASCAP-type solution, Relative Electron Density, Velocity Potential and Electrostatic Potential from the Velocity Potential.

Because there is no easy way to gradually approach the geometry of a corner, a series of solutions starting with a one-dimensional solution, as was presented for the strip geometry, will not be presented. Instead, we present a selection of calculations for different sized edges and out to different distances.

The biased structure shown is 1/4 of a cross section through an infinitely long conducting bar. For such an object, a square calculation space is inappropriate because the equipotential lines of the electrostatic potentials would be pulled artificially toward the upper right-hand corner of the calculation space, although they would quickly become nearly circular as one proceeded inward. Because at large distances one expects the sheath to approximate a circle in cross section, anyway, the calculation space has been truncated to a circle of 40 grid spaces in radius and centered at the point (0,0). Thus the high circularity of potentials of the maximum possible radius is also artificial but less so than equipotentials calculated using square outer boundaries.

Figures 39-43 show calculations for 1/4 of a square conducting bar 0.346 meters on a side. With D_{CL} = .5247 meters, the calculation space goes out to 1 D_{CL} from the bar above its flat surfaces. The grid is 41x41 points. The voltage on the outer boundary is 2.47 Volts. The effective scale length determined from the adjusted value of γ in the outer sheath is 2 grid spaces. The Debye Length is 0.135 grid space so that features of the order of a Debye length are unresolved. Table II indicates that good particle conservation was achieved for the flow shown in Fig. 42.

Notice that the NASCAP-type solution (Fig.40) is nearly the same as the Laplace solution (Fig.39). However, the electrostatic potential derived from the velocity potential (Fig.43) is pulled very much inward relative to the NASCAP-type potential. These two potentials are very different, a condition implying that neither is the correct solution of the fluid model equations. The correct solution must lie in-between these solutions.

Figures 44-48 show results for a 0.92m x 0.66m bar. The calculation space is the same as that of the previous figures. Again the Laplace and NASCAP-type solutions are similar although the

solutions on the lower right boundary are artificially pushed toward the bar. In this direction the sheath thickness is forced to be less than 1 D_{CL}.

As in the previous case, particle conservation is obtained to high precision. Also, the ratio of fluxes to the top and to the side of the corner are very nearly the same as the ratio of the extents of these surfaces, i.e., 14/10. As before, the electrostatic potential derived from the velocity potential is much pulled-in relative to the NASCAP-type potential.

Figures 49-53 show the same results as do Figures 39-43 but a different scale is used. The grid spacing is 0.05 D_{CL} in these figures rather than 0.033 D_{CL}. Thus the bar's dimensions are 0.525 m on a side. The calculation space goes out to 1.5 D_{CL} = 0.787 m above the flat surfaces of the bar. For calculational stability, the outer boundary has been set to 4.3 Volts.

Notice in the first two of these figures that the Laplace and NASCAP-type solutions are no longer similar. As expected, the Laplace solution extends out to the calculational boundary but the NASCAP-type solution of Fig. 50 terminates before this, at about 0.95 D_{CL}. The sheath radius compares to a radius of 0.86 D_{CL} in the NASCAP-type solution of Fig. 40. The slightly greater sheath radius in Fig. 50 is perhaps due to the larger boundary voltage, which would force the equipotentials outward somewhat. Nevertheless, the calculations shown in Fig. 50 have resulted in a sheath of the expected, finite thickness, namely, about 1 D_{CL}.

Reference to Table II shows that the flow of Fig. 52 conserves particles very well. Fig. 53 shows, again, that the final electrostatic potential and the NASCAP-type potential are very different. The wiggles on the outer equipotential in Figures . 53 and 49 do not represent real variation. They are probably due either to plotting artifacts, the fact that a smooth, circular boundary cannot be achieved on a square grid of points or budding numerical instabilities in the outer sheath.

Figures 54-58 show the same kind of information as do Figures 44-48 but with a grid spacing of 0.05 D_{CL}. Thus the bar size

in these figures is 0.735 m x 0.525 m. The calculation space is the same as that of Figures 44-48. The outer boundary voltage is 4.29 Volts.

One sees in these figures that the NASCAP-type solution shows a sheath of definite radius, about 1 D_{CL}, and that the final potential disagrees strongly with the NASCAP-type potential. As before, the Equation of Continuity is well solved and particles are conserved to high precision. Note, particularly, that in Fig. 55 the outer equipotentials are very circular even though the calculation space boundary is quite a bit further out. Indeed, this circularity is not lost until one approaches to within about 0.5 D_{CL} of the corner.

Figures 59-63 show calculations for a square bar of the same dimensions as that of the bar shown in Figures 39-43, i.e., 0.66 D_{CL} on a side. In these figures, however, the calculation space is extended to 1.56 D_{CL} above the flat surfaces of the bar. For numerical stability, the effective scale length of the outer sheath has been increased from 2 to 2.1 grid spaces. This means that the outer boundary electrostatic potential is 4.2 Volts.

One sees in the NASCAP-type solution of Fig. 60 that the sheath extends out only to about 0.71D_{CL} above the flat surfaces. This is to be compared to Fig. 40, in which the sheath extends out to about 0.86 D_{CL} but the calculation space extends only out to 1 D_{CL}. This difference may be due to proximity of the calculation boundary to the outer sheath surface in Fig. 40, i.e., the boundary may be pulling the sheath outward. The sheath shown in Fig. 60 is less affected by the boundary, which is farther away. One should note here once again that the boundary of the calculation space is a circle, 40 grid spaces in radius and centered at (0,0).

As in the other cases presented, Fig. 62 shows a flow that conserves particles quite well (see Table II). Also, the final potential is very much different from the NASCAP-type solution, as before.

C. Summary and Conclusions

The modeling of the Debye Approximation electron sheaths in the edge and strip geometries was completed in the summer of 1989. Electrostatic potentials in these sheaths were compared to NASCAP/LEO solutions for similar geometries. Velocity fields, charge densities and particle fluxes to the biased surfaces were calculated for all cases.

The major conclusion to be drawn from the comparisons of our Debye Approximation calculations with NASCAP-LEO output is that, where comparable biased structures can be defined and sufficient resolution obtained, these results are in general agreement.

Numerical models for the Child-Langmuir, high-voltage electron sheaths in the edge and strip geometries were constructed in 1989. Electrostatic potentials were calculated for several cases in each of both geometries. Velocity fields and particle fluxes were calculated. The self-consistent solution process was carried through one cycle and output electrostatic potentials compared to NASCAP-type input potentials.

The major conclusions to be drawn from the Child-Langmuir analysis of the strip and edge geometries are as follows:

1) Equations for the electron sheath that connect the electrostatic potential, electron density and velocity field can be derived from a multi-dimensional, warm fluid plasma model. These equations reduce to those used in the NASCAP-LEO code in one dimension.

2) NASCAP-type electrostatic potentials, which are solutions of the multi-dimensional Poisson's Equation but using the one-dimensional relation between charge density, velocity and electrostatic potential, are not compatible with the warm plasma fluid model near points of severe voltage or shape discontinuity. The incompatibility becomes more pronounced as voltage or shape discontinuities are made larger.

3) If particle velocity fields are assumed irrotational, the Equation of Continuity becomes an equation for the velocity potential, which can be solved to high precision. This requires imposing a non-linear boundary condition on the biased surface. The Continuity Equation approach to determining particle flow is an alternative to particle tracking and has the feature that it embodies particle interactions during the flow.

4) Sheath thicknesses of the NASCAP-type solutions in the edge geometry are approximately equal to but somewhat less than the expected value of one Child-Langmuir length. However, the electrostatic potentials calculated from the velocity fields have much smaller sheath thicknesses. If the self-consistent solution cycle were to be pursued to convergence, one might expect that the final solutions would show intermediate sheath thicknesses. This would imply generally thinner sheaths than are predicted by NASCAP/LEO-type solutions.

References

1) R.N. Metz, "Circuit Transients due to Arcs on a High-Voltage Solar Array", Journal of Spacecraft and Rockets, Vol. 23, No. 5, Sept.-Oct., 1986.

2) R.N. Metz, "Circuit Transients Due to Negative Bias Arcs-II", AIAA 24th Aerospace Sciences Meeting, Reno, Nevada, January, 1986

3) R.N. Metz, "LEO High Voltage Solar Array Arcing Response Model Final Report", January, 1986, NASA Grant NAG 3-576

4) R.N. Metz, "LEO High Voltage Solar Array Arcing Response Model Interim Report", February, 1987, NASA Grant NAG 3-576.

5) S.R. Seshadri, Fundamentals of Plasma Physics, American Elsevier, New York, 1973.

6) R.N. Metz, "LEO High Voltage Solar Array Arcing Response Model Interim Report", February, 1988, NASA Grant NAG 3-576.

7) I. Katz, M.J. Mandell, G.W. Schnuelle, D.E. Parks and P.C. Steen, "Plasma Collection by High Voltage Spacecraft at Low Earth Orbit", AIAA-80-0042, 18th Aerospace Sciences Meeting, January, 1980, Pasadena, California.

8) M.J. Mandell, I. Katz and D.L. Cooke, "Potentials on Large Spacecraft in LEO", IEEE Transactions on Nuclear Science, Vol. NS-29, No. 6, December, 1982.

9) R.N. Metz, "LEO High Voltage Solar Array Arcing Response Model Interim Report - Continuation IV", March, 1989, NASA Grant NAG 3-576.

Table I

Particle Fluxes for the Strip Geometry

100 Volt Surface +/- Modulation
(arbitrary units)

Fig.#	% Mod.	LFlux	RFlux	TFlux	%NC	%RtShift
12	0	.1783	.1783	.3565	-.03	0
17	10	.1763	.1757	.3519	-.03	-.2
22	30	.1748	.1756	.3503	-.03	.2
27	50	.1722	.1745	.3467	0	.6
32	70	.1669	.1722	.3391	0	1.6
37	90	.1514	.1671	.3187	+.06	5.0

LFlux = integrated normal flux on lower left (low voltage) boundary

RFlux = integrated normal flux on lower right (high voltage) boundary

TFlux = integrated normal flux on upper boundary

%NC = 100*[1-(lflux+rflux)/topflux] = % non-conservation of flux

%RtShift = 100*(rflux-lflux)/topflux = % of flux shifted to higher voltage surface

Table II

Particle Fluxes for the Edge Geometry (arbitrary units)

Fig.#	CTFlux	CCFlux	CRFlux	TTFlux	TRFlux	%NC
42	.084	.0063	.084	.088	.088	.5
47	.117	.0063	.085	.104	.105	.3
52	.084	.0063	.084	.088	.088	.5
57	.117	.0063	.085	.104	.105	.4
62	.059	.0063	.059	.063	.063	.8

CTFlux = integrated normal flux onto top of edge

CCFlux = flux to corner

CRFlux = integrated normal flux onto right side of edge

TTFlux = integrated normal flux crossing top boundary

TRFlux = integrated normal flux crossing right boundary

%NC = 100*[1-(total outer boundary flux/total flux to edge) = % non-conservation of flux

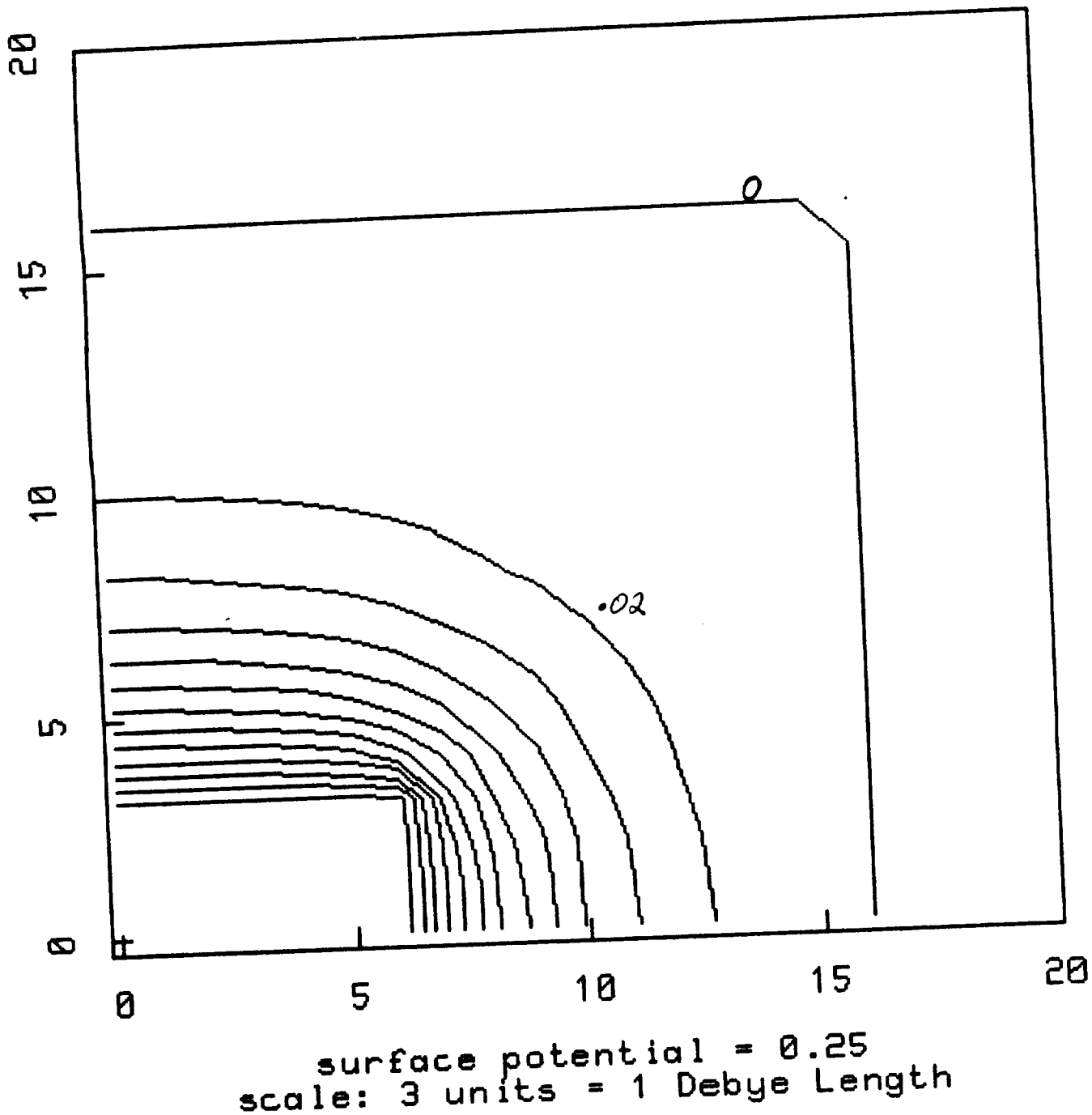

Fig.2

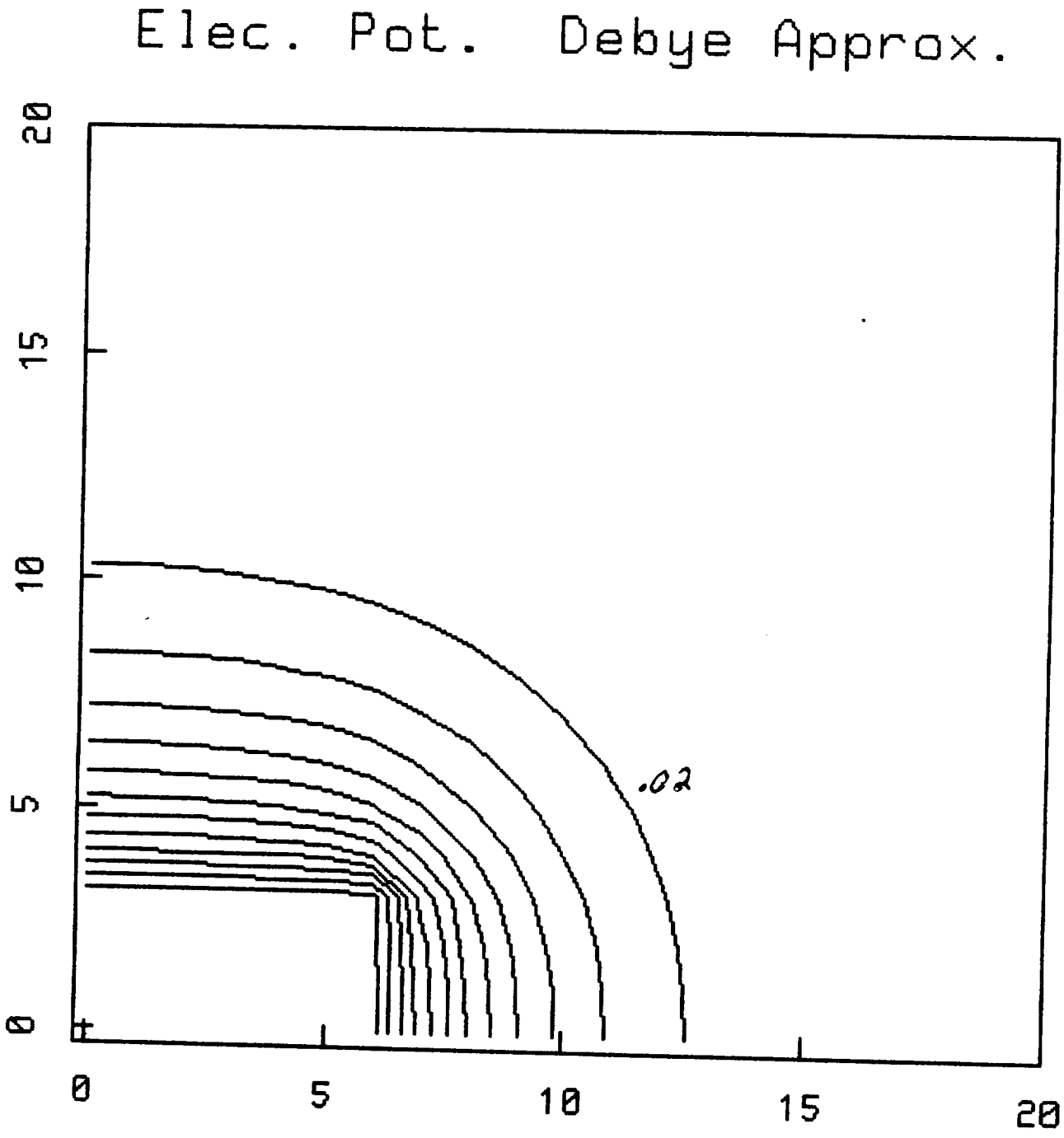
Elec. Pot. Debye Approx.
20
15
10
5
0
0
5
10
15
20
.02
surface potential = 0.25
scale: 3 units = 1 Debye Length

Fig.3

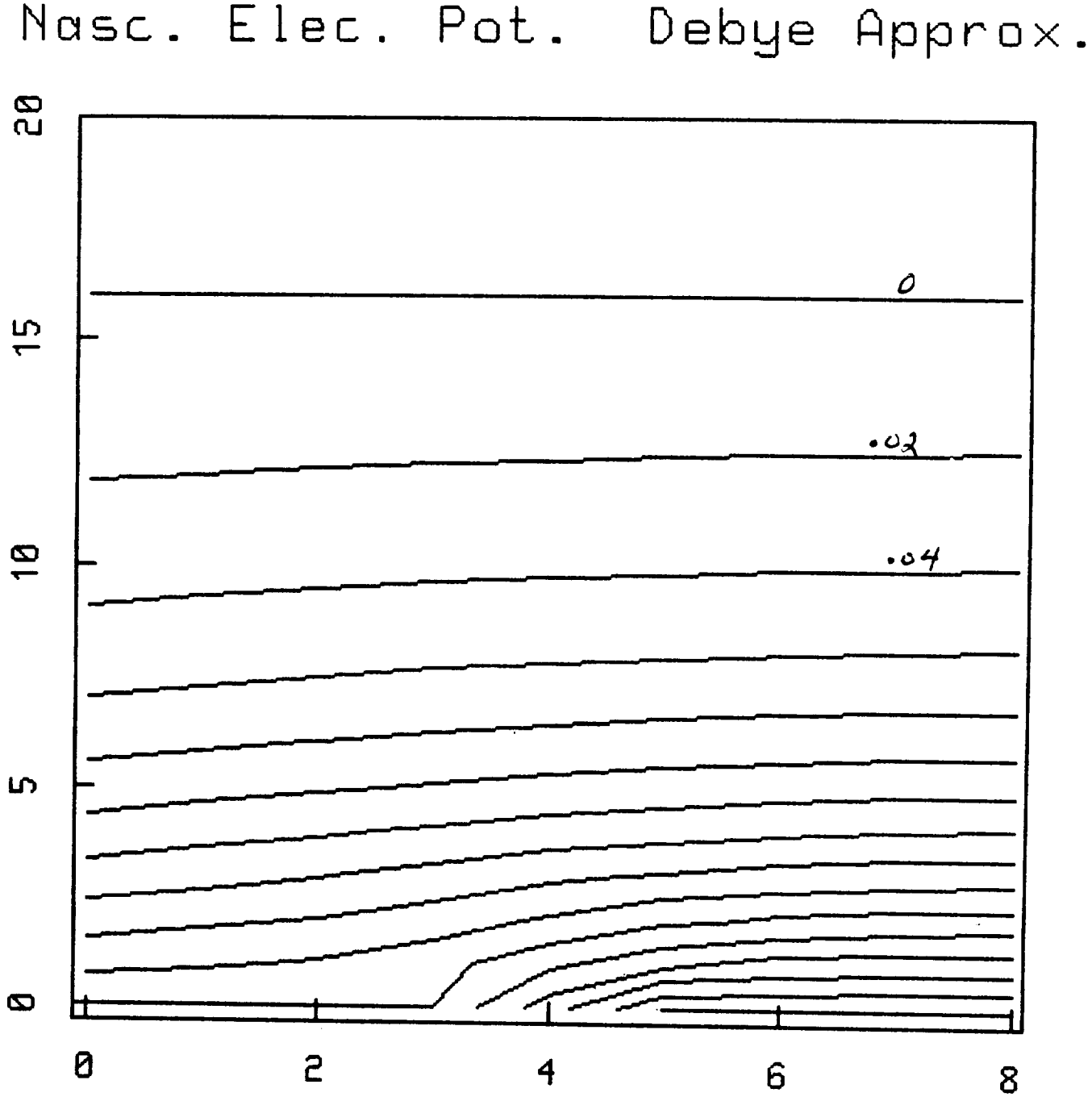
Nasc. Elec. Pot. Debye Approx.
20
15
10
5
0
0
.02
.04
0
2
4
6
8
strip surface: Voo = 0.25 Vo = 0.05
scale: 8 units = 1 Debye Length

Fig.4

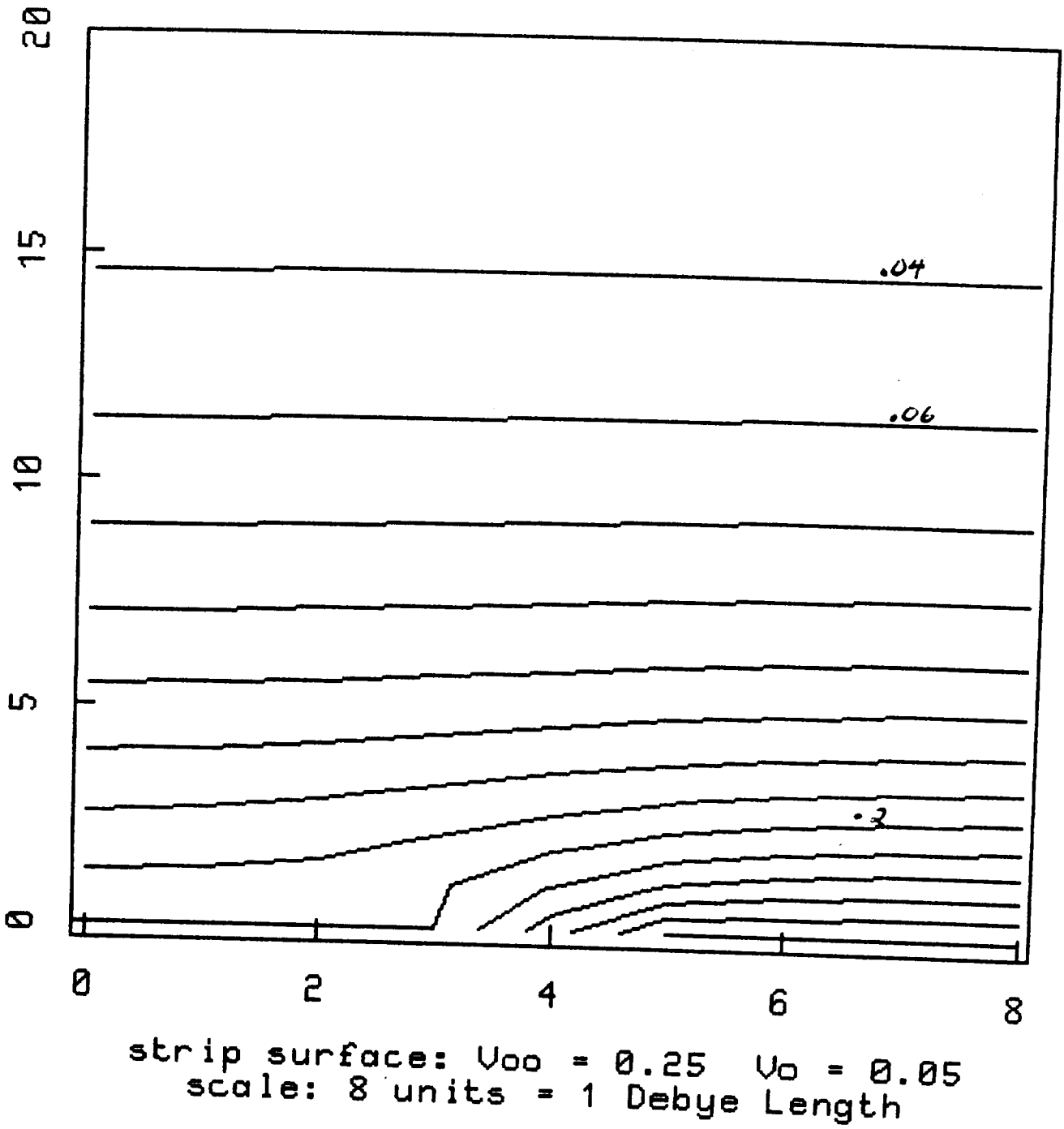
Elec. Pot. Debye Approx.
20
15
10
5
0
.04
.06
.2
0
2
4
6
8
strip surface: Voo = 0.25 Vo = 0.05
scale: 8 units = 1 Debye Length

Fig.5

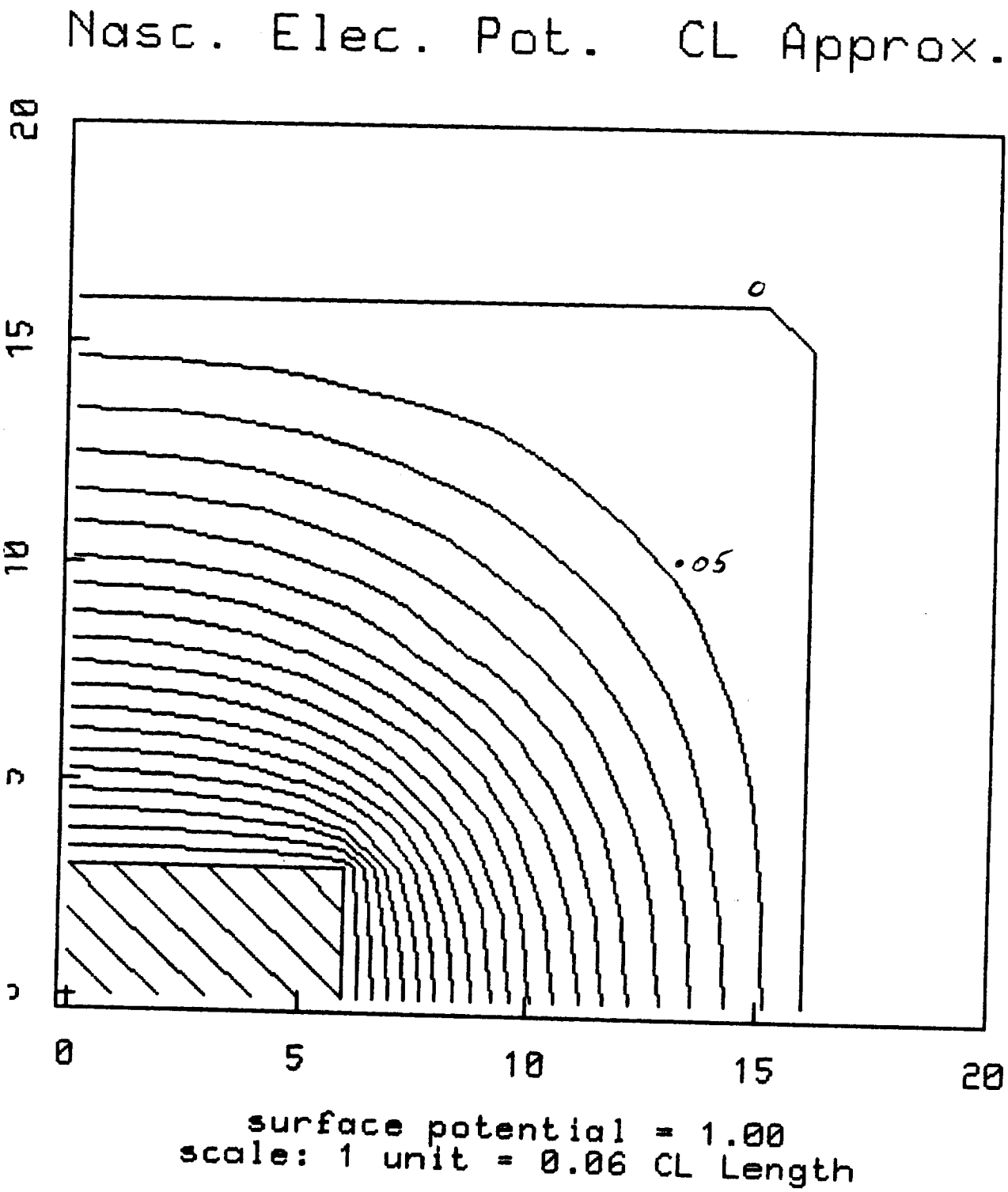

Fig.7

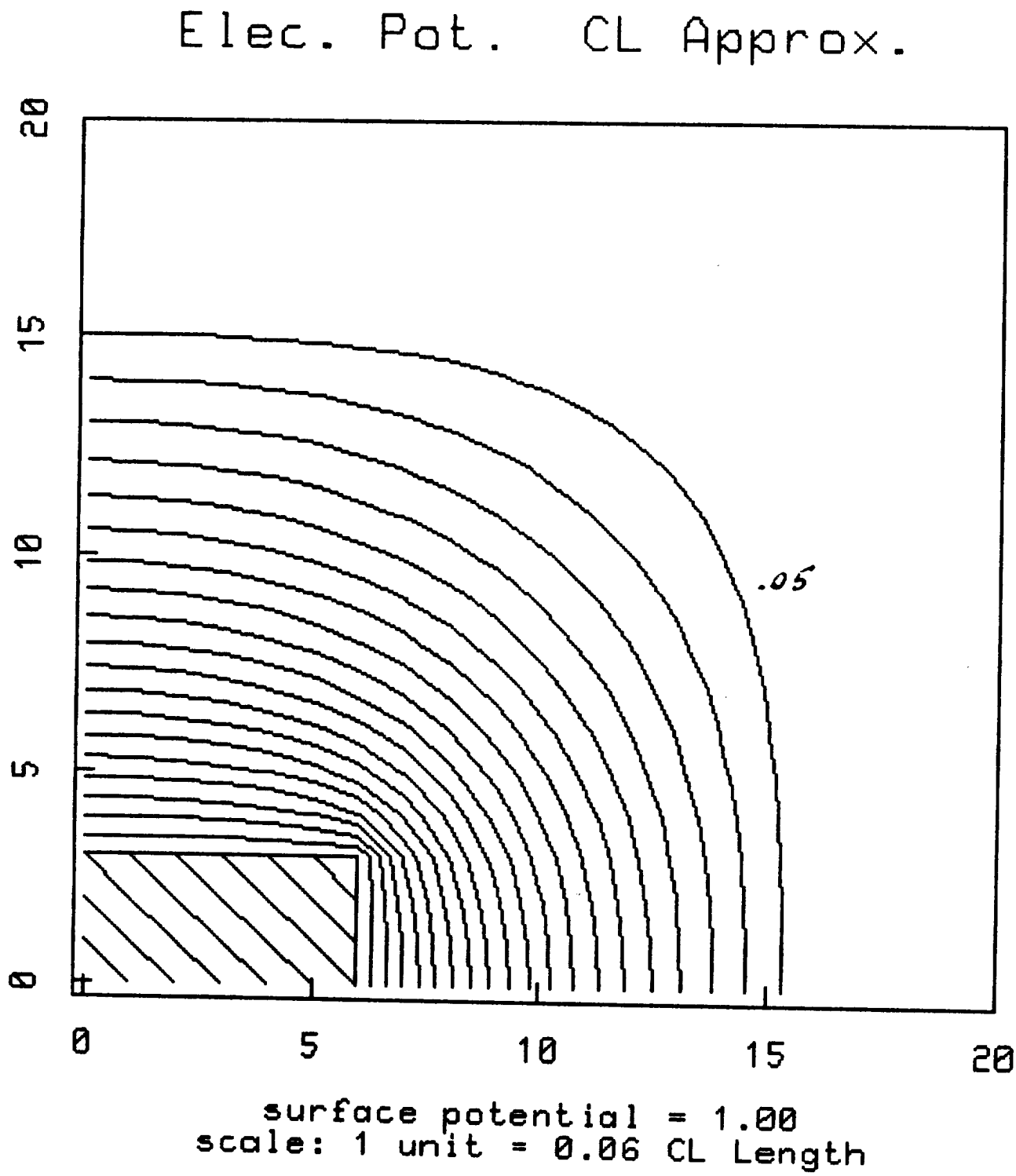
Elec. Pot. CL Approx.
20
15
10
5
0
.05
0
5
10
15
20
surface potential = 1.00
scale: 1 unit = 0.06 CL Length

Fig.8

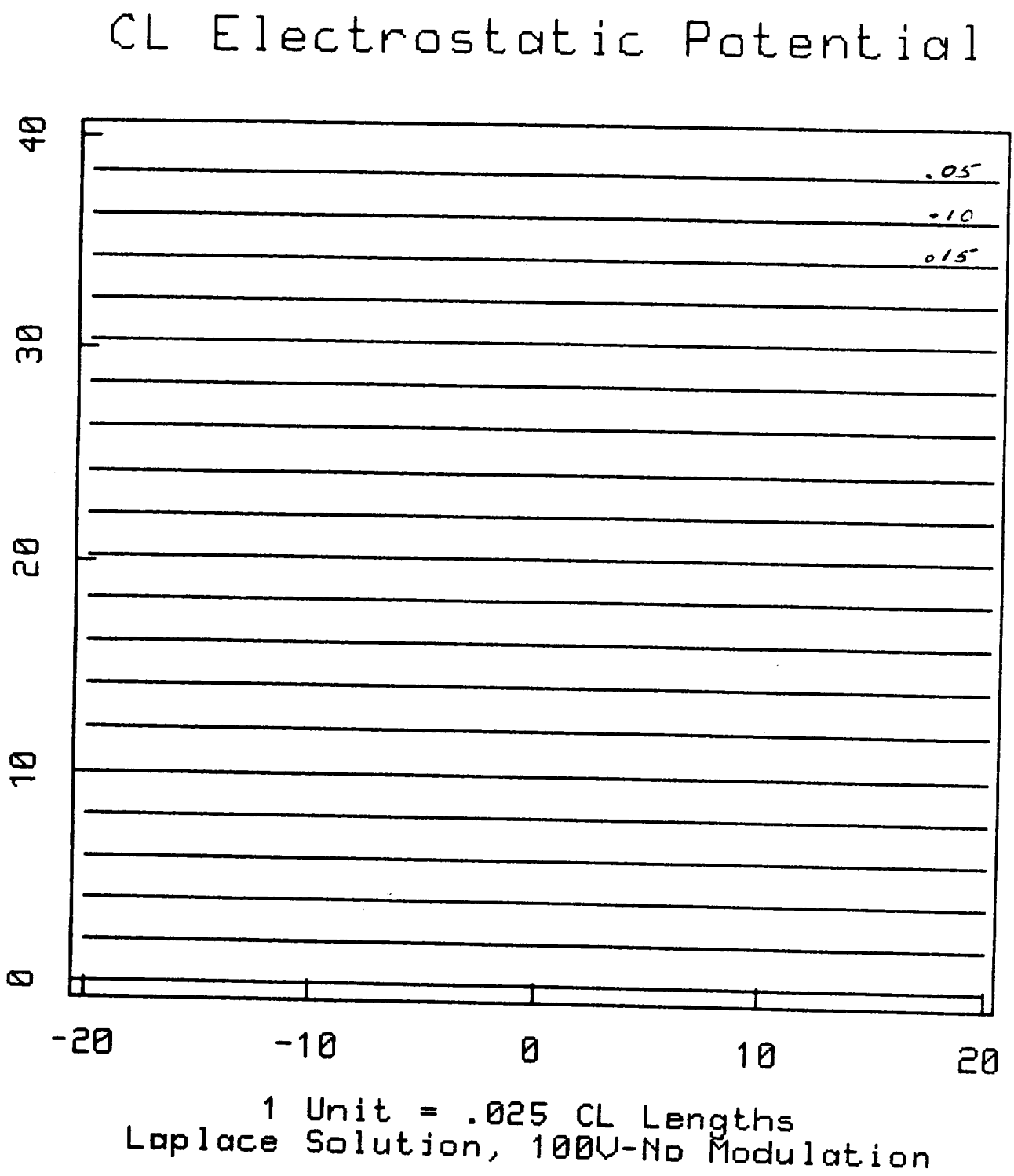
CL Electrostatic Potential
40
30
20
10
0
.05
.10
.15
-20
-10
0
10
20
1 Unit = .025 CL Lengths
Laplace Solution, 100V-No Modulation

Fig.9

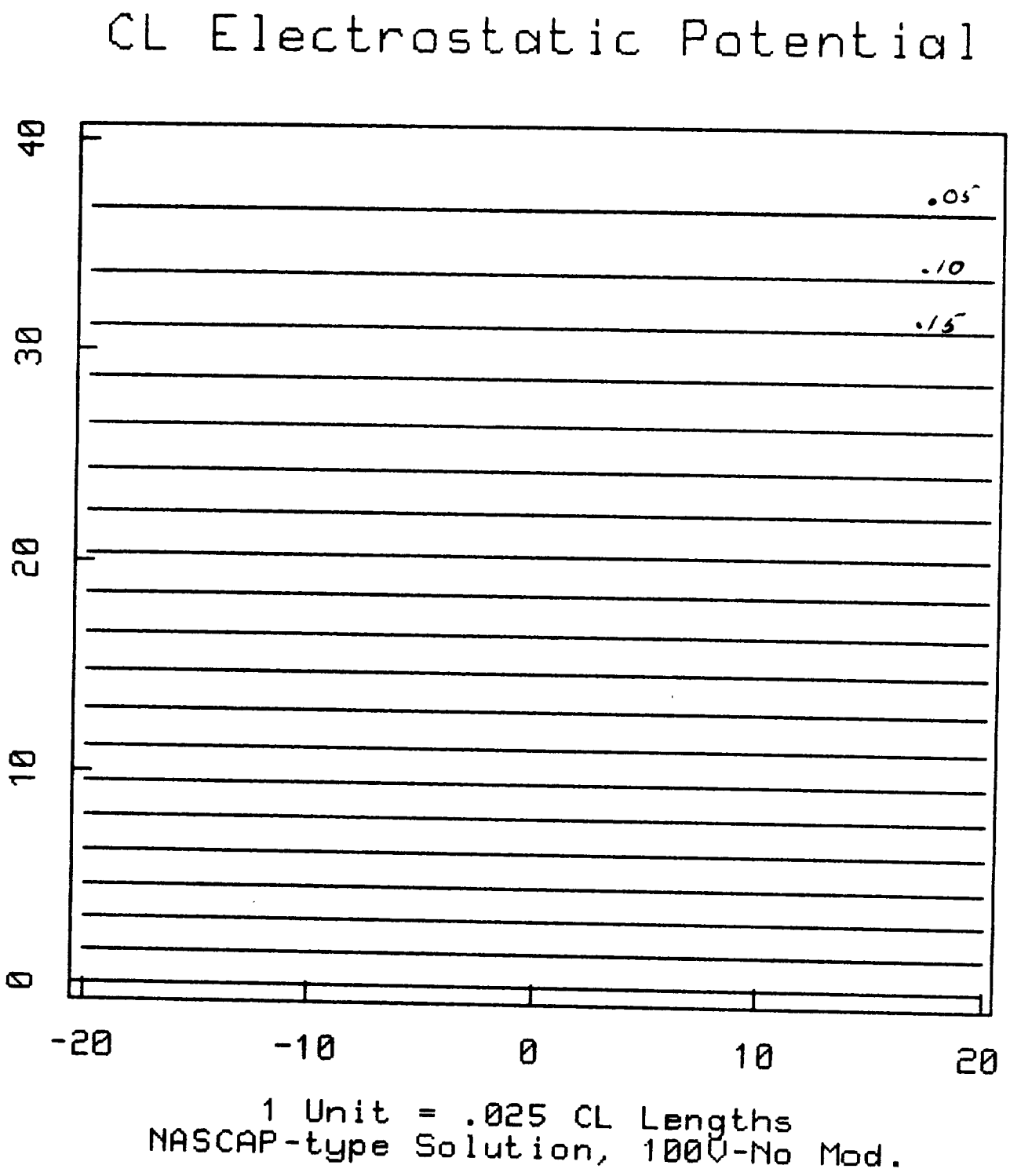
CL Electrostatic Potential
40
30
20
10
0
.05
.10
.15
-20
-10
0
10
20
1 Unit = .025 CL Lengths
NASCAP-type Solution, 100V-No Mod.

Fig.10

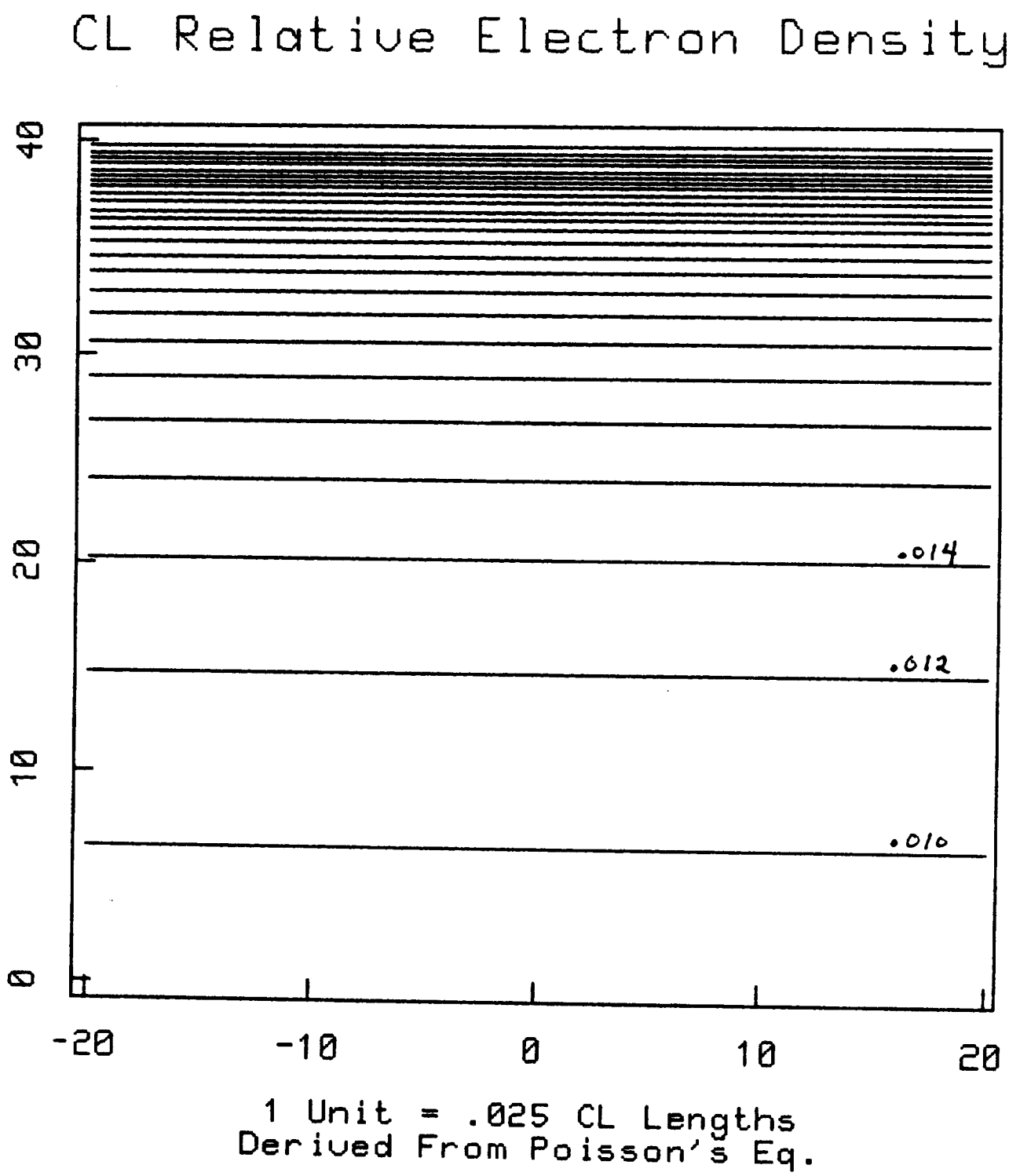
CL Relative Electron Density
40
30
20
10
0
.014
.012
.010
-20
-10
0
10
20
1 Unit = .025 CL Lengths
Derived From Poisson's Eq.

Fig.11

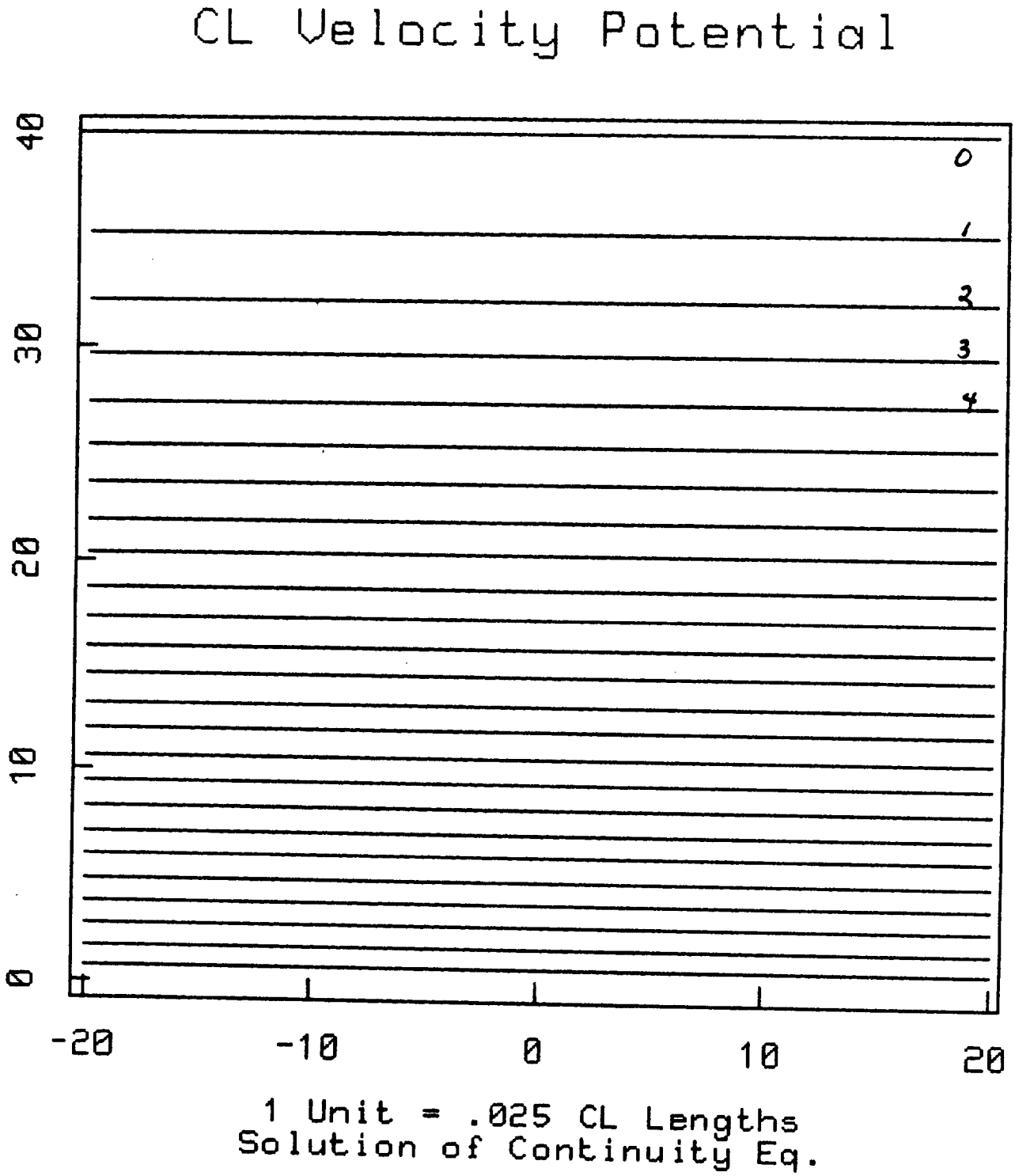
CL Velocity Potential
40
30
20
10
0
0
1
3
3
4
-20
-10
0
10
20
1 Unit = .025 CL Lengths
Solution of Continuity Eq.

Fig.12

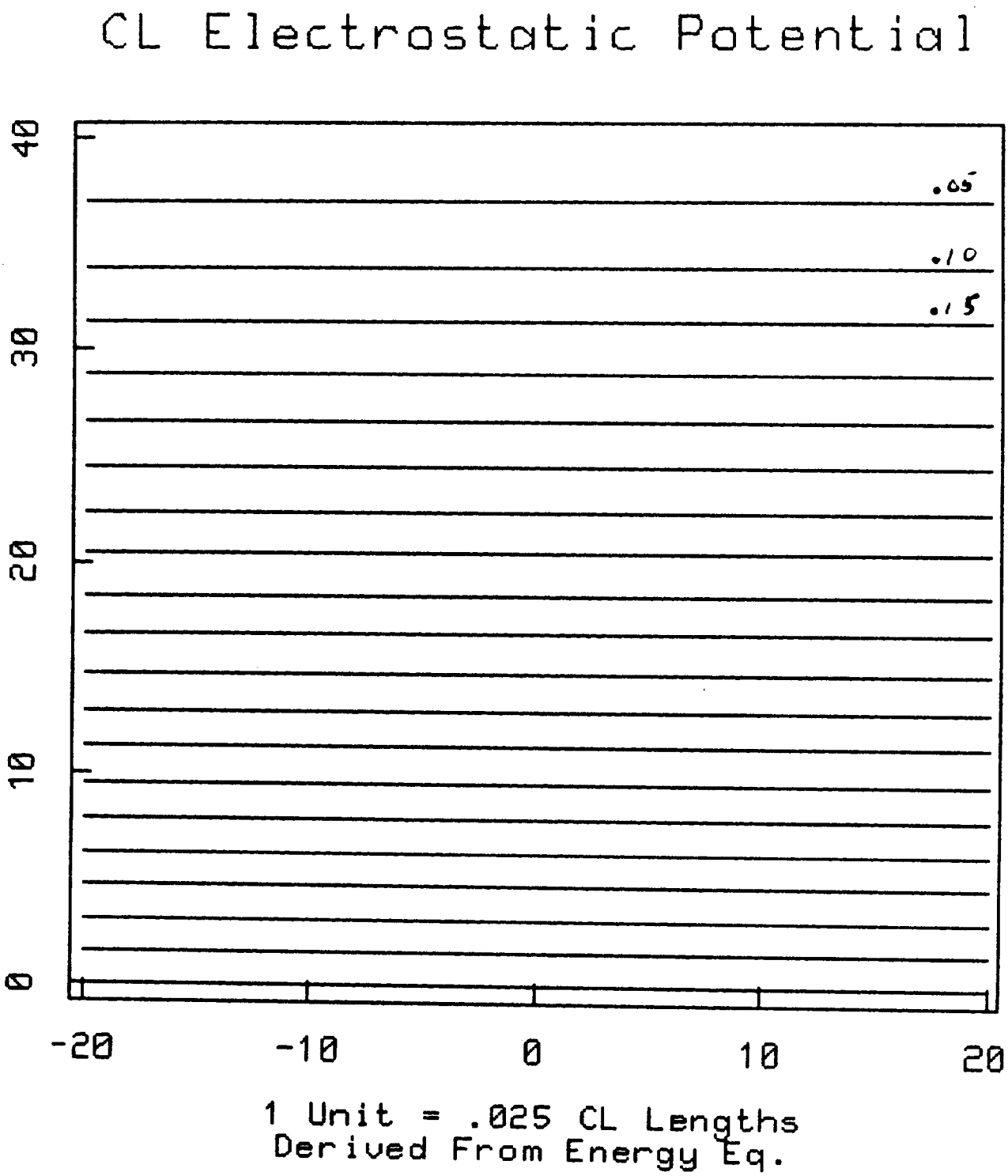
CL Electrostatic Potential
40
30
20
10
0
.05
.10
.15
-20
-10
0
10
20
1 Unit = .025 CL Lengths
Derived From Energy Eq.

Fig.13

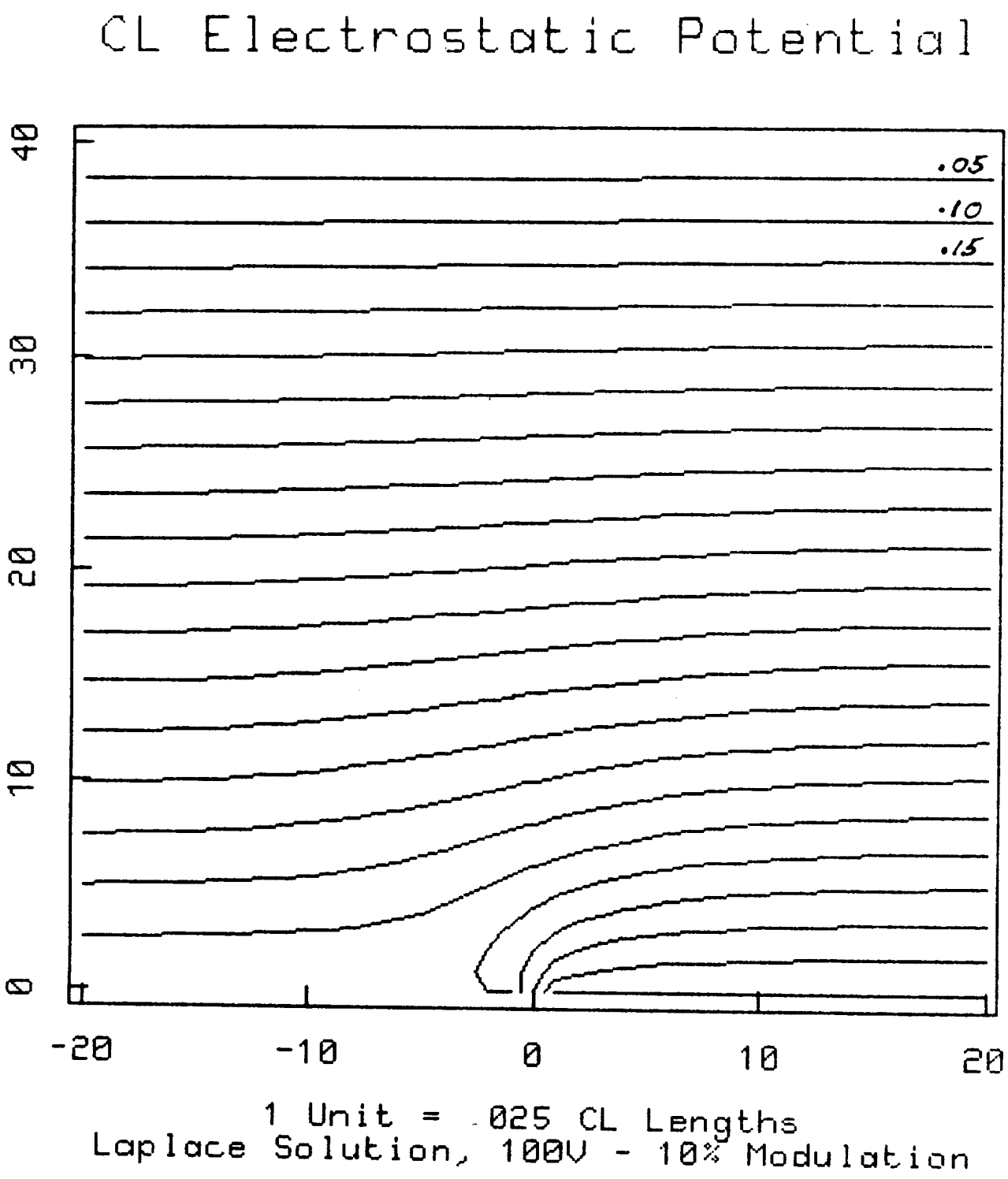
CL Electrostatic Potential
40
30
20
10
0
.05
.10
.15
-20
-10
0
10
20
1 Unit = .025 CL Lengths
Laplace Solution, 100V - 10% Modulation

Fig.14

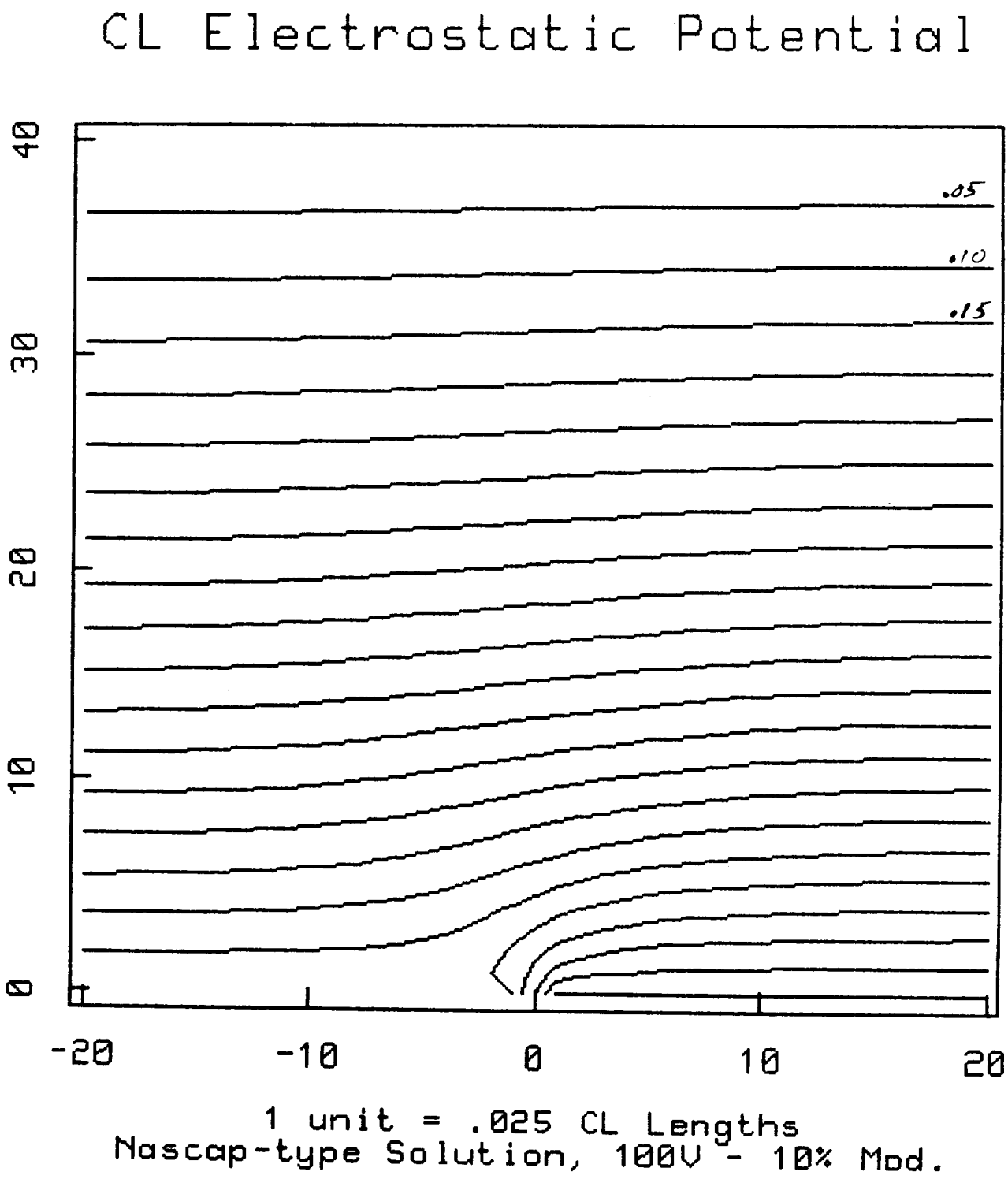
CL Electrostatic Potential
40
30
20
10
0
.05
.10
.15
-20
-10
0
10
20
1 unit = .025 CL Lengths
Nascap-type Solution, 100V - 10% Mod.

Fig.15

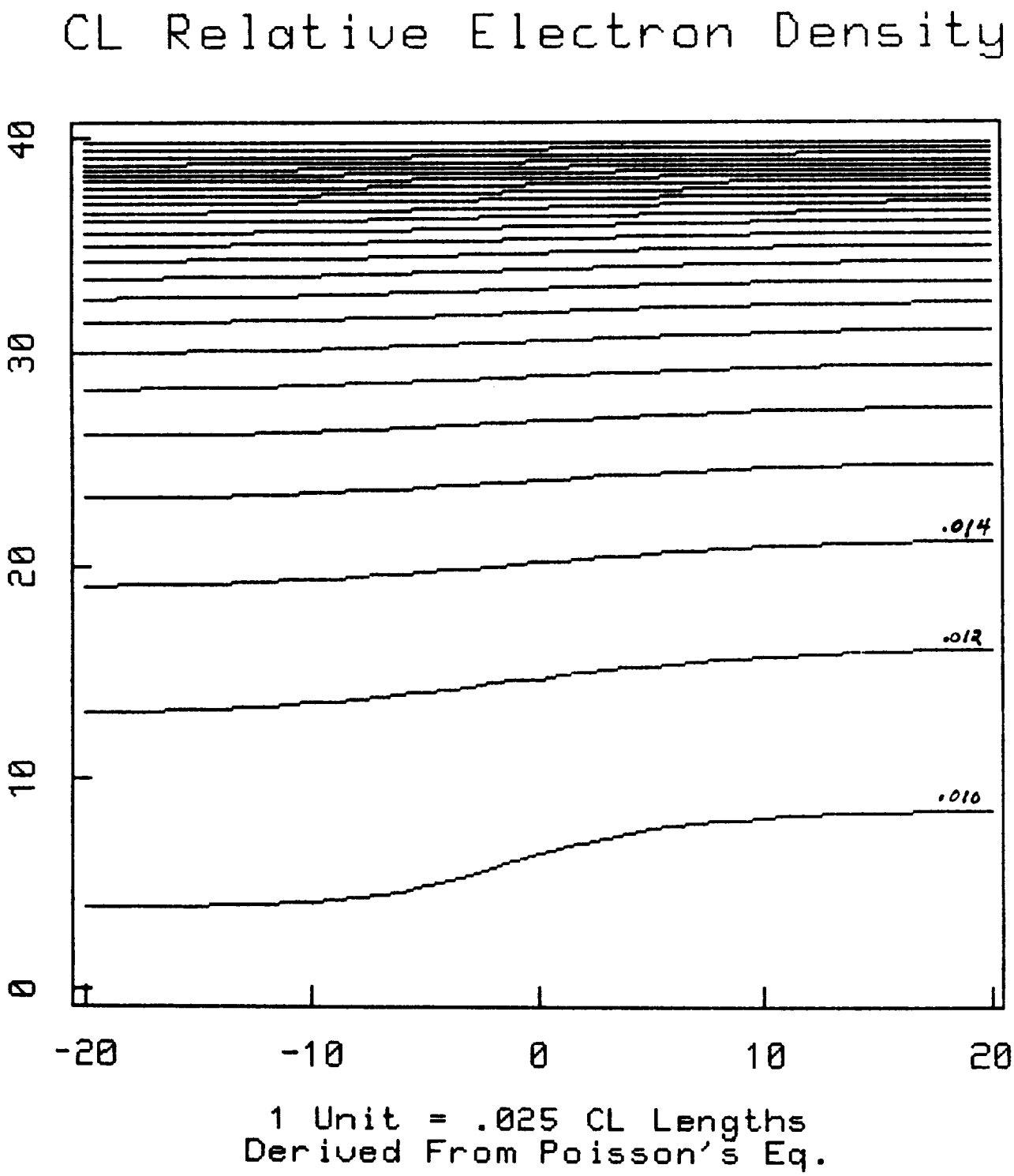
CL Relative Electron Density
40
30
20
10
0
.014
.012
.010
-20
-10
0
10
20
1 Unit = .025 CL Lengths
Derived From Poisson's Eq.

Fig.16

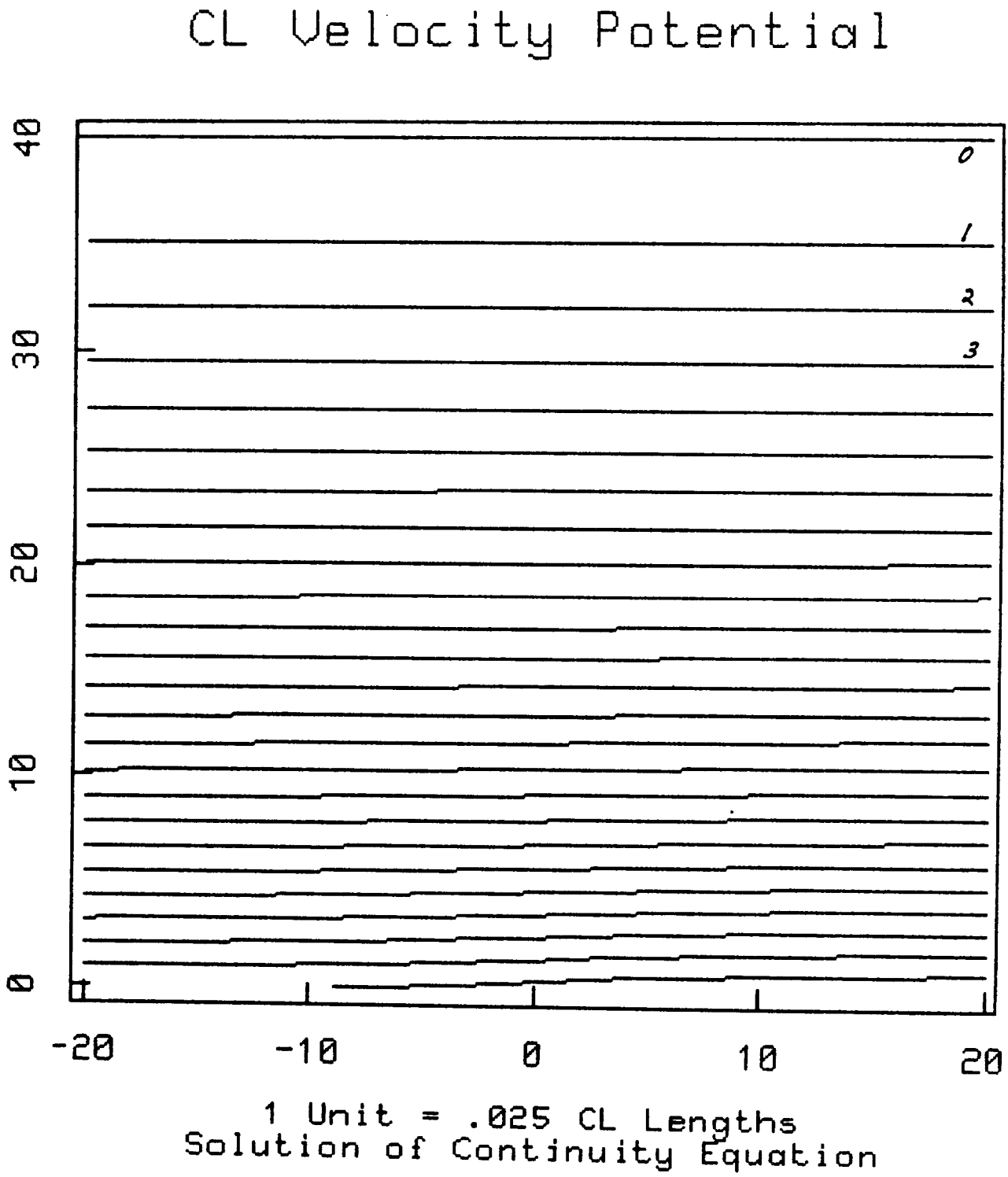
CL Velocity Potential
40
30
20
10
0
0
1
2
3
-20
-10
0
10
20
1 Unit = .025 CL Lengths
Solution of Continuity Equation

Fig.17

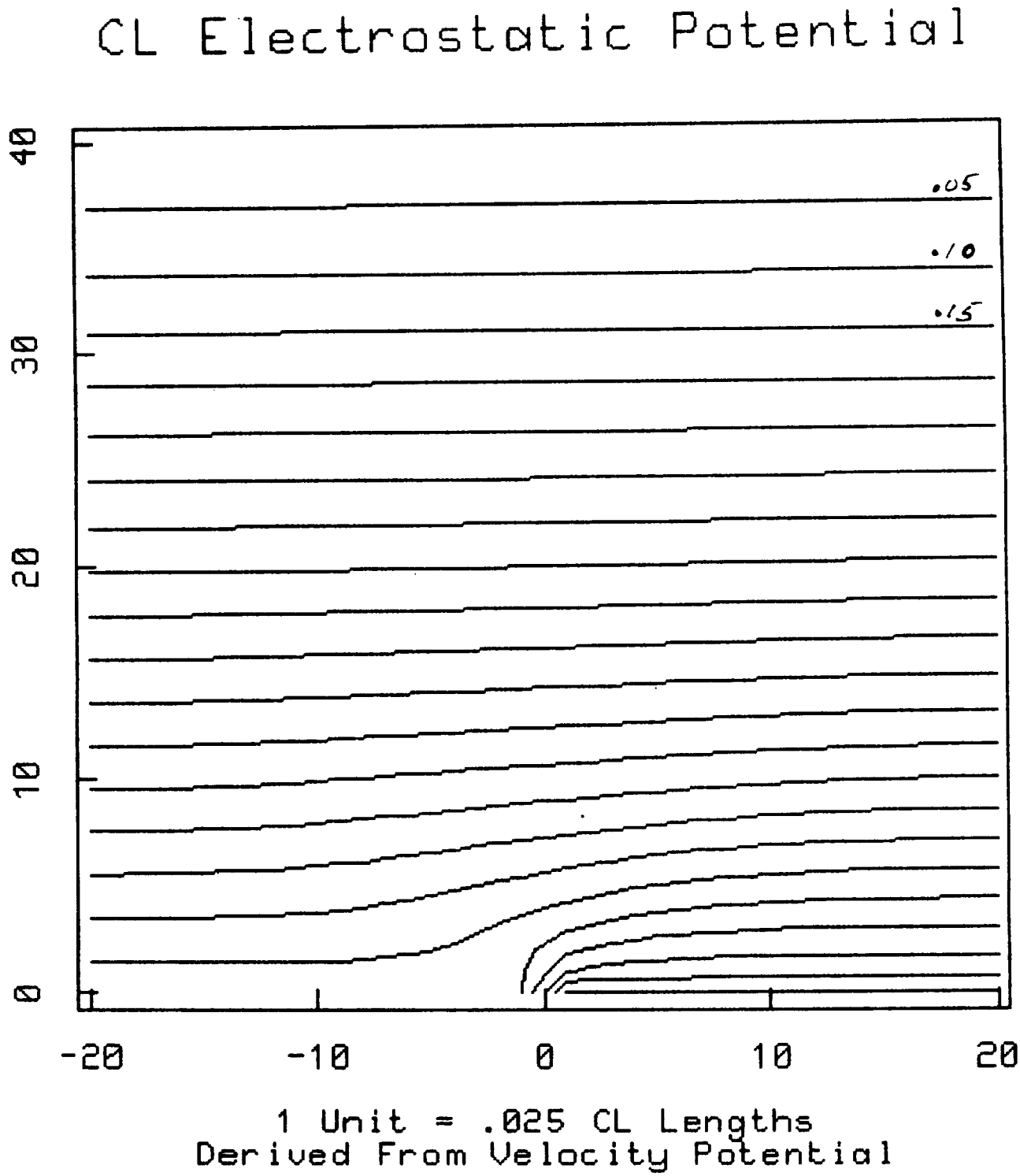
CL Electrostatic Potential
40
30
20
10
0
.05
.10
.15
-20
-10
0
10
20
1 Unit = .025 CL Lengths
Derived From Velocity Potential

Fig.18

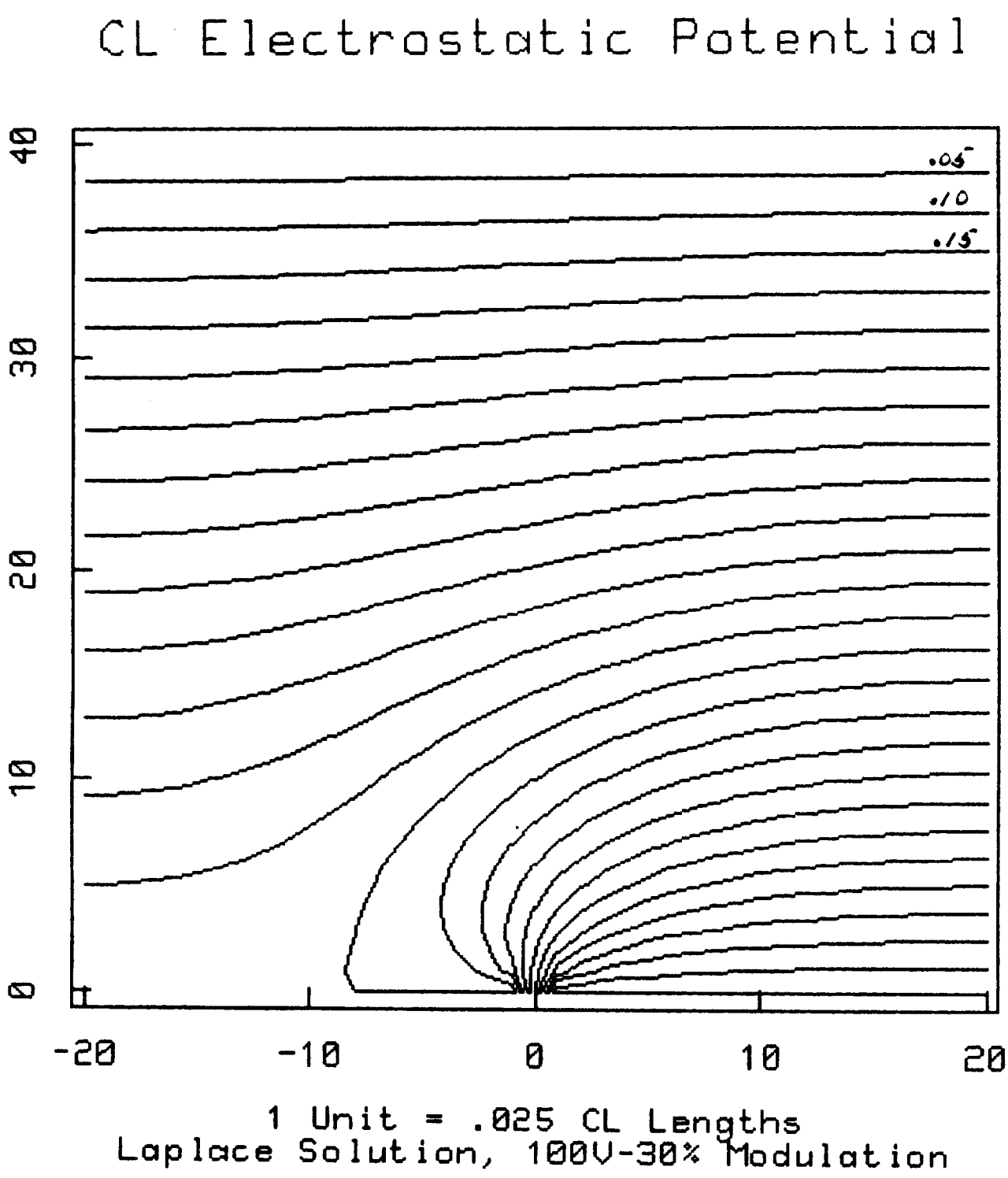
CL Electrostatic Potential
40
30
20
10
0
.05
.10
.15
-20
-10
0
10
20
1 Unit = .025 CL Lengths
Laplace Solution, 100V-30% Modulation

Fig.19

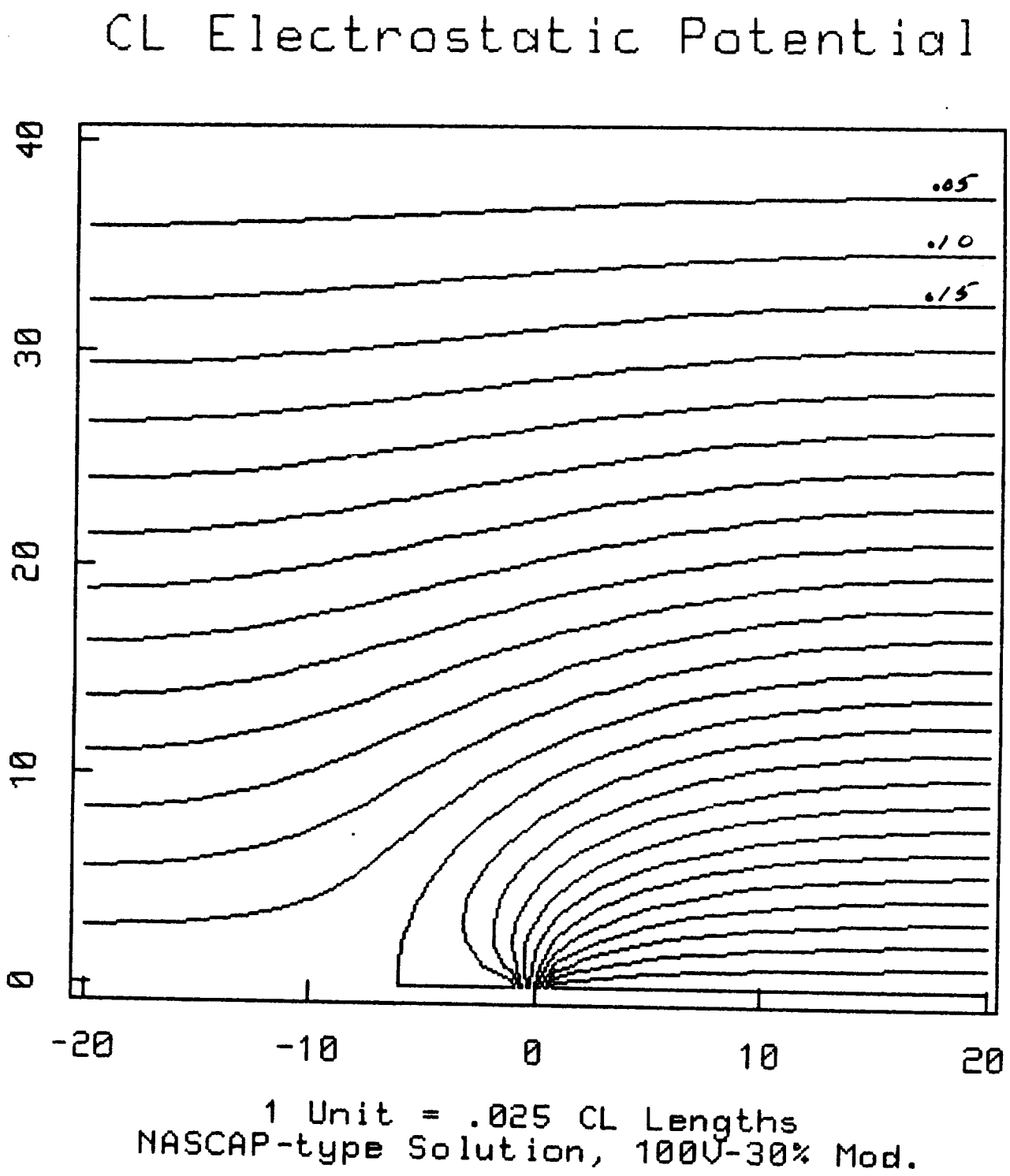
CL Electrostatic Potential
40
30
20
10
0
.05
.10
.15
-20
-10
0
10
20
1 Unit = .025 CL Lengths
NASCAP-type Solution, 100V-30% Mod.

Fig.20

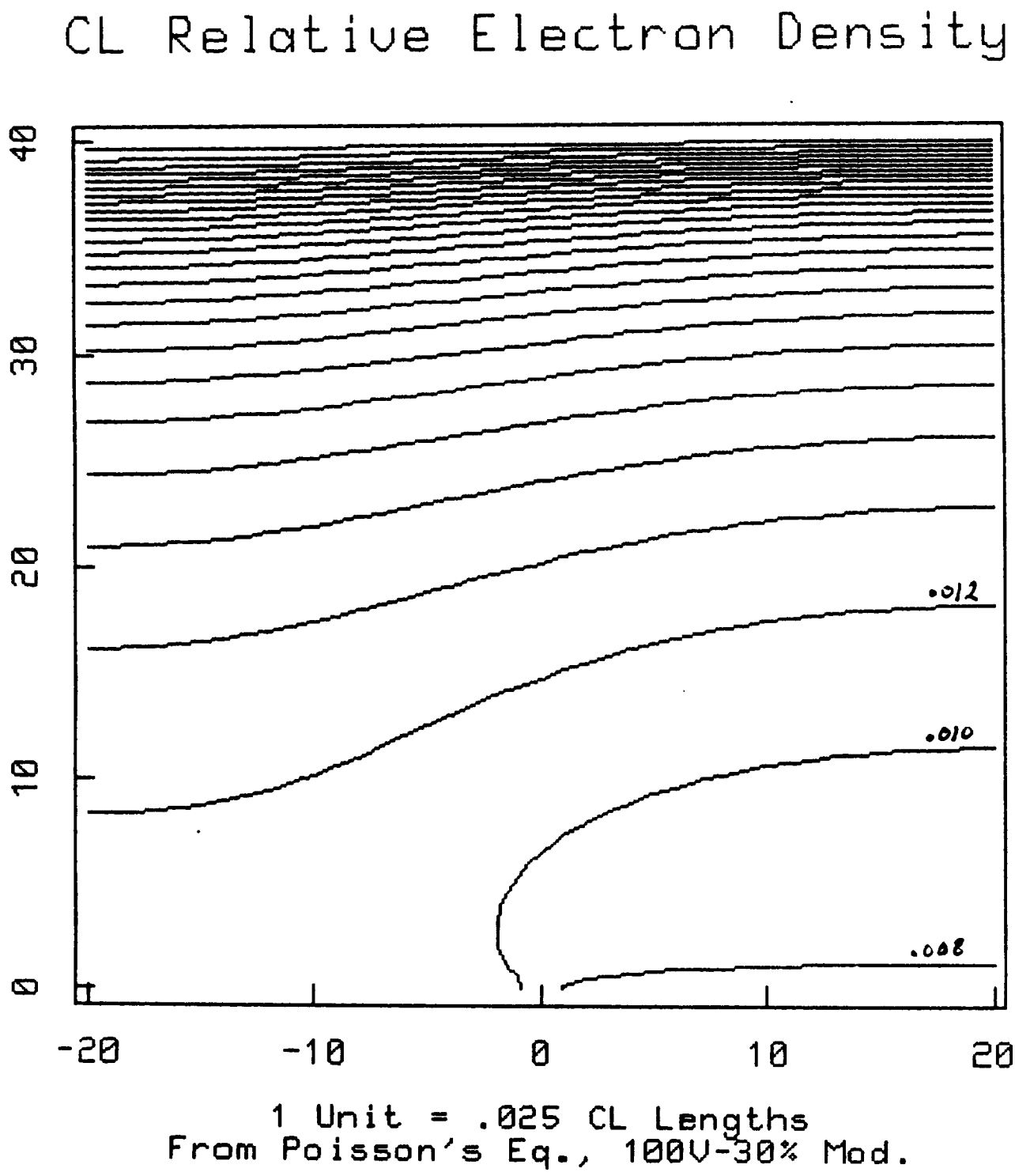
CL Relative Electron Density
40
30
20
10
0
.012
.010
.008
-20
-10
0
10
20
1 Unit = .025 CL Lengths
From Poisson's Eq., 100V-30% Mod.

Fig.21

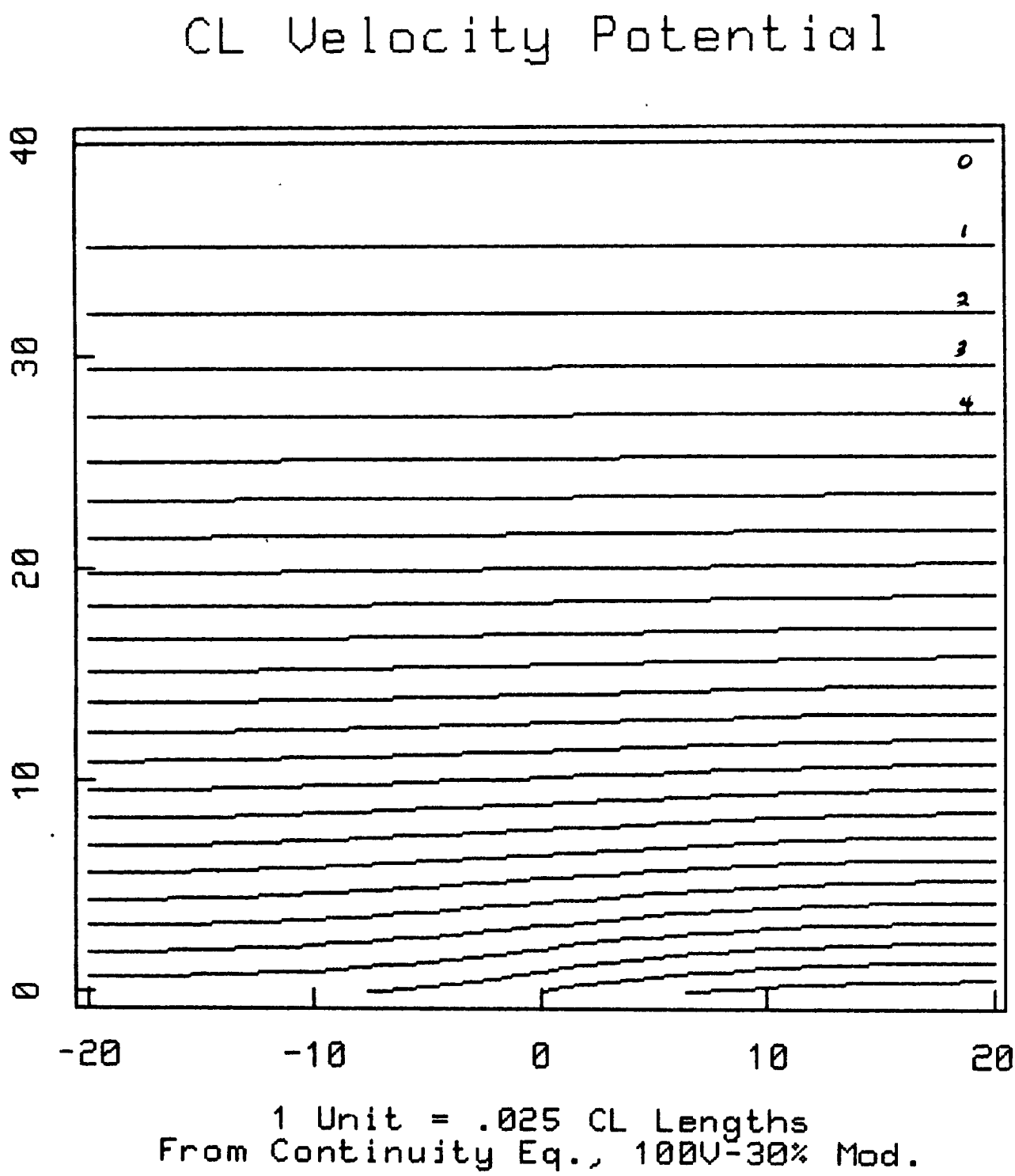
CL Velocity Potential
40
30
20
10
0
0
1
2
3
4
-20
-10
0
10
20
1 Unit = .025 CL Lengths
From Continuity Eq., 100V-30% Mod.

Fig.22

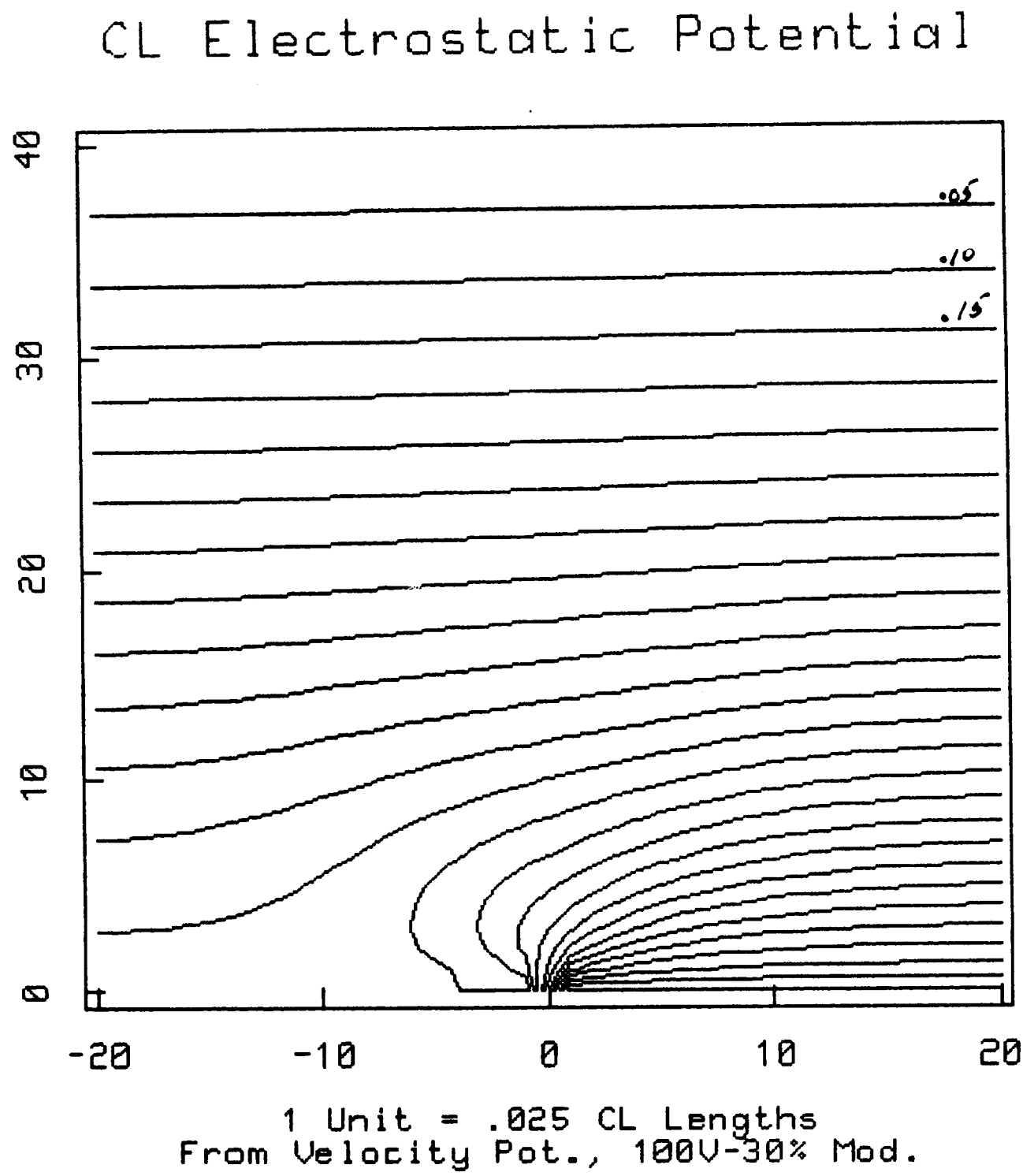
CL Electrostatic Potential
40
30
20
10
0
.05
.10
.15
-20
-10
0
10
20
1 Unit = .025 CL Lengths
From Velocity Pot., 100V-30% Mod.

Fig.23

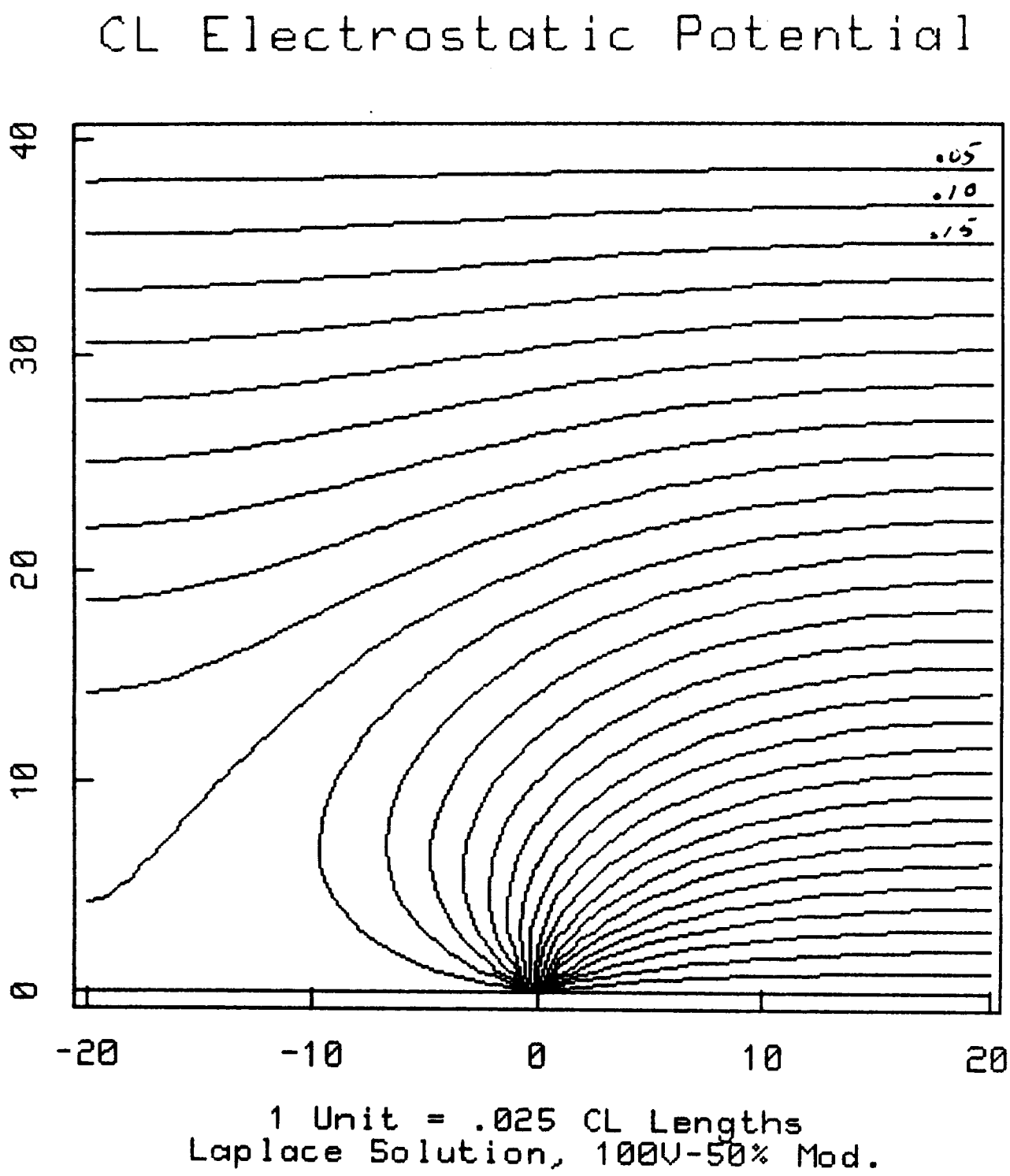
CL Electrostatic Potential
.05
.10
.15
40
30
20
10
0
-20
-10
0
10
20
1 Unit = .025 CL Lengths
Laplace Solution, 100V-50% Mod.

Fig.24

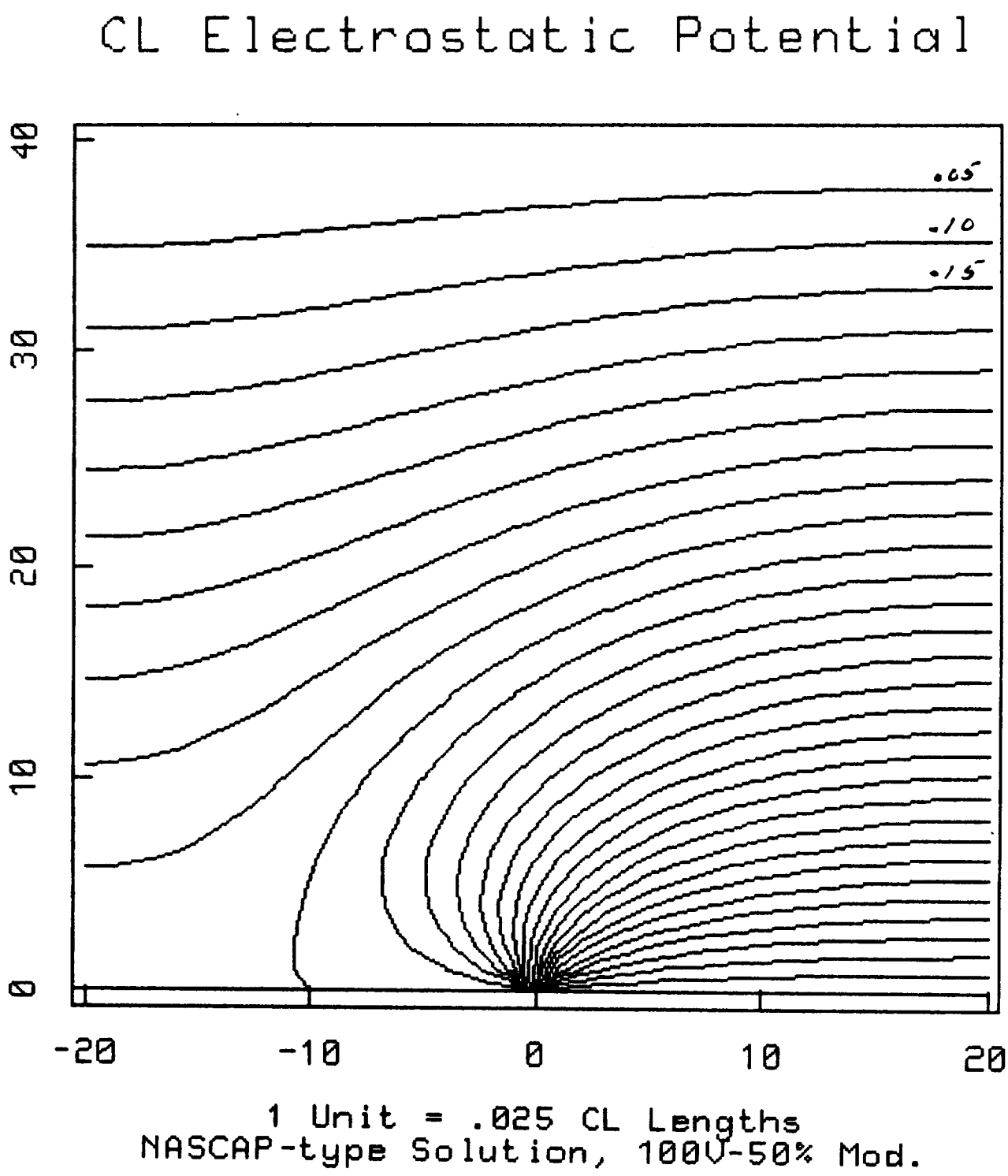
CL Electrostatic Potential
40
30
20
10
0
.05
.10
.15
-20
-10
0
10
20
1 Unit = .025 CL Lengths
NASCAP-type Solution, 100V-50% Mod.

Fig.25

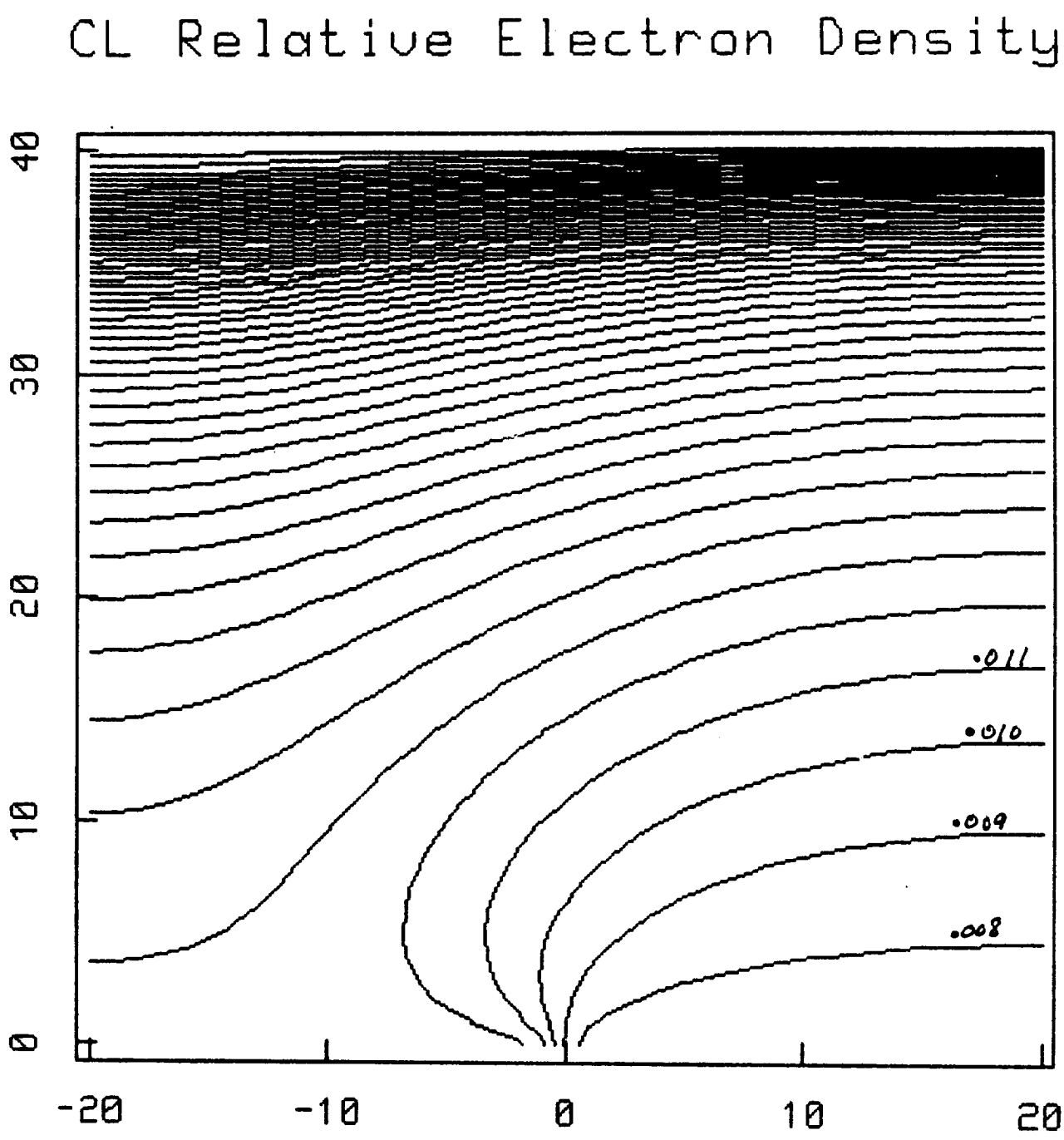
CL Relative Electron Density
40
30
20
10
0
.011
.010
.009
.008
-20
-10
0
10
20
1 Unit = .025 CL Lengths
From Poisson's Eq., 100V-50% Mod.

Fig.26

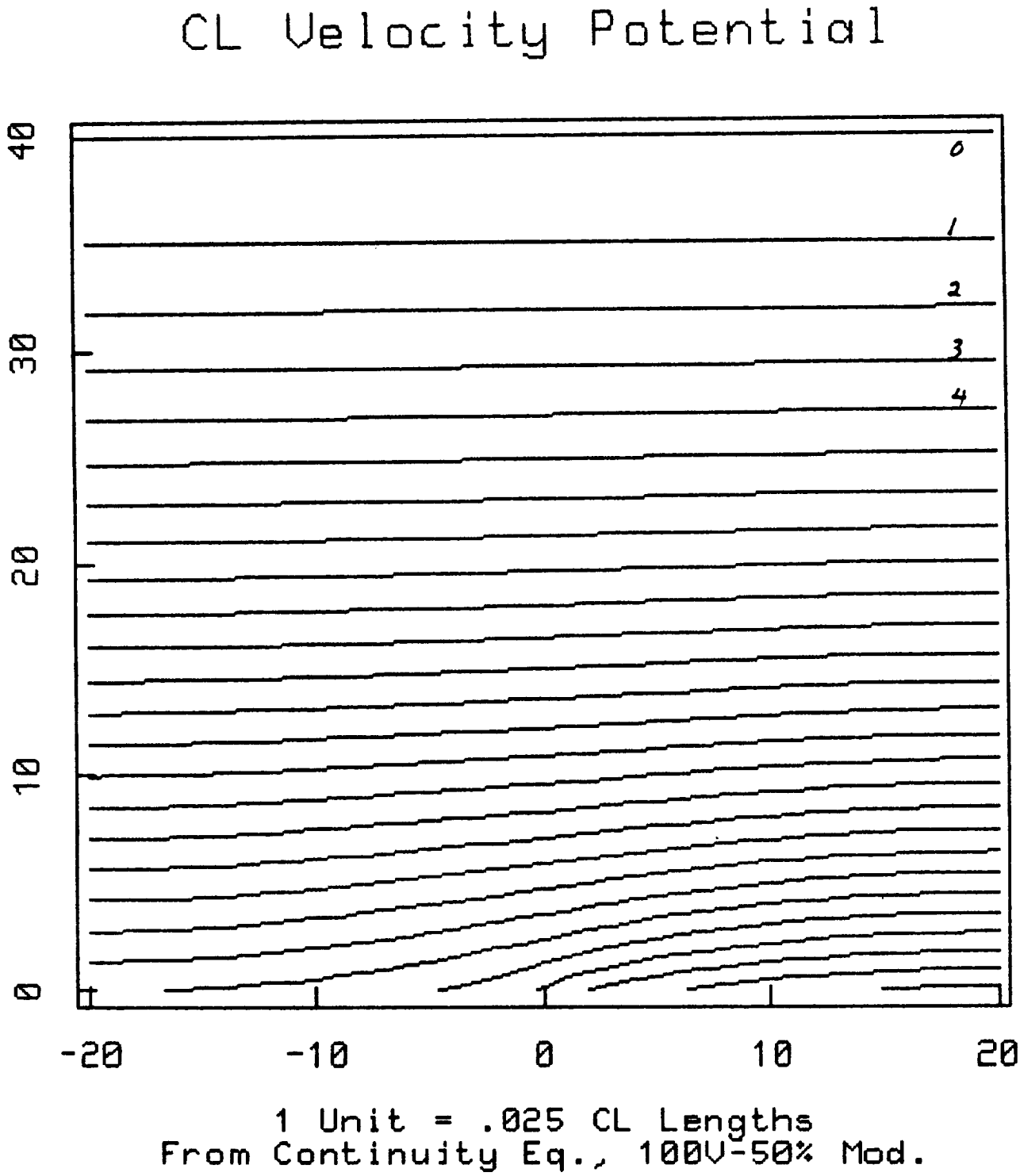
CL Velocity Potential
40
30
20
10
0
0
1
2
3
4
-20
-10
0
10
20
1 Unit = .025 CL Lengths
From Continuity Eq., 100V-50% Mod.

Fig.27

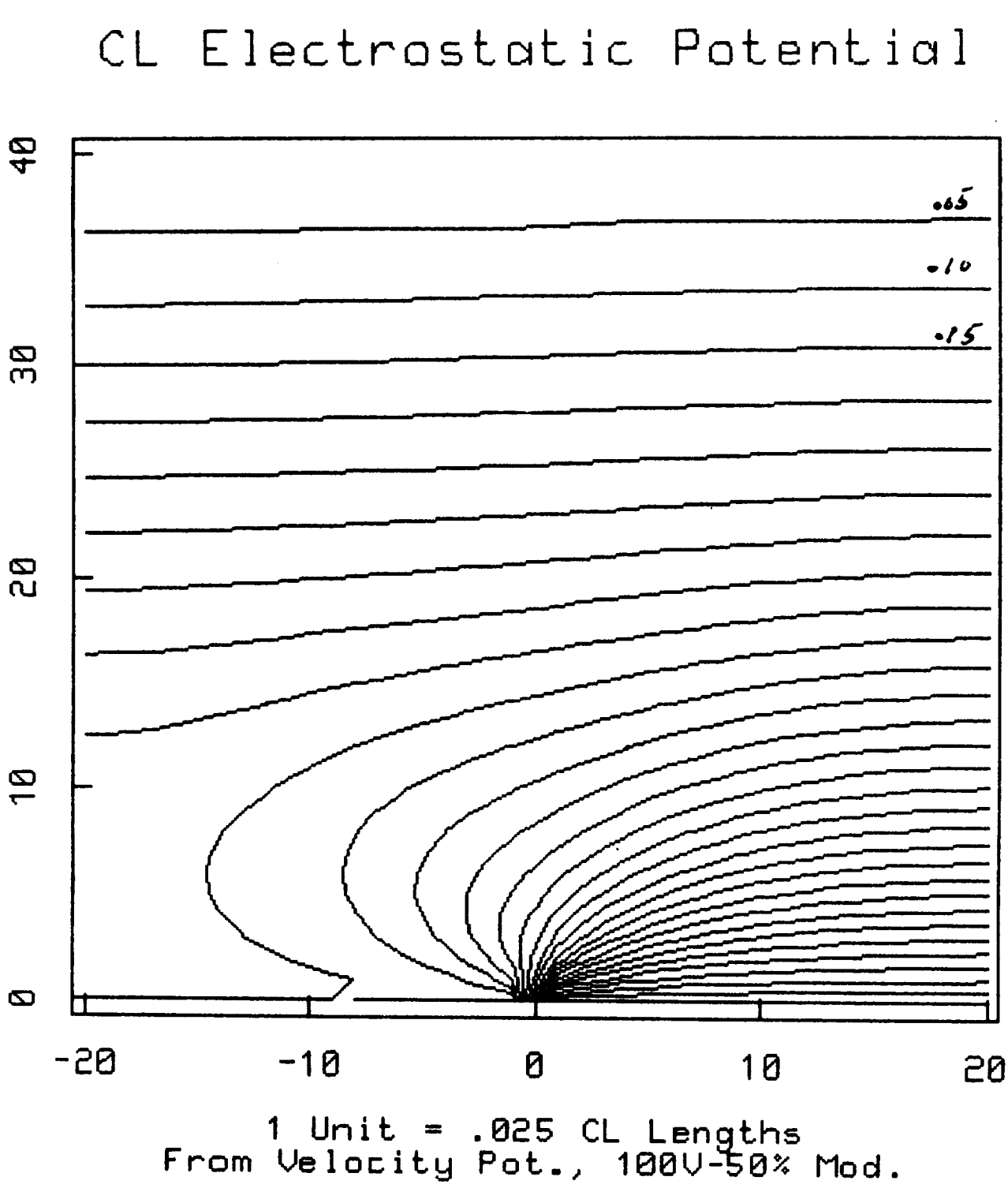
CL Electrostatic Potential
40
30
20
10
0
.05
.10
.15
-20
-10
0
10
20
1 Unit = .025 CL Lengths
From Velocity Pot., 100V-50% Mod.

Fig.28

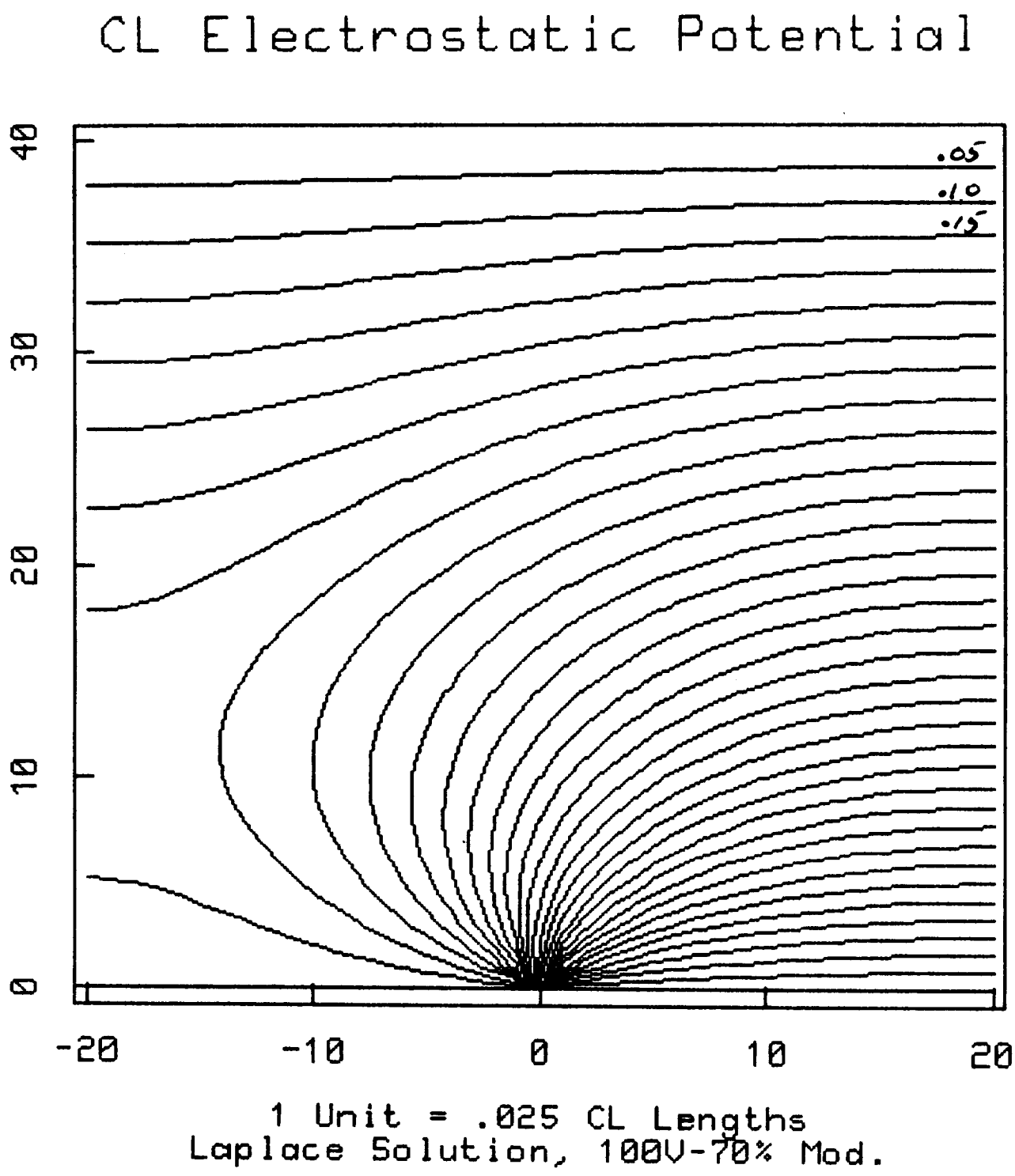
CL Electrostatic Potential
40
30
20
10
0
.05
.10
.15
-20
-10
0
10
20
1 Unit = .025 CL Lengths
Laplace Solution, 100V-70% Mod.

Fig.29

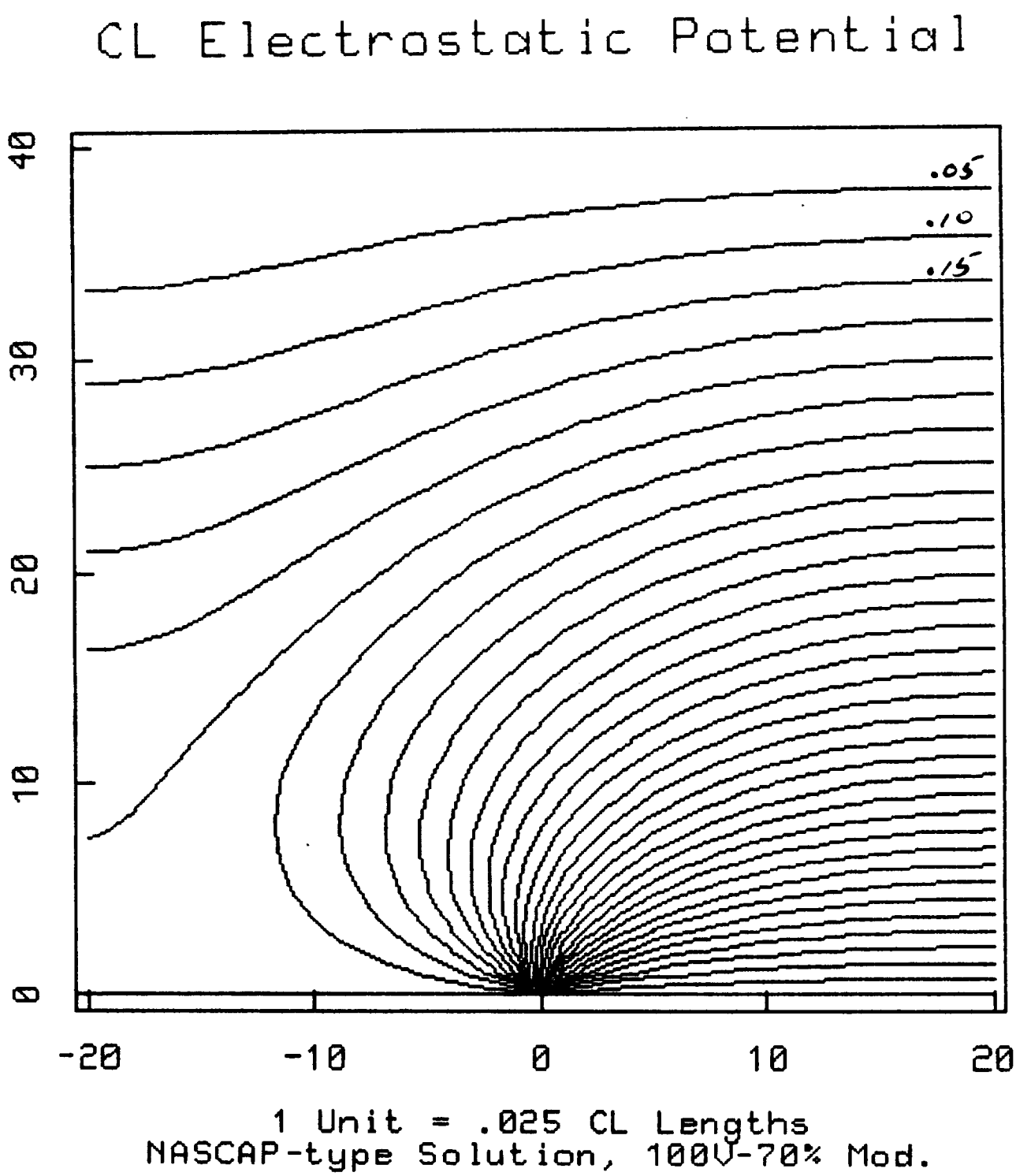
CL Electrostatic Potential
40
30
20
10
0
.05
.10
.15
-20
-10
0
10
20
1 Unit = .025 CL Lengths
NASCAP-type Solution, 100V-70% Mod.

Fig.30

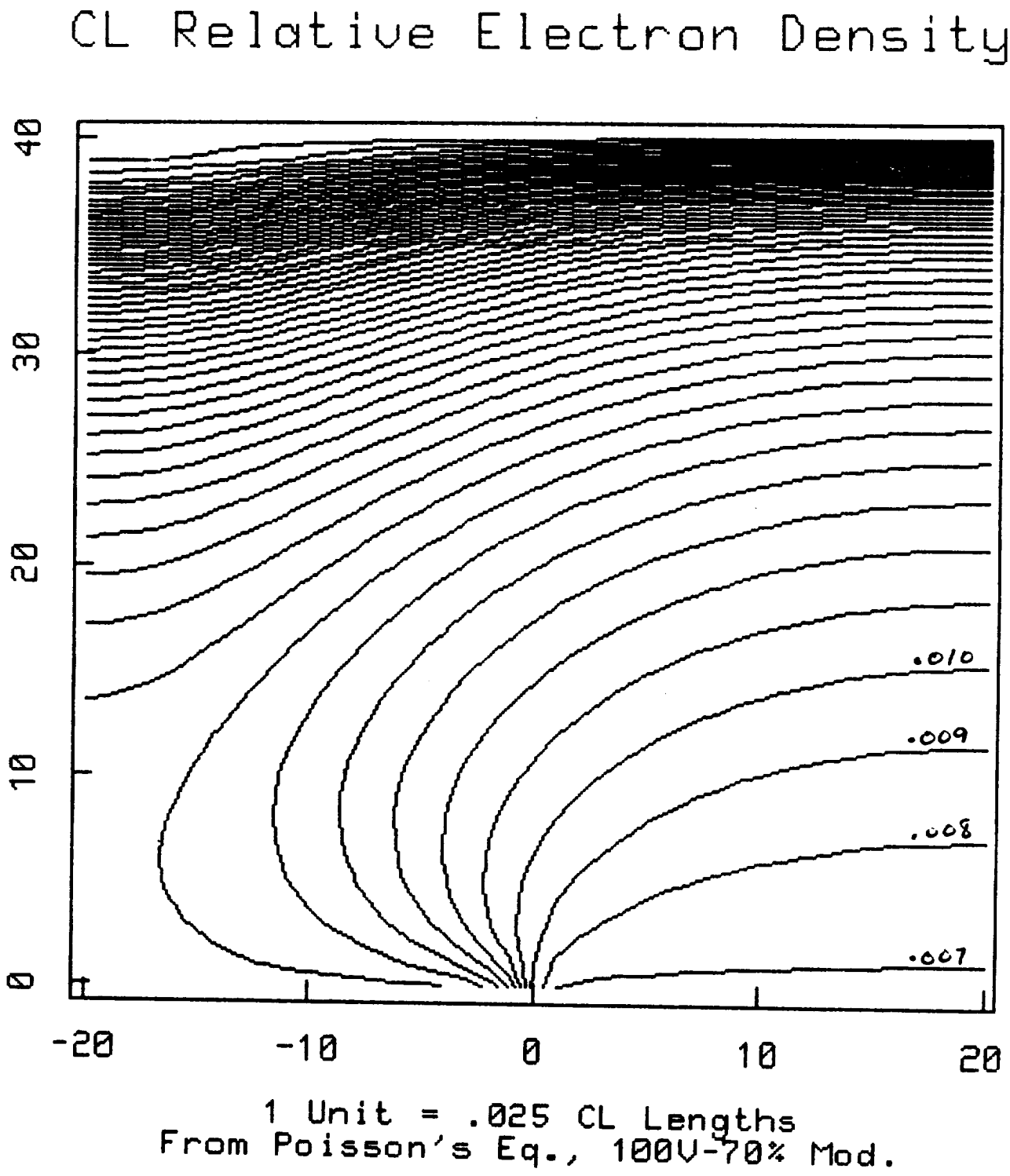
CL Relative Electron Density
40
30
20
10
0
-20
-10
0
10
20
.010
.009
.008
.007
1 Unit = .025 CL Lengths
From Poisson's Eq., 100V-70% Mod.

Fig.31

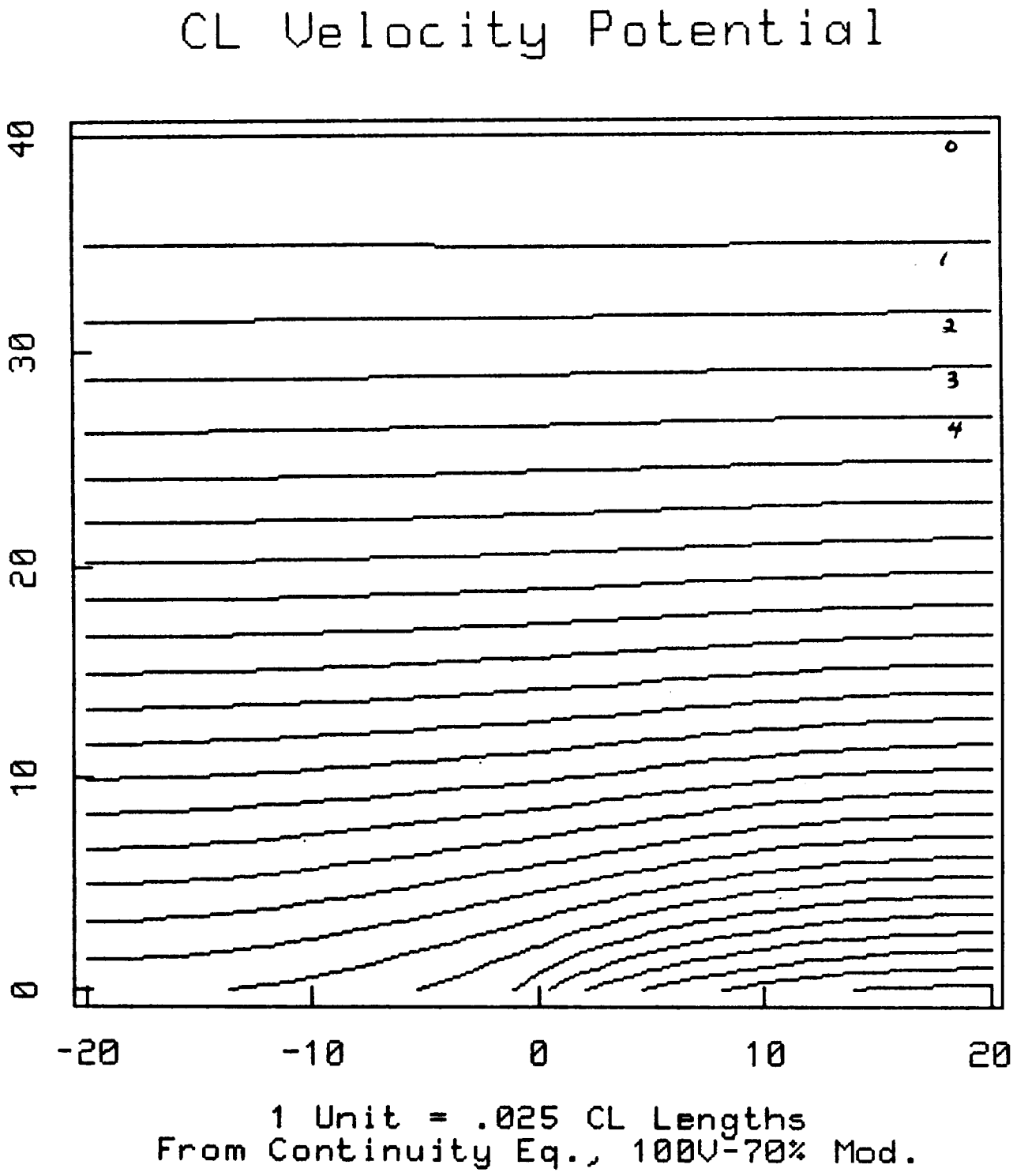
CL Velocity Potential
40
30
20
10
0
0
1
2
3
4
-20
-10
0
10
20
1 Unit = .025 CL Lengths
From Continuity Eq., 100V-70% Mod.

Fig.32

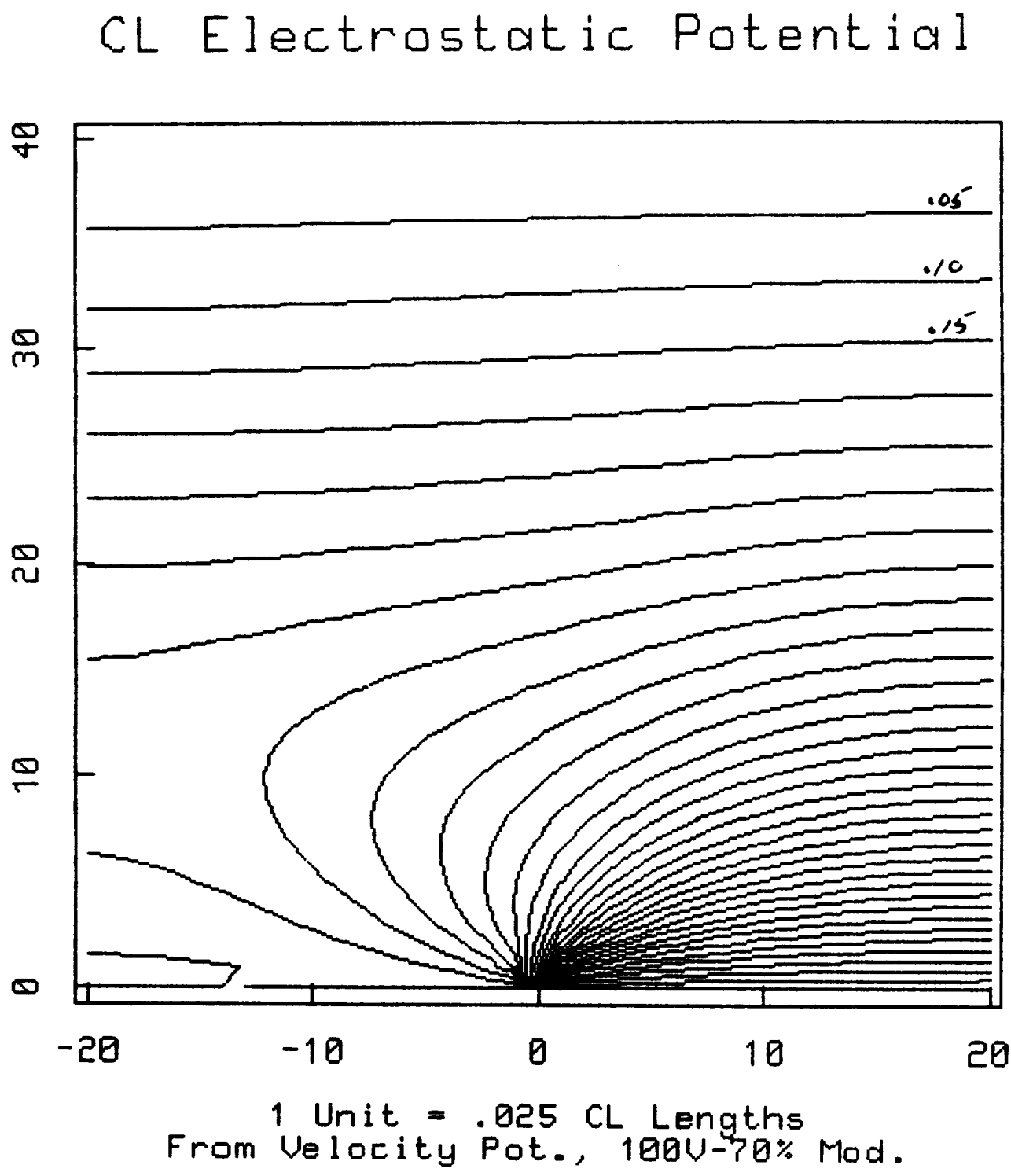
CL Electrostatic Potential
40
30
20
10
0
.05
.10
.15
-20
-10
0
10
20
1 Unit = .025 CL Lengths
From Velocity Pot., 100V-70% Mod.

Fig.33

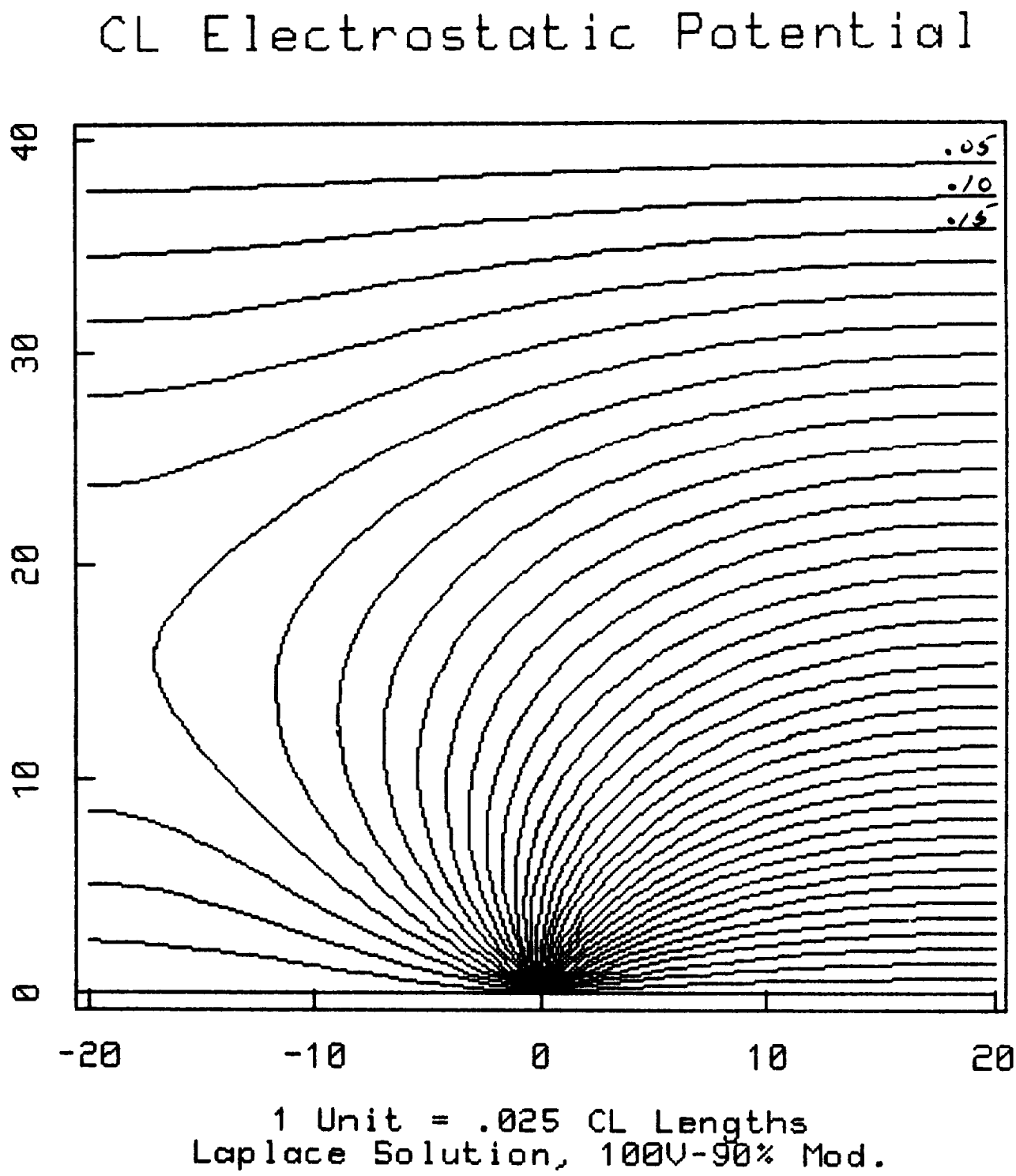
CL Electrostatic Potential
.05
.10
.15
40
30
20
10
0
-20
-10
0
10
20
1 Unit = .025 CL Lengths
Laplace Solution, 100V-90% Mod.

Fig.34

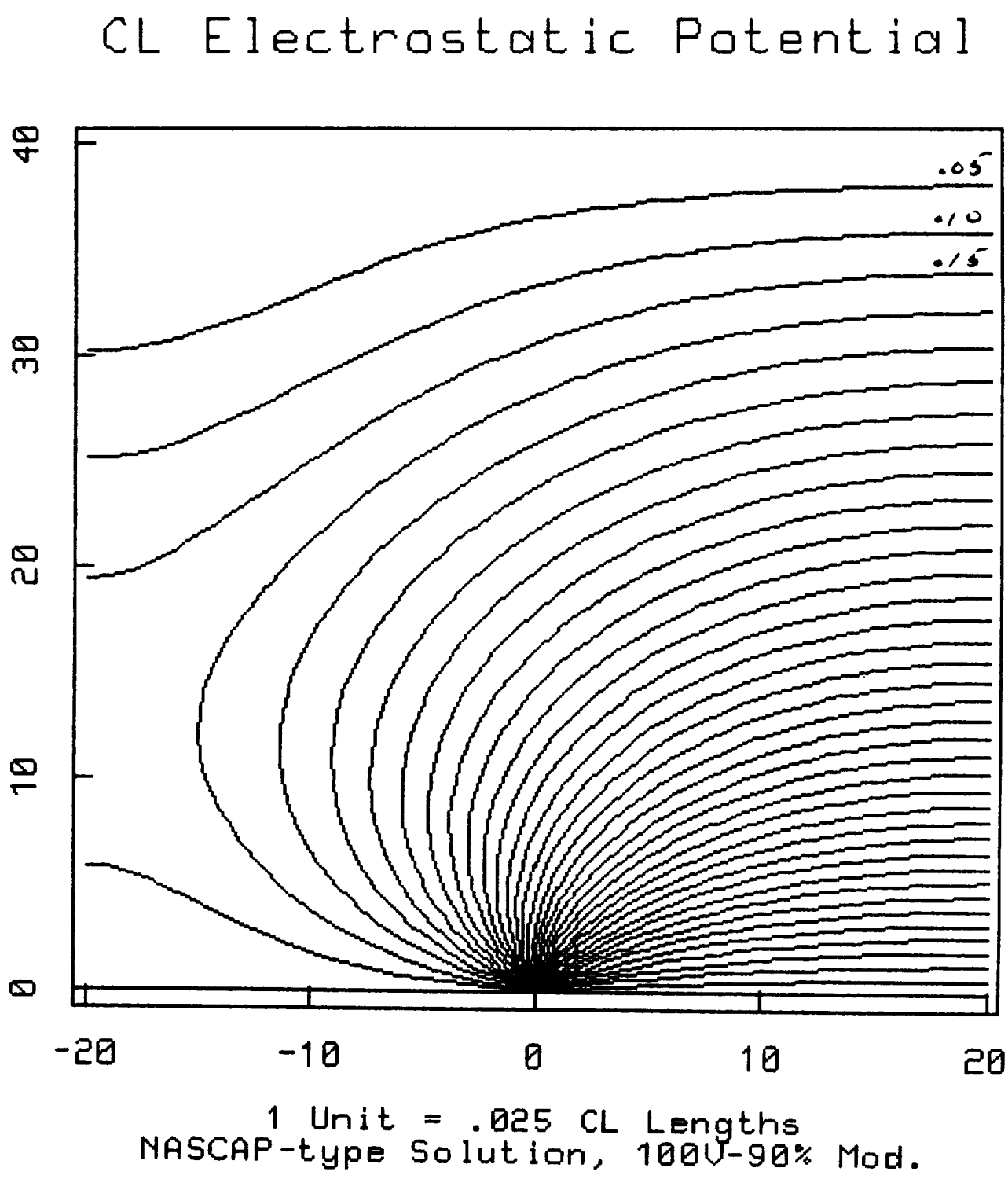
CL Electrostatic Potential
40
30
20
10
0
.05
.10
.15
-20
-10
0
10
20
1 Unit = .025 CL Lengths
NASCAP-type Solution, 100V-90% Mod.

Fig.35

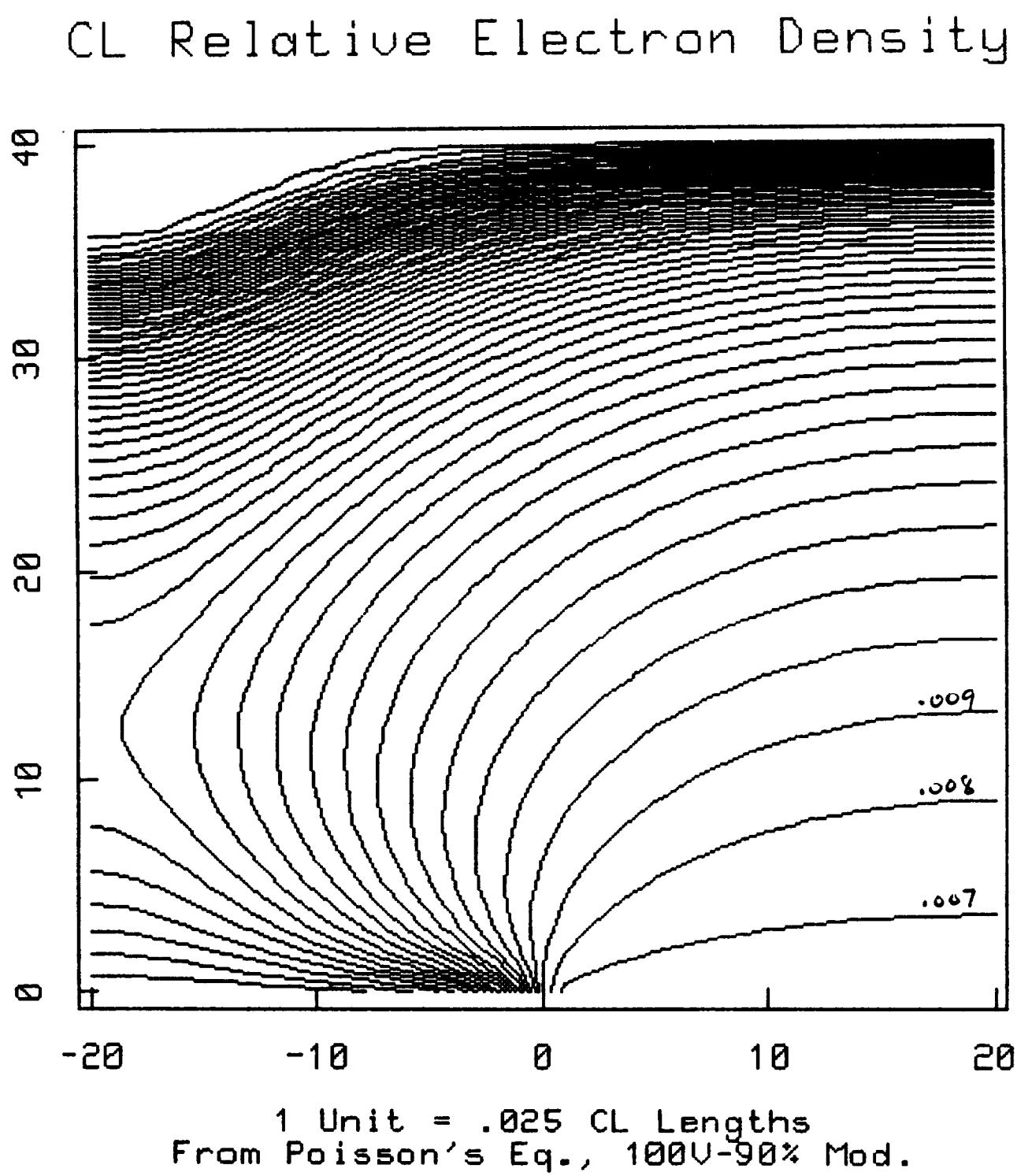
CL Relative Electron Density
40
30
20
10
0
-20
-10
0
10
20
.009
.008
.007
1 Unit = .025 CL Lengths
From Poisson's Eq., 100V-90% Mod.

Fig.36

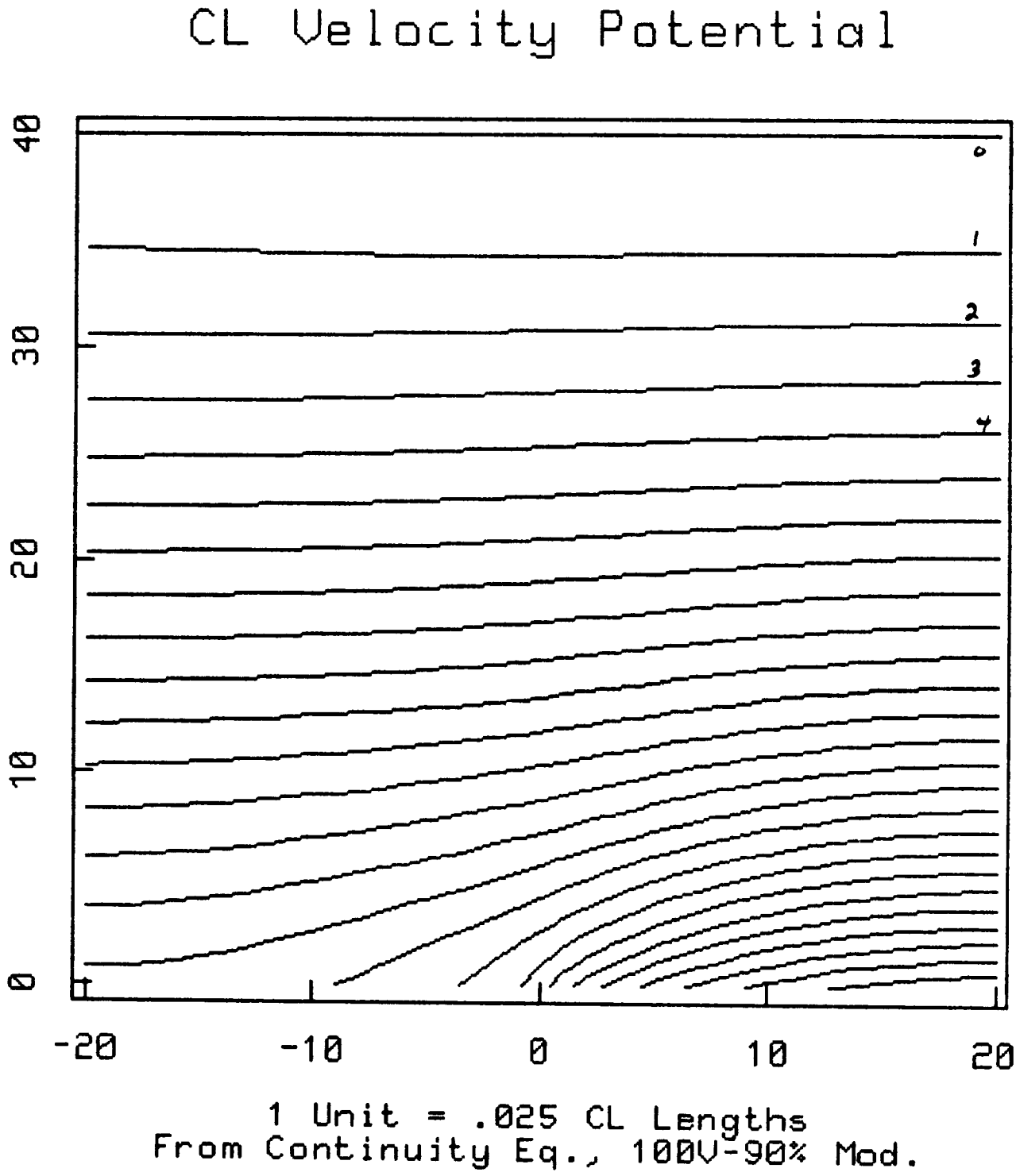
CL Velocity Potential
40
30
20
10
0
-20
-10
0
10
20
0
1
2
3
4
1 Unit = .025 CL Lengths
From Continuity Eq., 100V-90% Mod.

Fig.37

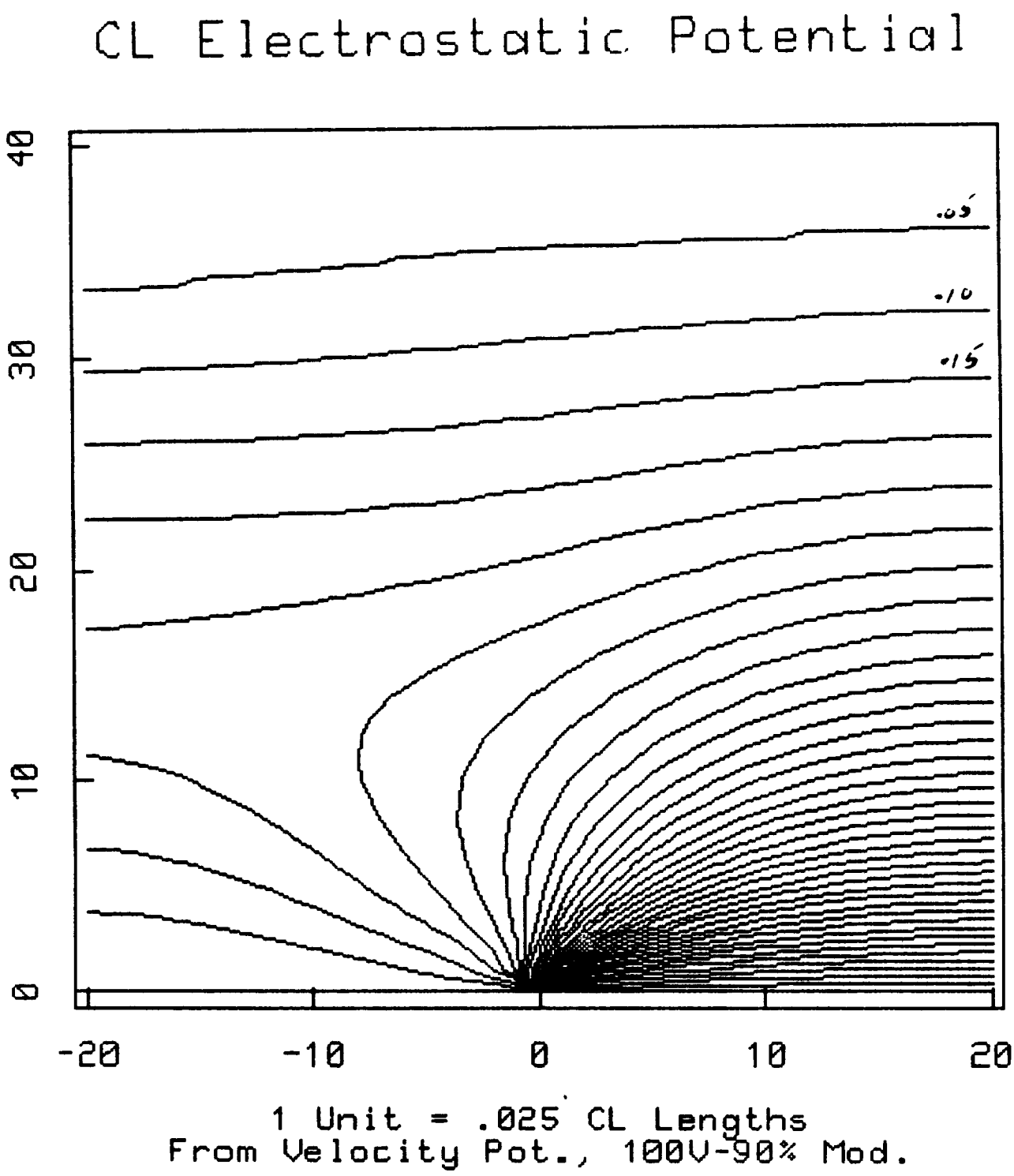
CL Electrostatic Potential
40
30
20
10
0
.05
.10
.15
-20
-10
0
10
20
1 Unit = .025 CL Lengths
From Velocity Pot., 100V-90% Mod.

Fig.38

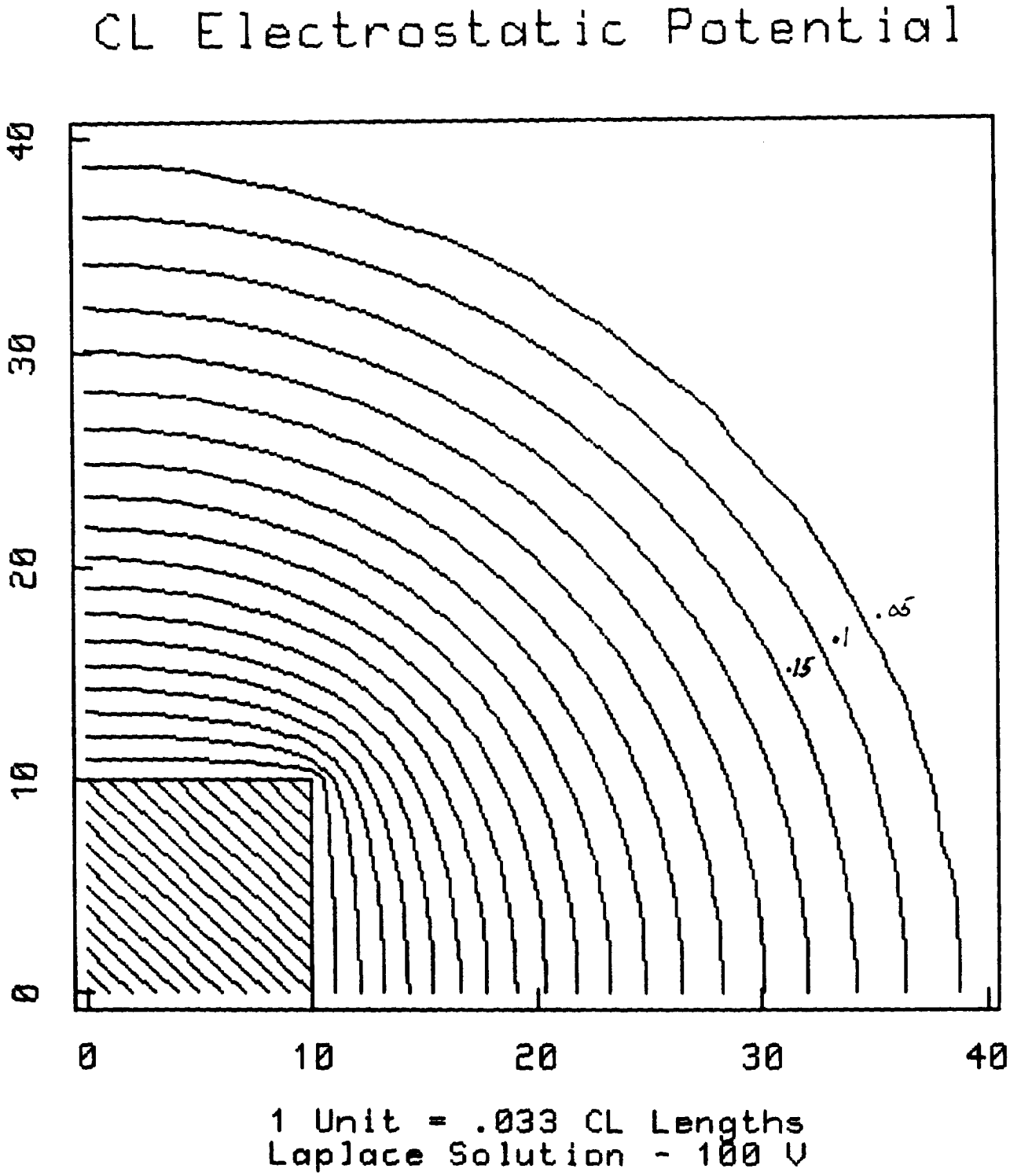
CL Electrostatic Potential
40
30
20
10
0
0
10
20
30
40
.85
.1
.15
1 Unit = .033 CL Lengths
Laplace Solution - 100 V

Fig.39

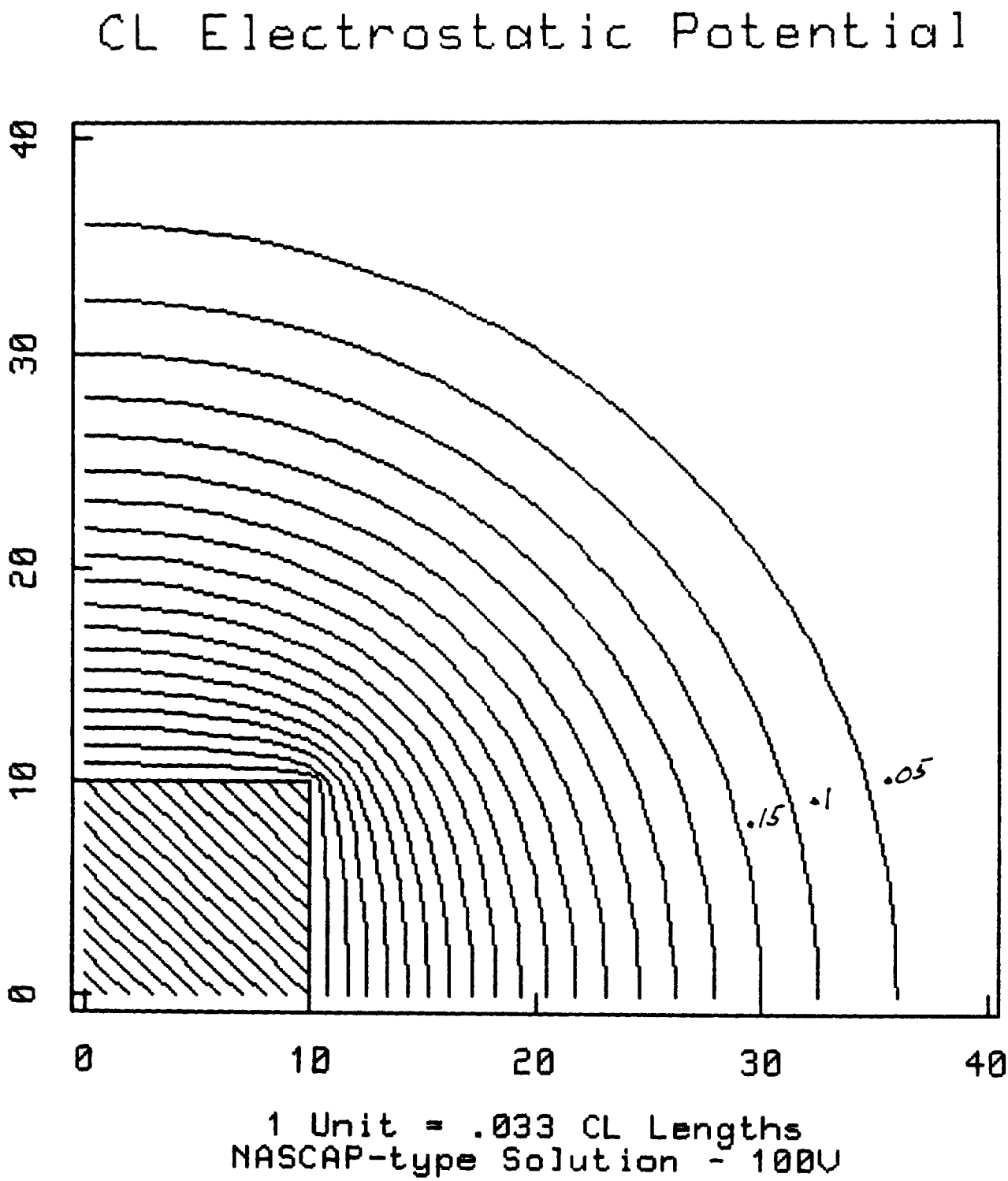
CL Electrostatic Potential
40
30
20
10
0
0
10
20
30
40
.05
.1
.15
1 Unit = .033 CL Lengths
NASCAP-type Solution - 100V

Fig.40

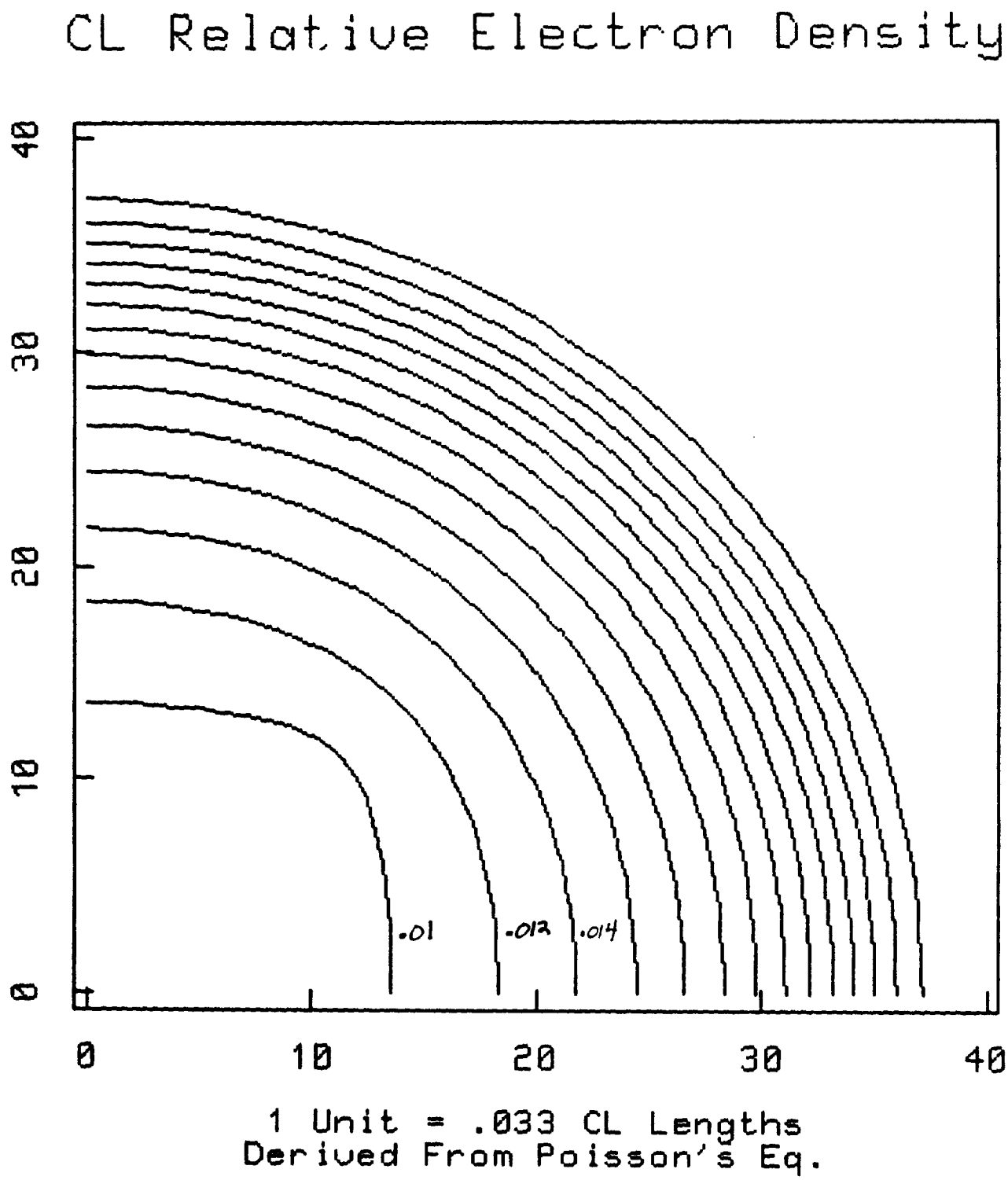
CL Relative Electron Density
40
30
20
10
0
0
10
20
30
40
.01
.012
.014
1 Unit = .033 CL Lengths
Derived From Poisson's Eq.

Fig.41

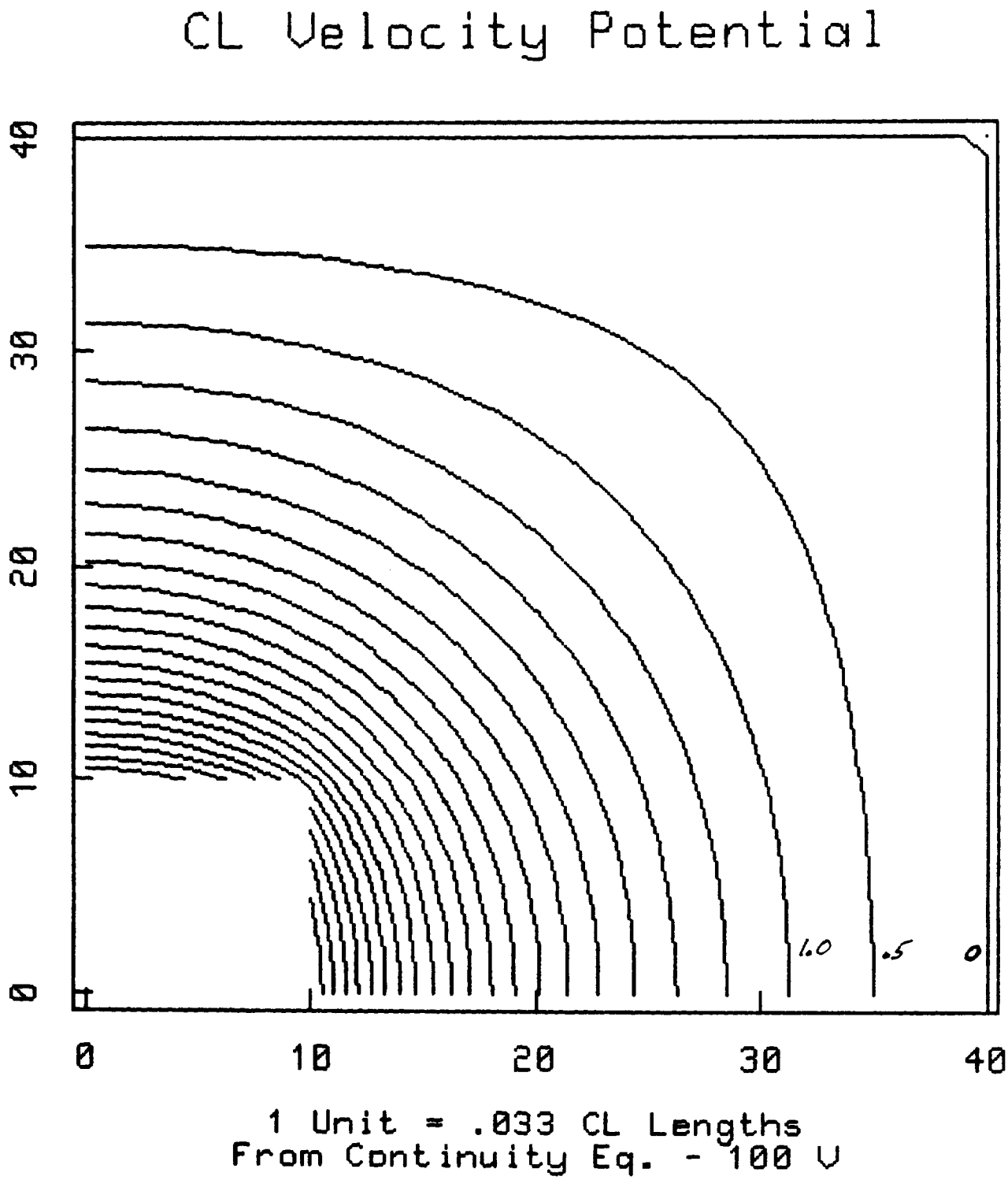
CL Velocity Potential
40
30
20
10
0
1.0
.5
0
0
10
20
30
40
1 Unit = .033 CL Lengths
From Continuity Eq. - 100 V

Fig.42

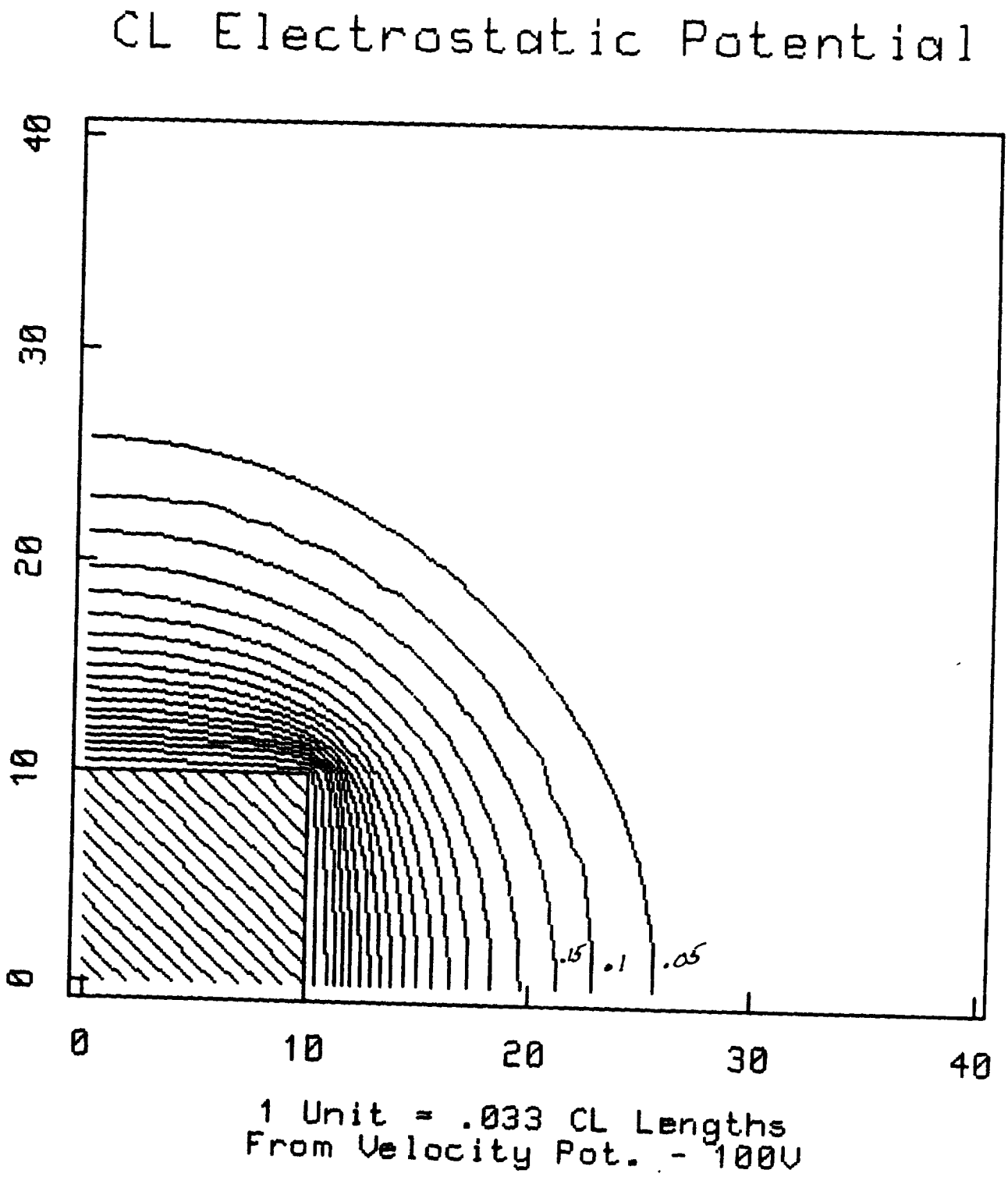
CL Electrostatic Potential
40
30
20
10
0
0
10
20
30
40
.15
.1
.05
1 Unit = .033 CL Lengths
From Velocity Pot. - 100V

Fig.43

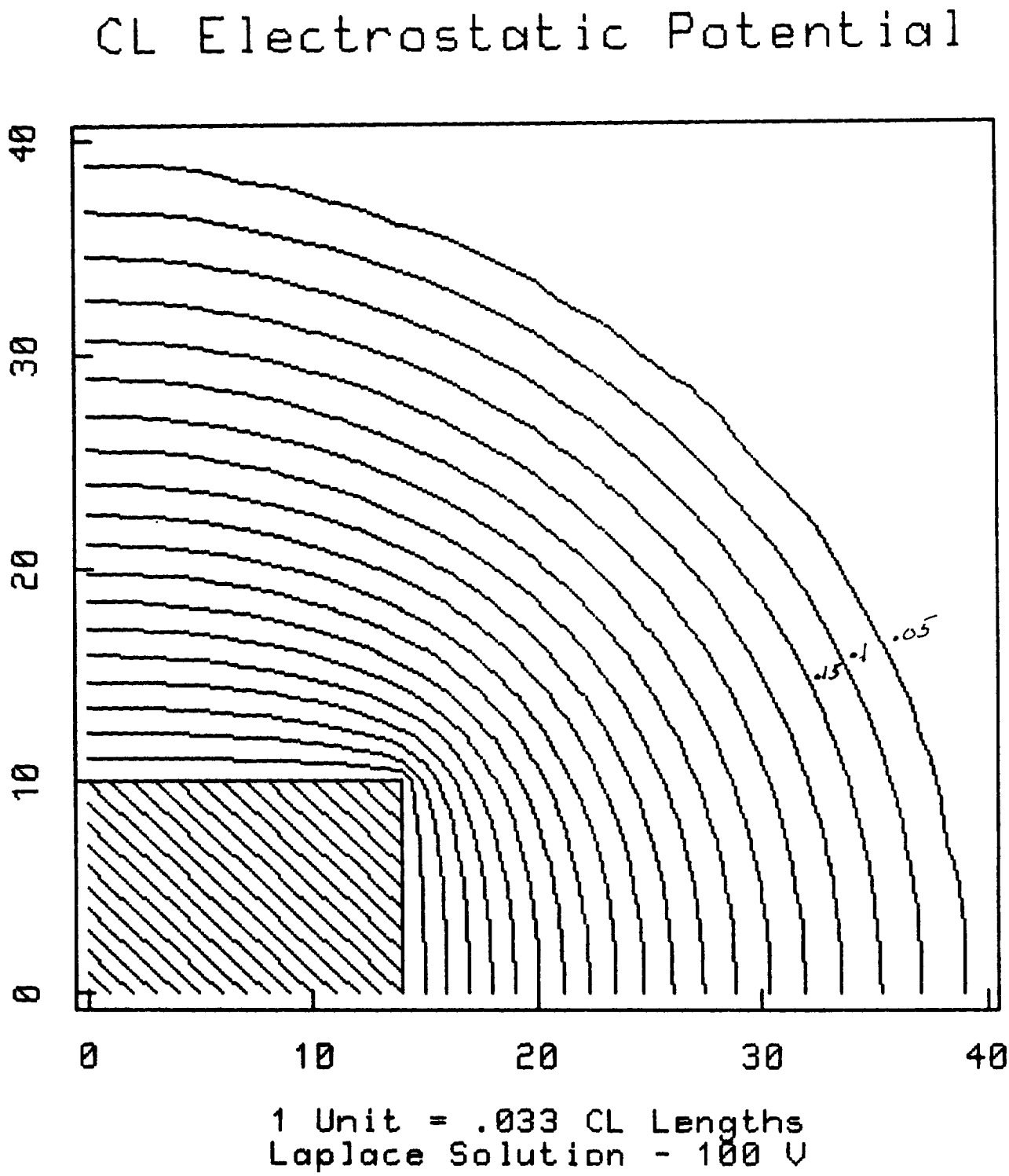
CL Electrostatic Potential
40
30
20
10
0
0
10
20
30
40
.05
.1
.15
1 Unit = .033 CL Lengths
Laplace Solution - 100 V

Fig.44

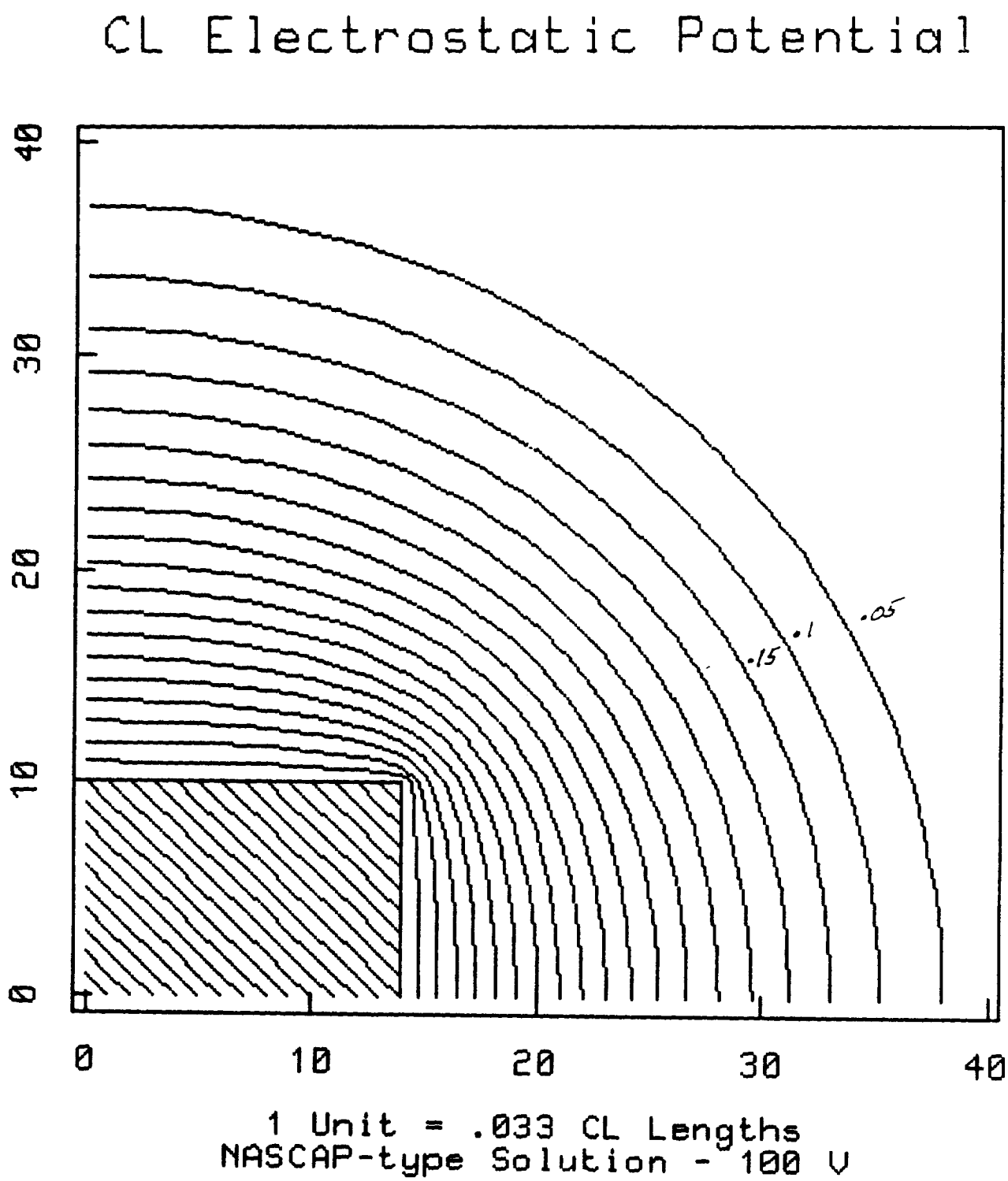
CL Electrostatic Potential
40
30
20
10
0
0
10
20
30
40
.05
.1
.15
1 Unit = .033 CL Lengths
NASCAP-type Solution - 100 V

Fig.45

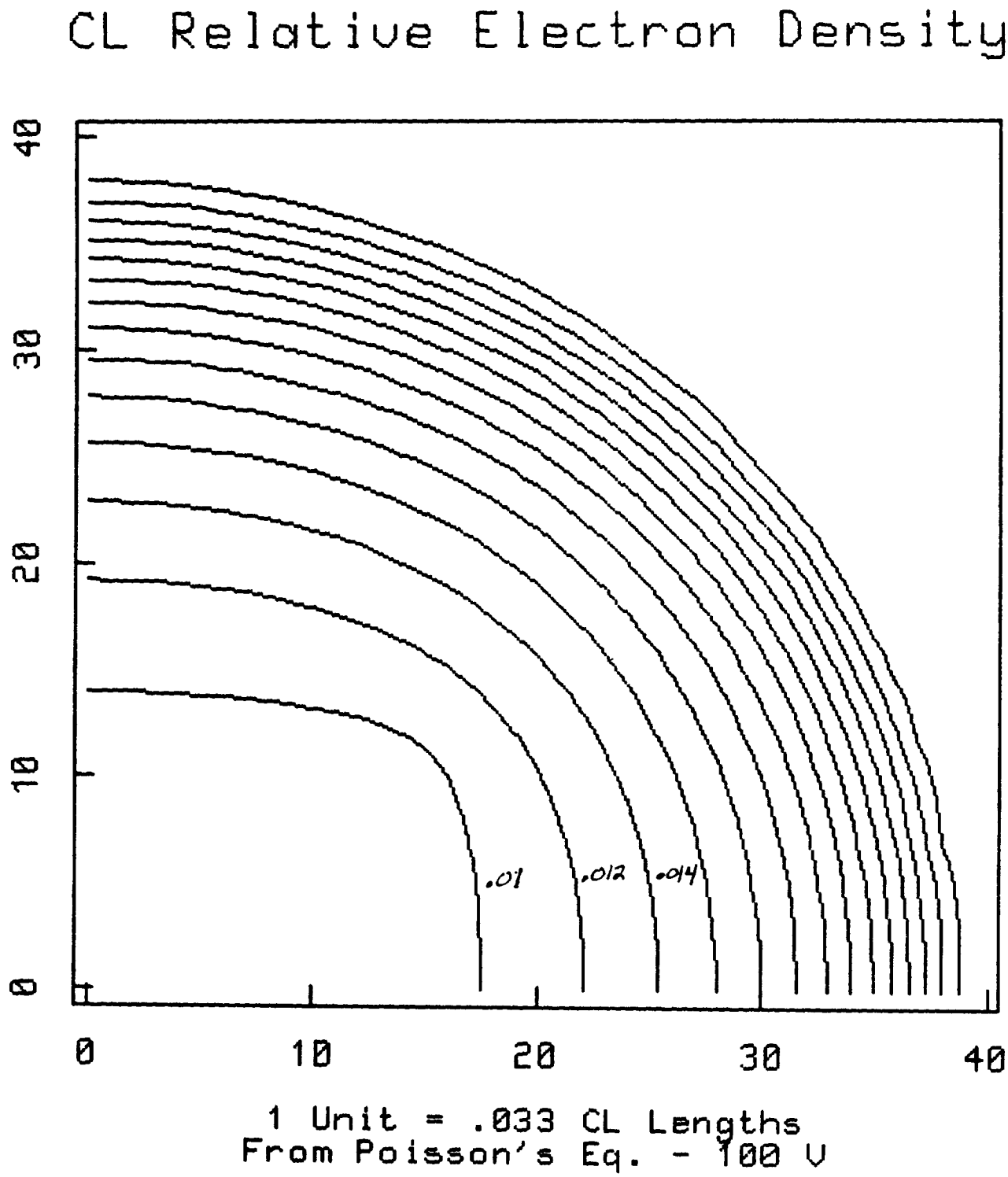
CL Relative Electron Density
40
30
20
10
0
0
10
20
30
40
.01
.012
.014
1 Unit = .033 CL Lengths
From Poisson's Eq. - 100 V

Fig.46

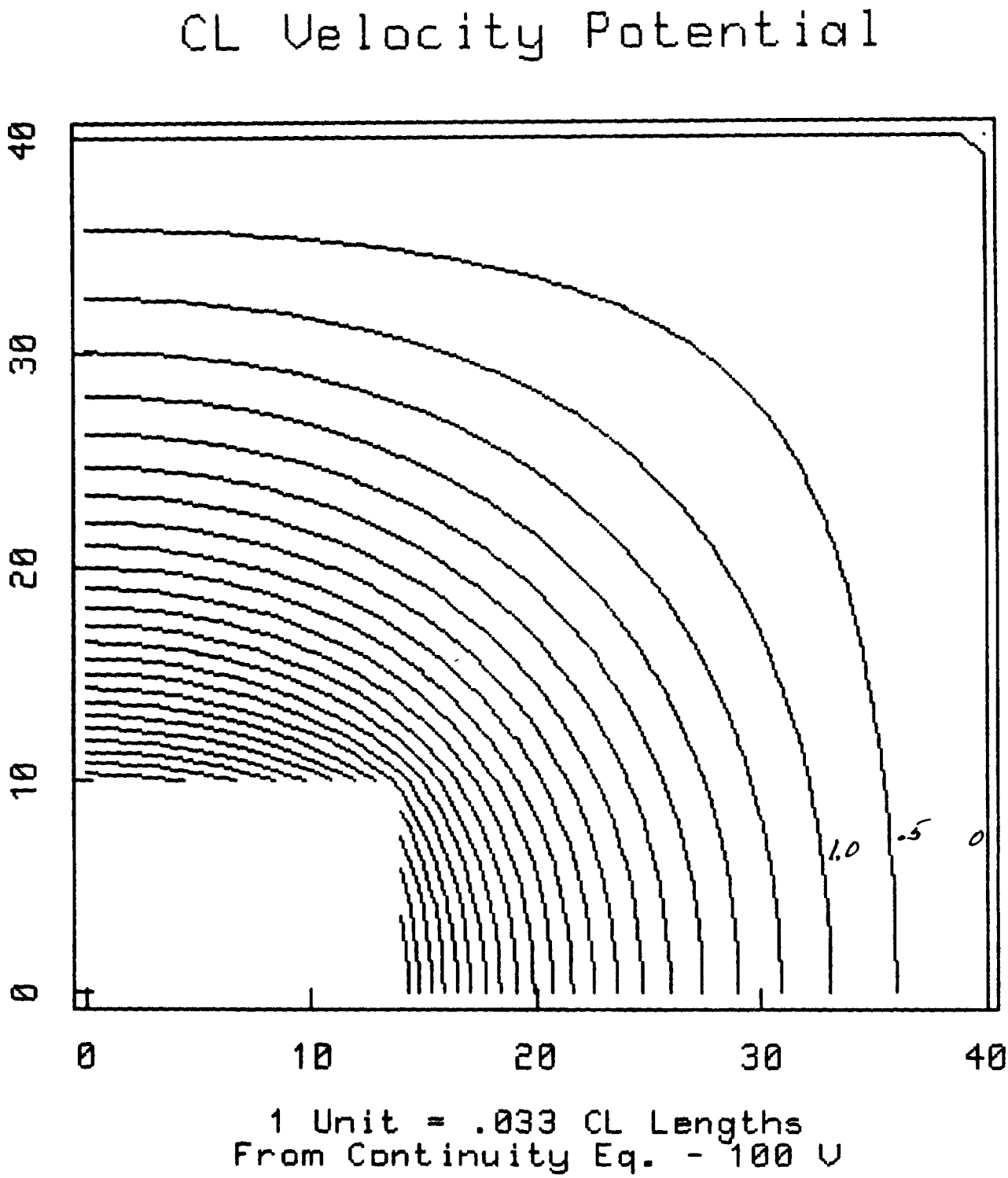
CL Velocity Potential
40
30
20
10
0
0
10
20
30
40
1.0
.5
0
1 Unit = .033 CL Lengths
From Continuity Eq. - 100 V

Fig.47

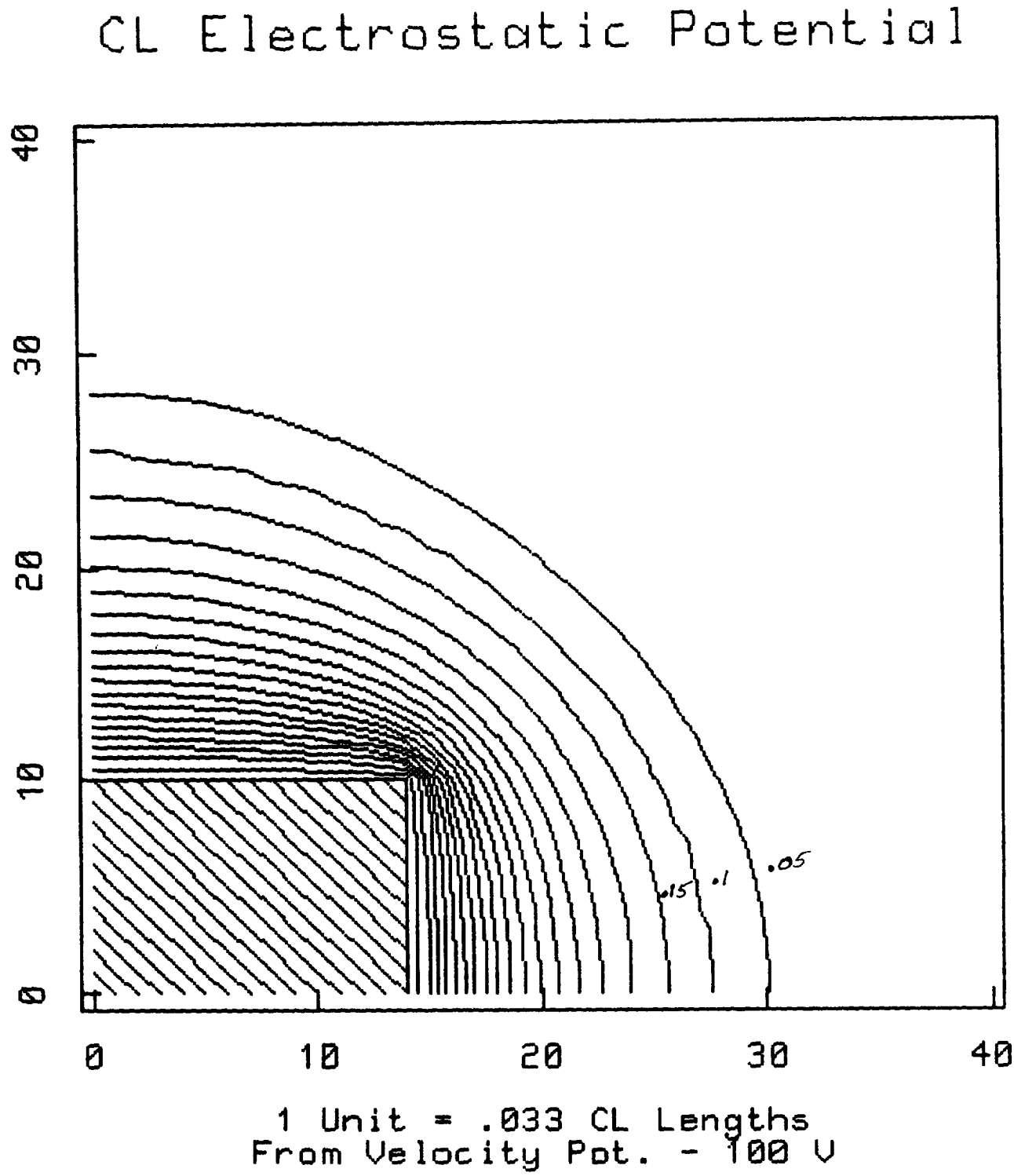
CL Electrostatic Potential
40
30
20
10
0
0
10
20
30
40
.05
.1
.15
1 Unit = .033 CL Lengths
From Velocity Pot. - 100 V

Fig.48

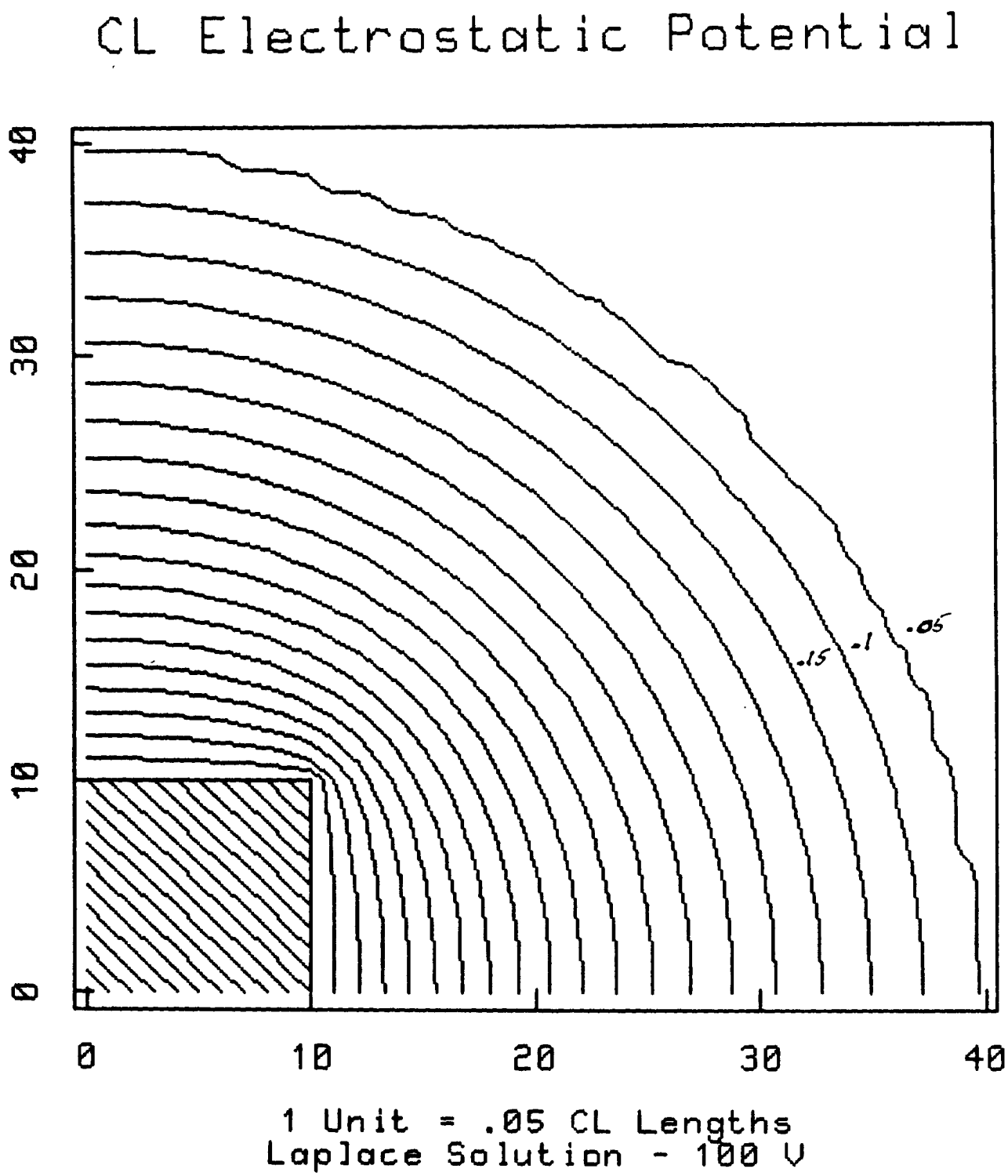
CL Electrostatic Potential
40
30
20
10
0
0
10
20
30
40
.05
.1
.15
1 Unit = .05 CL Lengths
Laplace Solution - 100 V

Fig.49

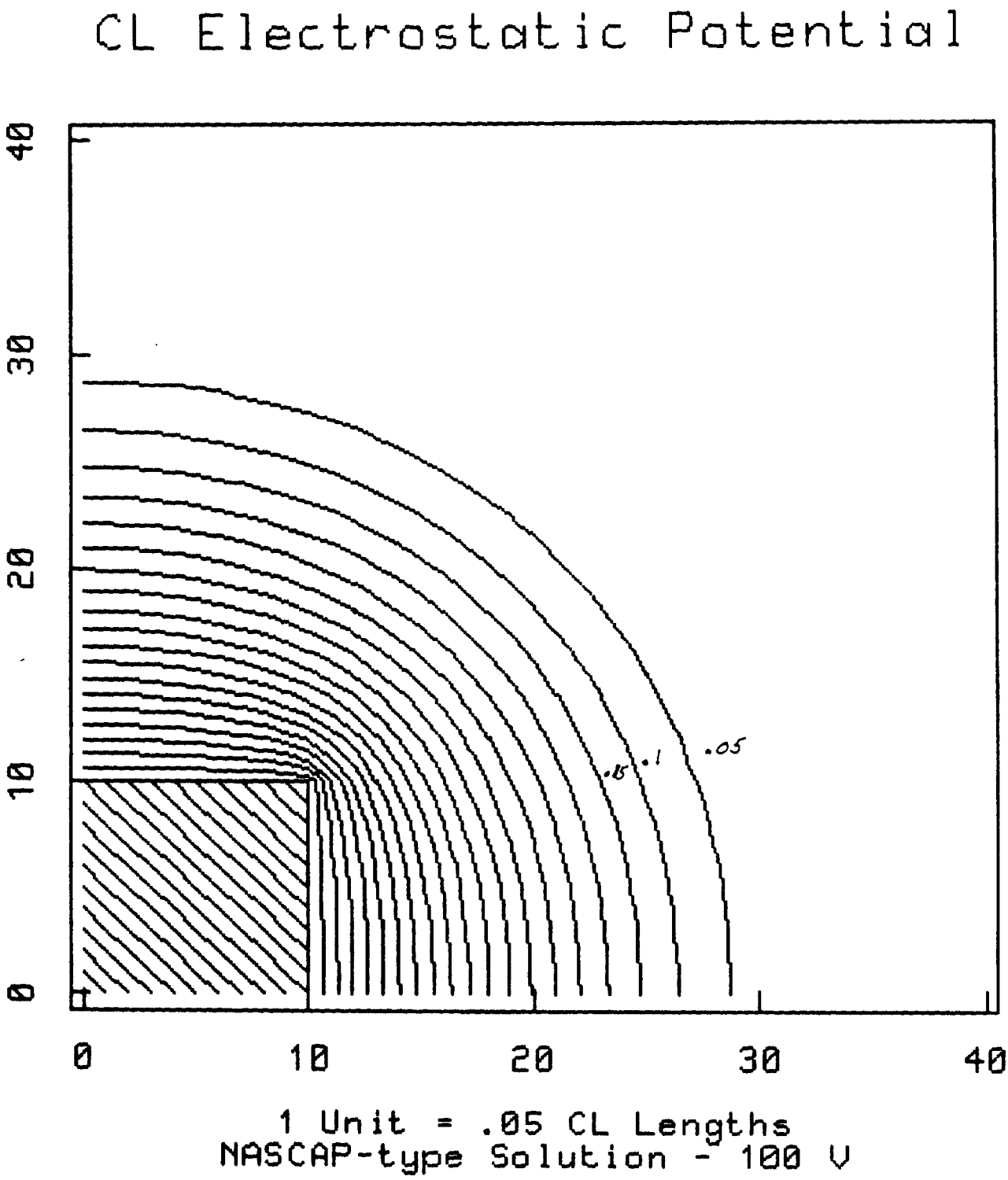
CL Electrostatic Potential
40
30
20
10
0
0
10
20
30
40
.05
.1
.15
1 Unit = .05 CL Lengths
NASCAP-type Solution - 100 V

Fig.50

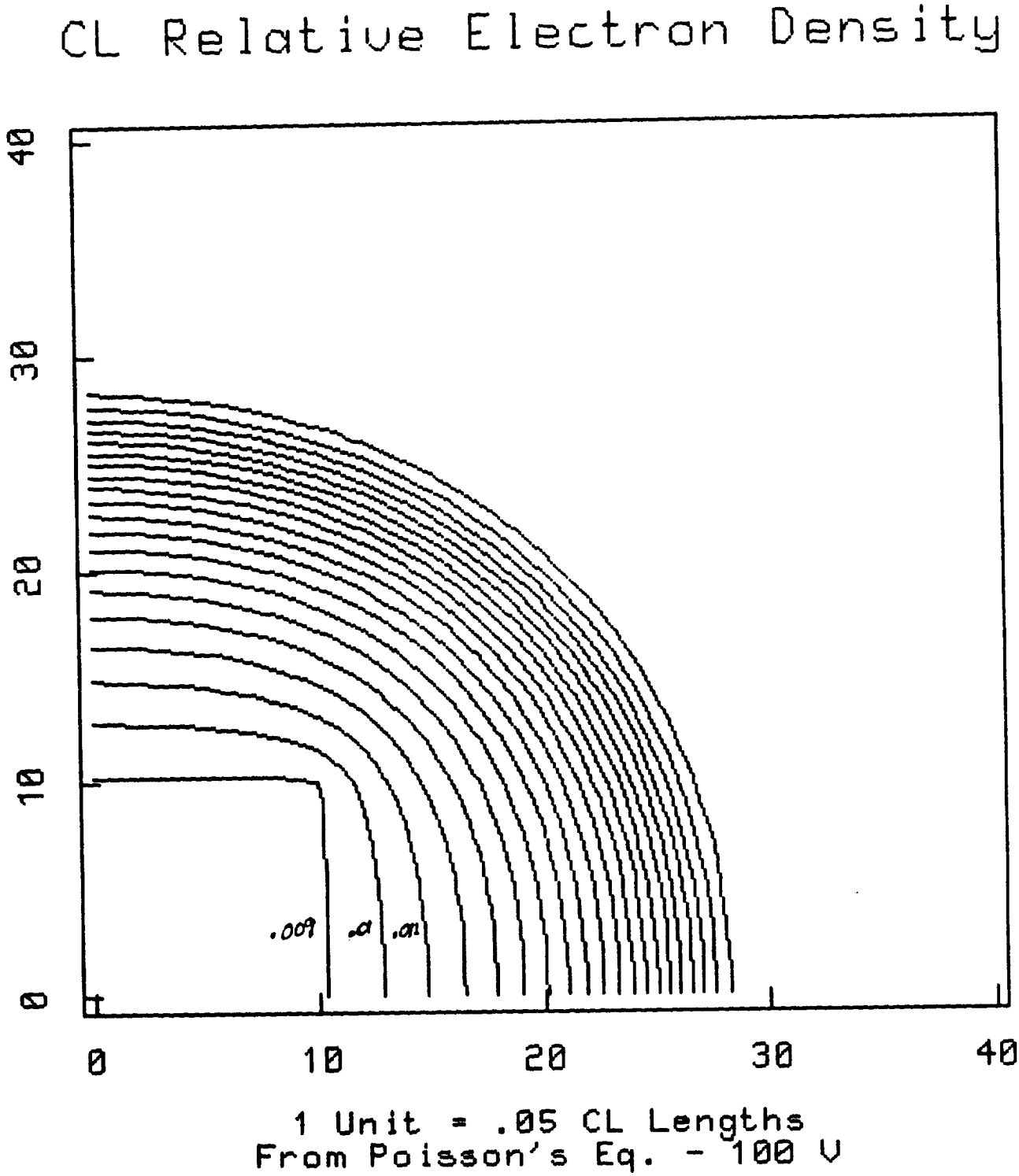
CL Relative Electron Density
40
30
20
10
0
0
10
20
30
40
.009
.01
1 Unit = .05 CL Lengths
From Poisson's Eq. - 100 V

Fig.51

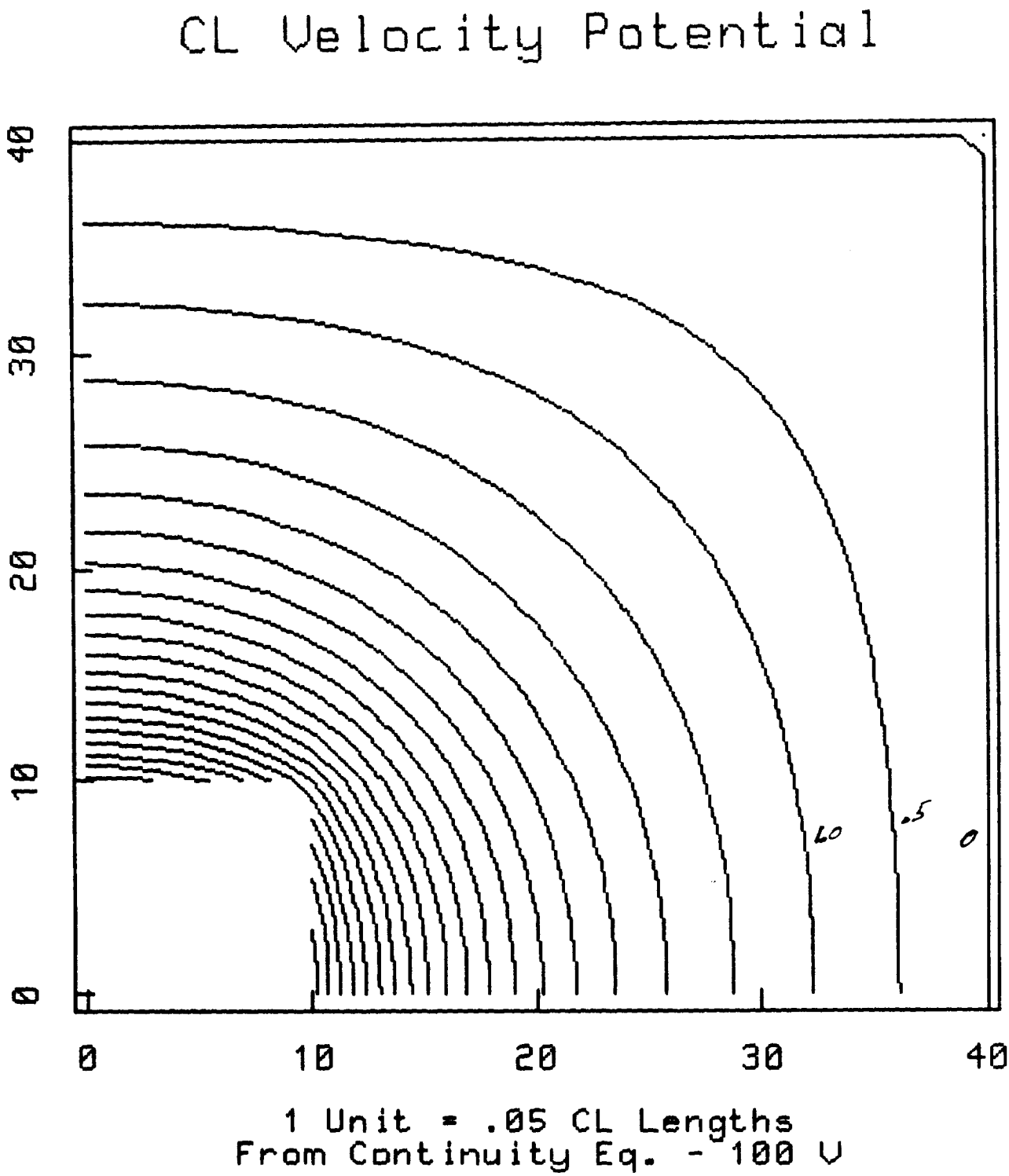
CL Velocity Potential
40
30
20
10
0
0
10
20
30
40
.5
0
1 Unit = .05 CL Lengths
From Continuity Eq. - 100 V

Fig.52

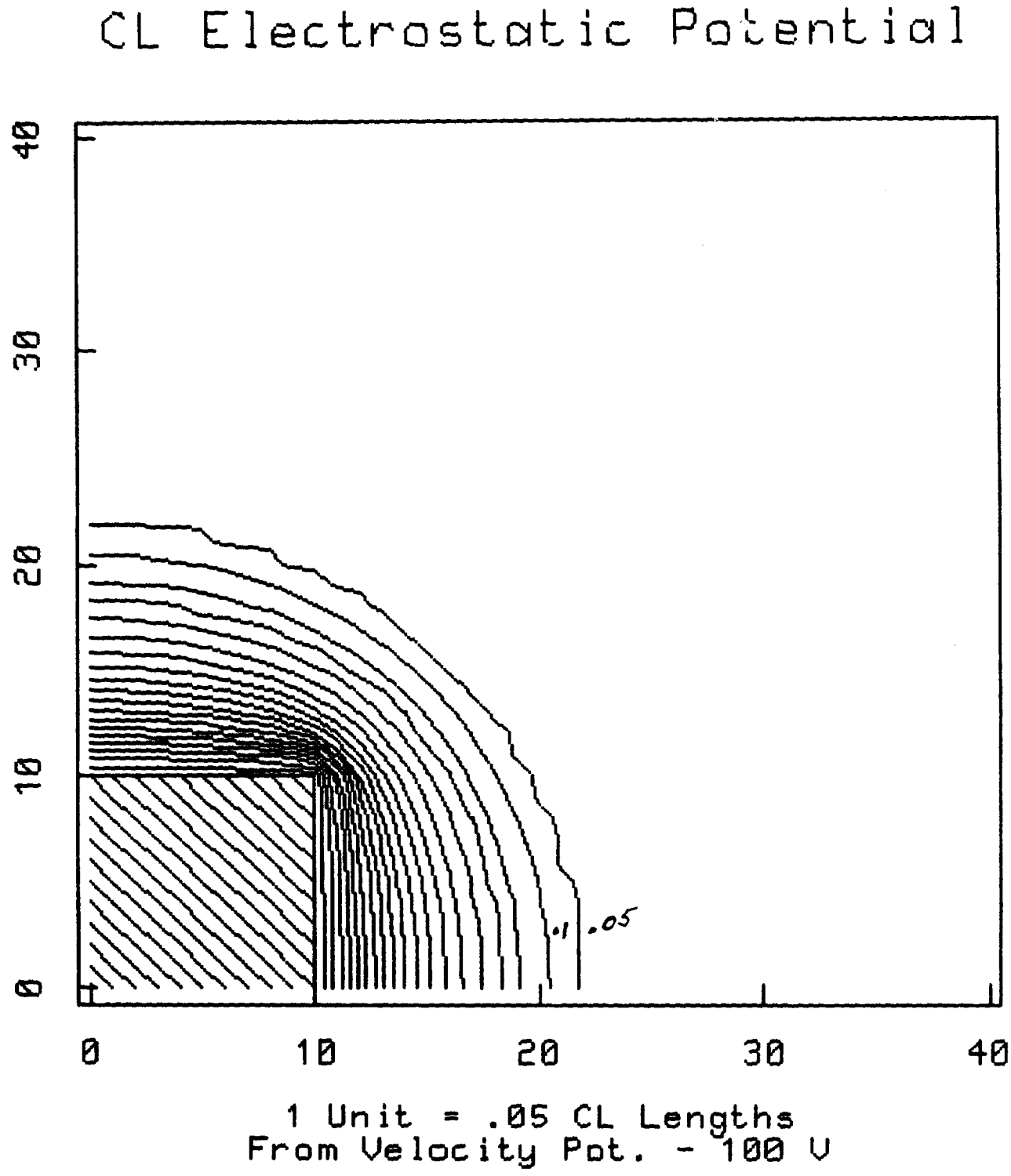
CL Electrostatic Potential
40
30
20
10
0
0
10
20
30
40
.1
.05
1 Unit = .05 CL Lengths
From Velocity Pot. - 100 V

Fig.53

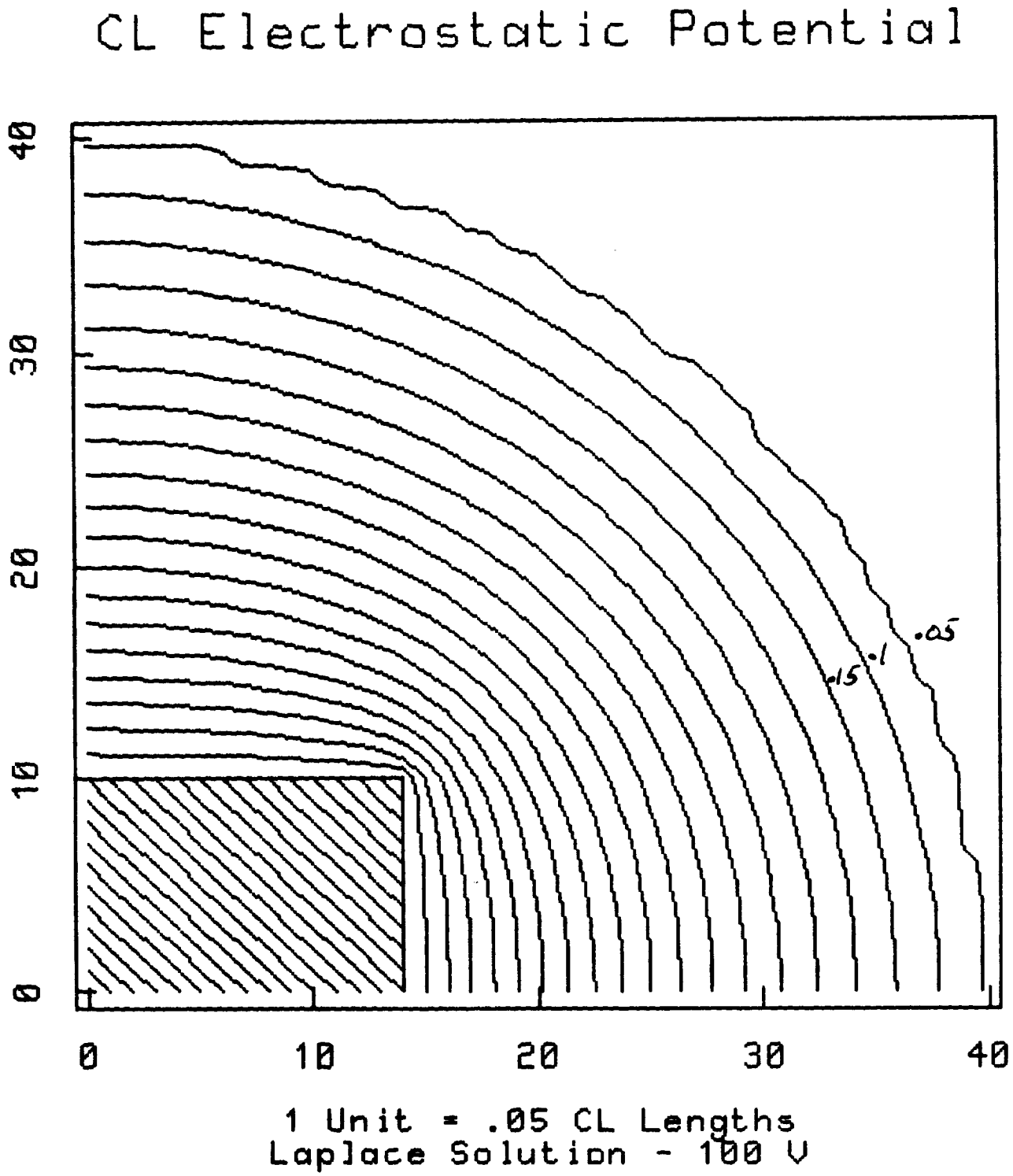
CL Electrostatic Potential
40
30
20
10
0
0
10
20
30
40
.05
.1
.15
1 Unit = .05 CL Lengths
Laplace Solution - 100 V

Fig.54

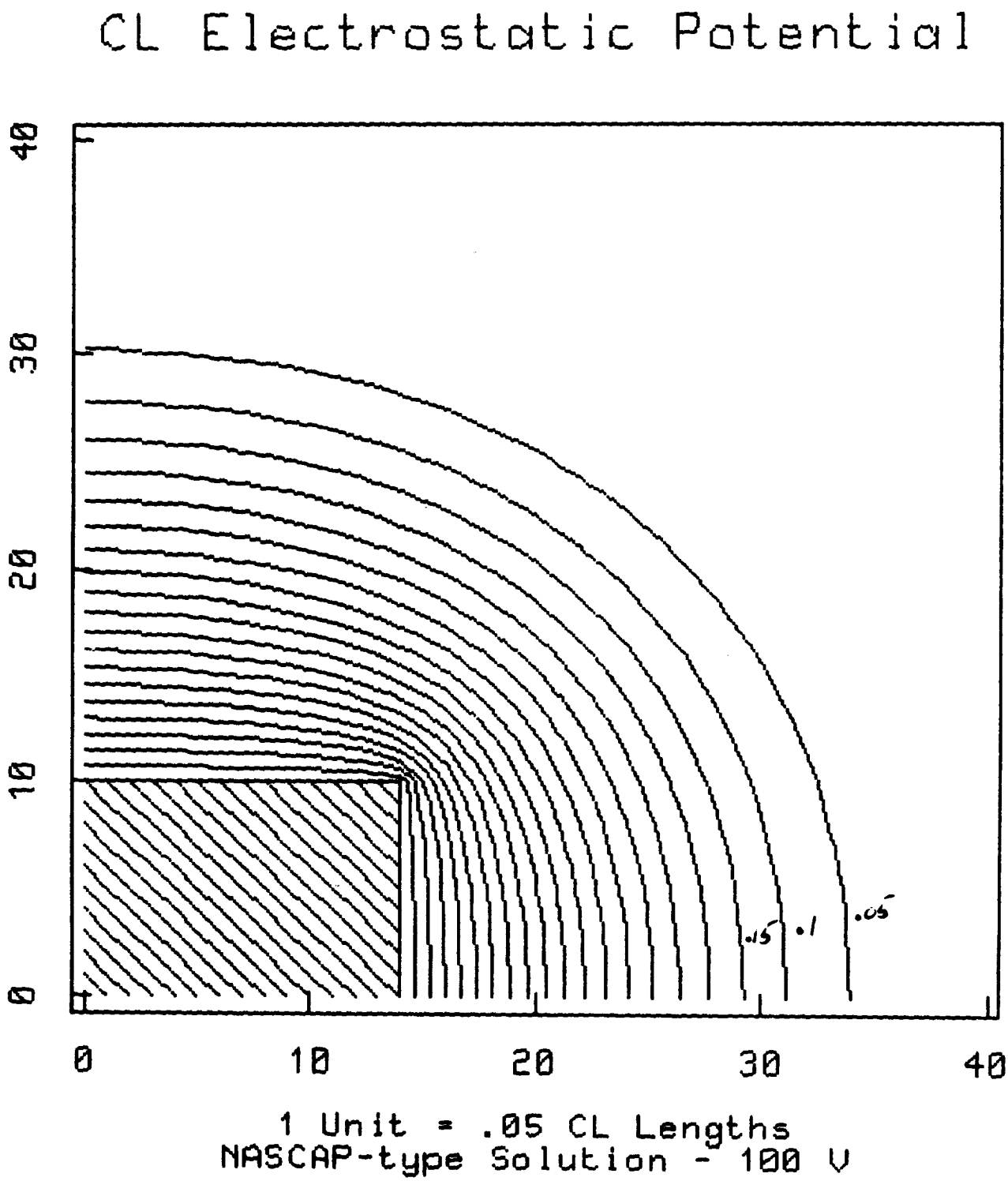
CL Electrostatic Potential
40
30
20
10
0
0
10
20
30
40
.15
.1
.05
1 Unit = .05 CL Lengths
NASCAP-type Solution - 100 V

Fig.55

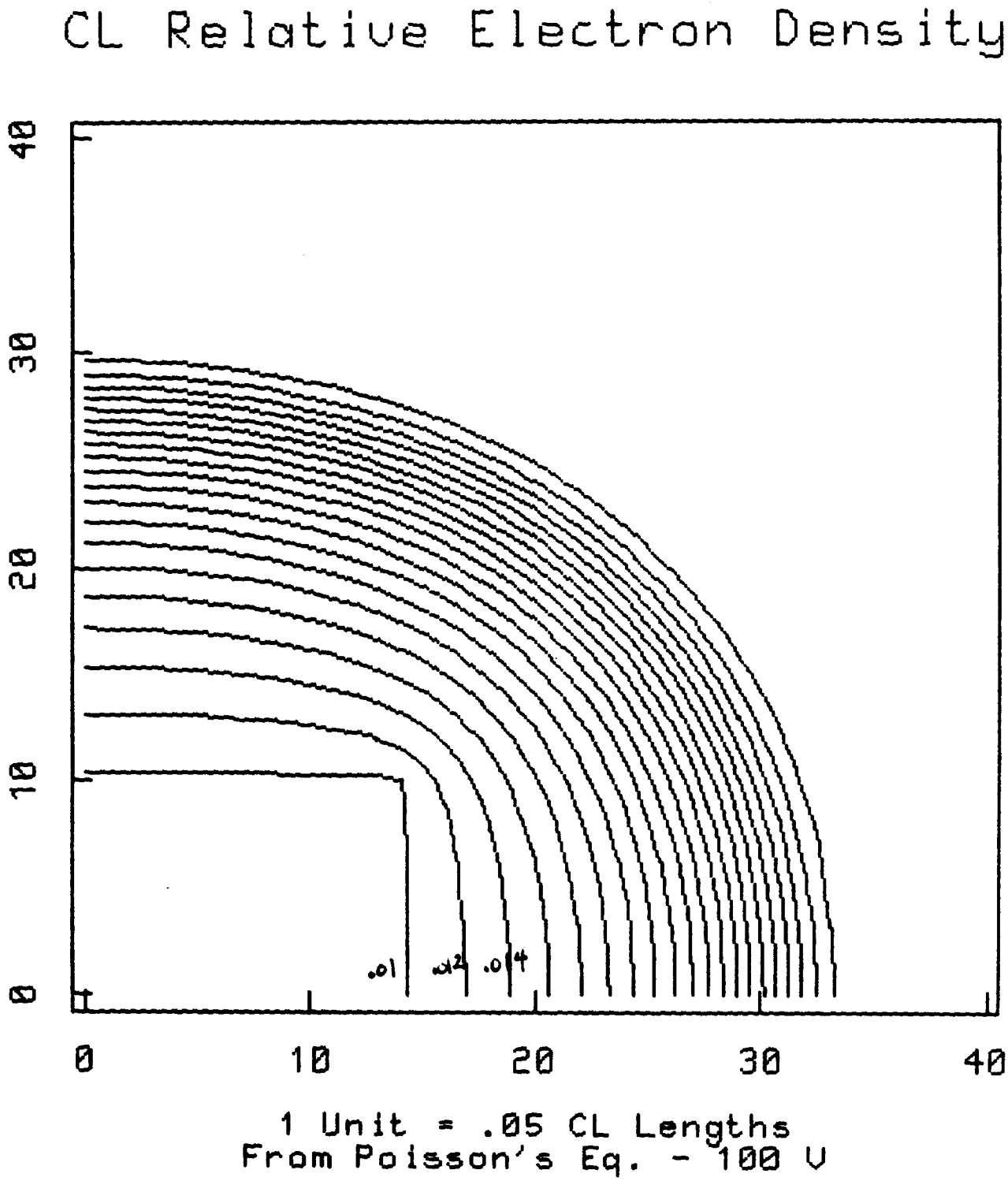
CL Relative Electron Density
40
30
20
10
0
.01
.02
.04
0
10
20
30
40
1 Unit = .05 CL Lengths
From Poisson's Eq. - 100 V

Fig.56

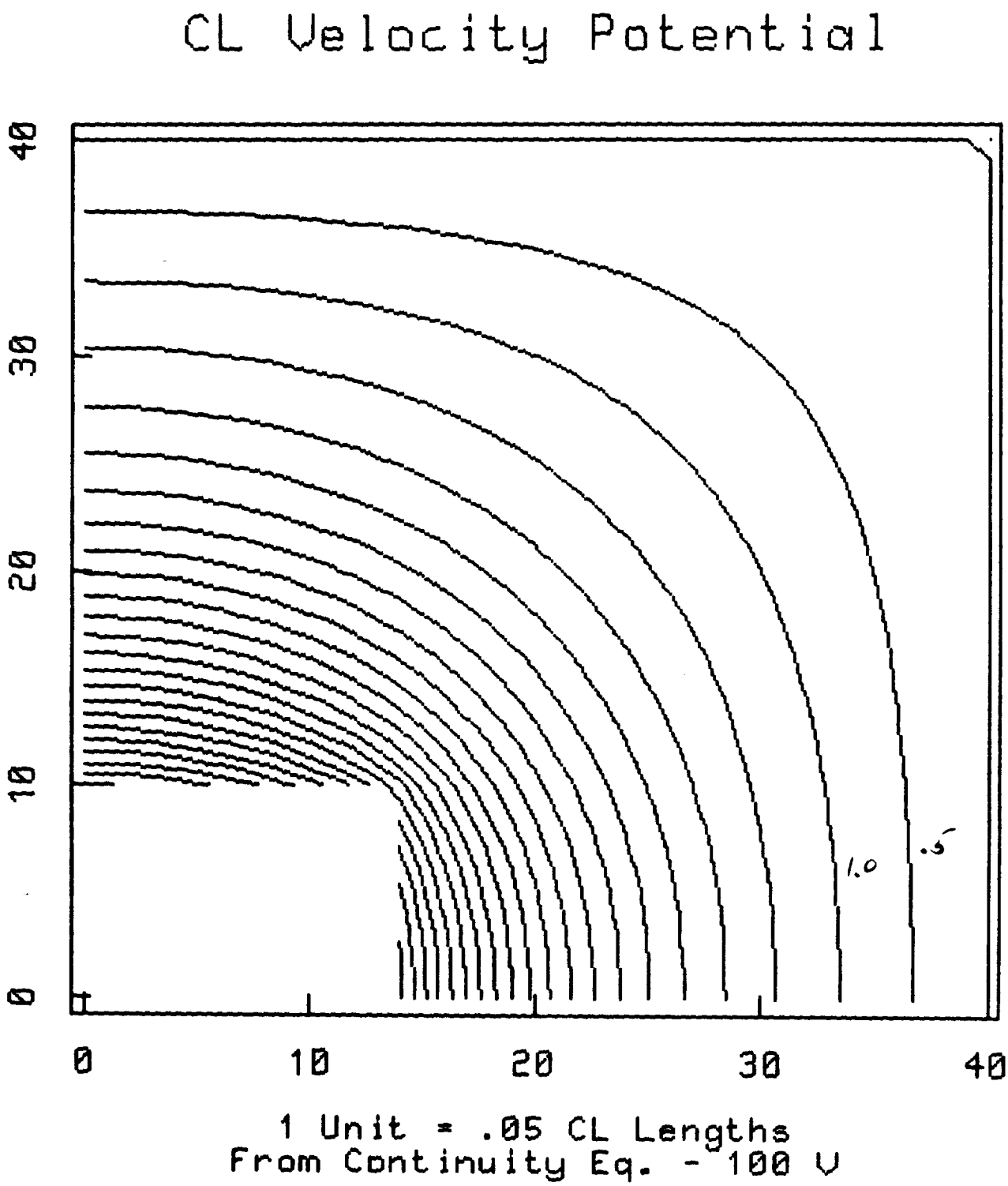
CL Velocity Potential
40
30
20
10
0
0
10
20
30
40
1.0
.5
1 Unit = .05 CL Lengths
From Continuity Eq. - 100 V

Fig.57

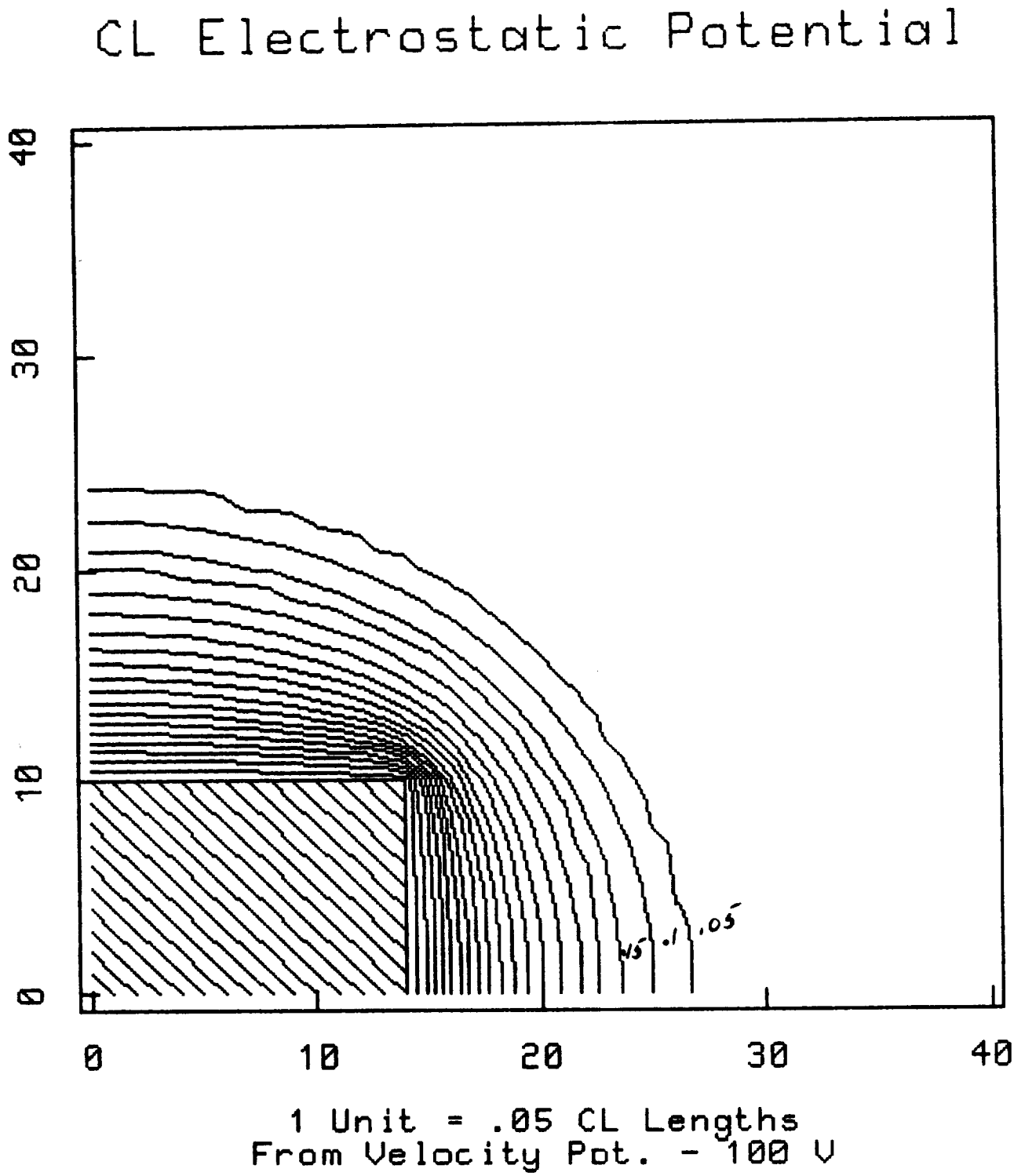
CL Electrostatic Potential
40
30
20
10
0
0
10
20
30
40
.05
.1
.05
1 Unit = .05 CL Lengths
From Velocity Pot. - 100 V

Fig.58

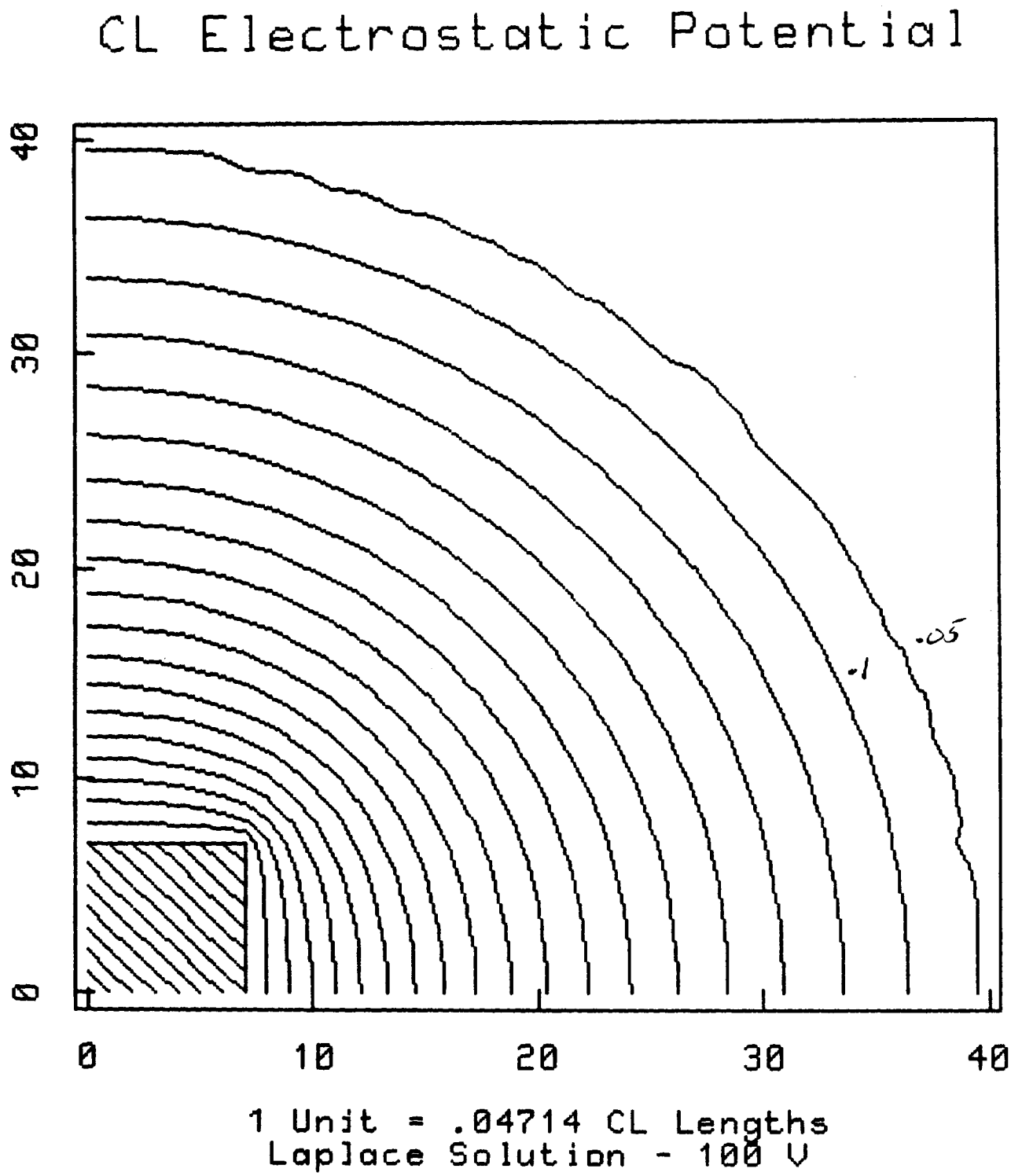
CL Electrostatic Potential
40
30
20
10
0
0
10
20
30
40
.05
.1
1 Unit = .04714 CL Lengths
Laplace Solution - 100 V

Fig.59

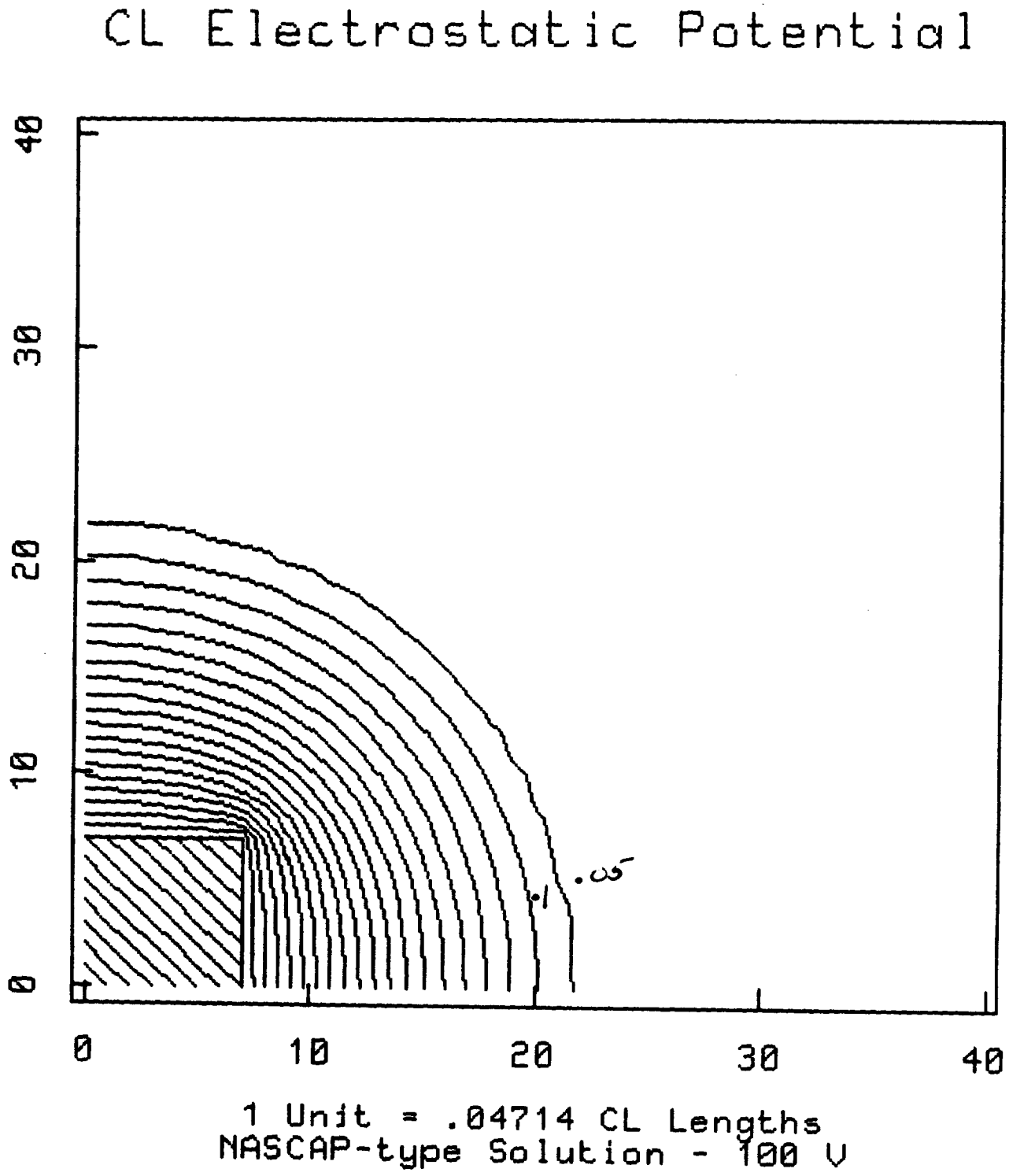
CL Electrostatic Potential
40
30
20
10
0
0
10
20
30
40
.05
.1
1 Unit = .04714 CL Lengths
NASCAP-type Solution - 100 V

Fig.60

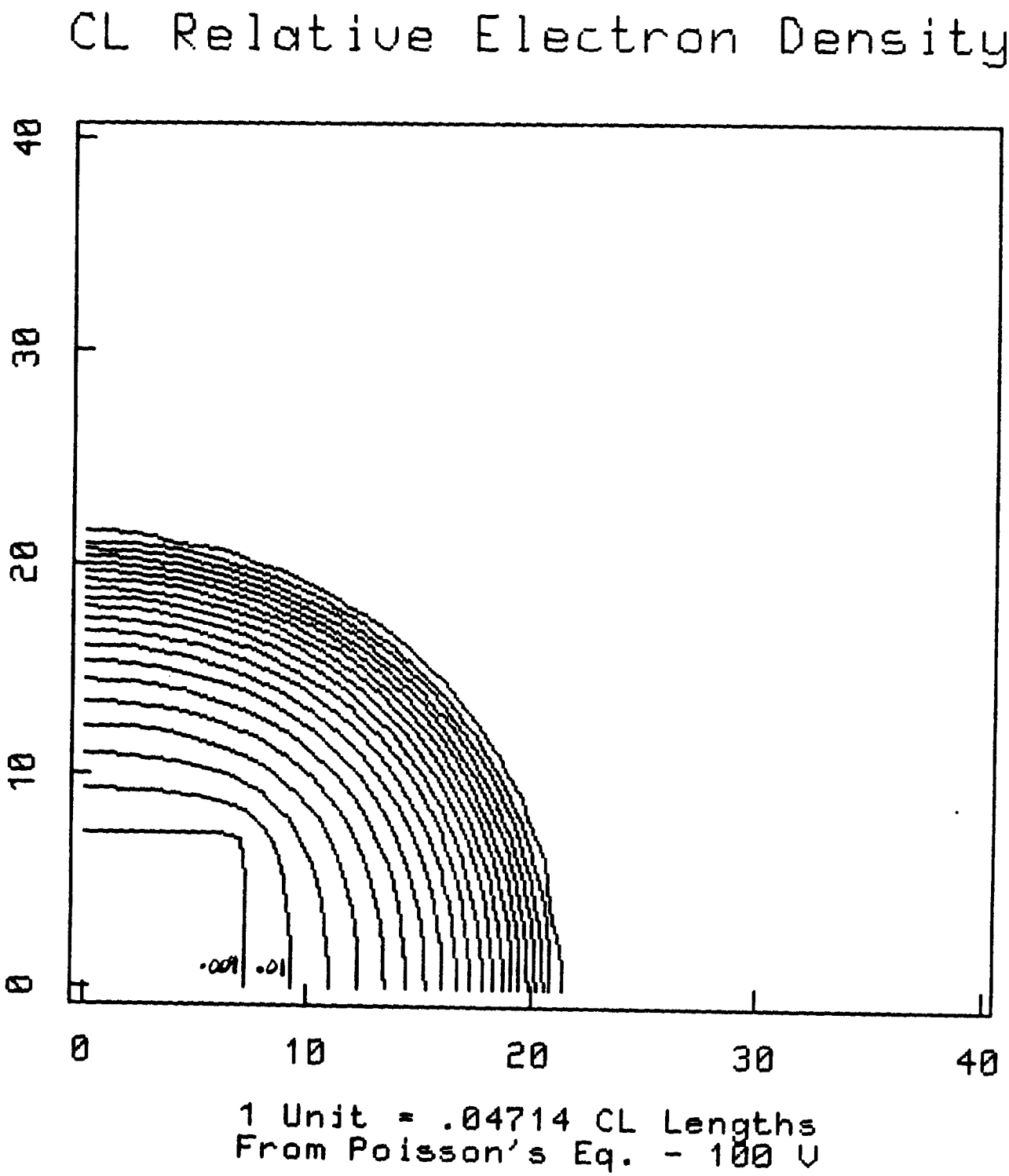
CL Relative Electron Density
40
30
20
10
0
0
10
20
30
40
.009
.01
1 Unit = .04714 CL Lengths
From Poisson's Eq. - 100 V

Fig.61

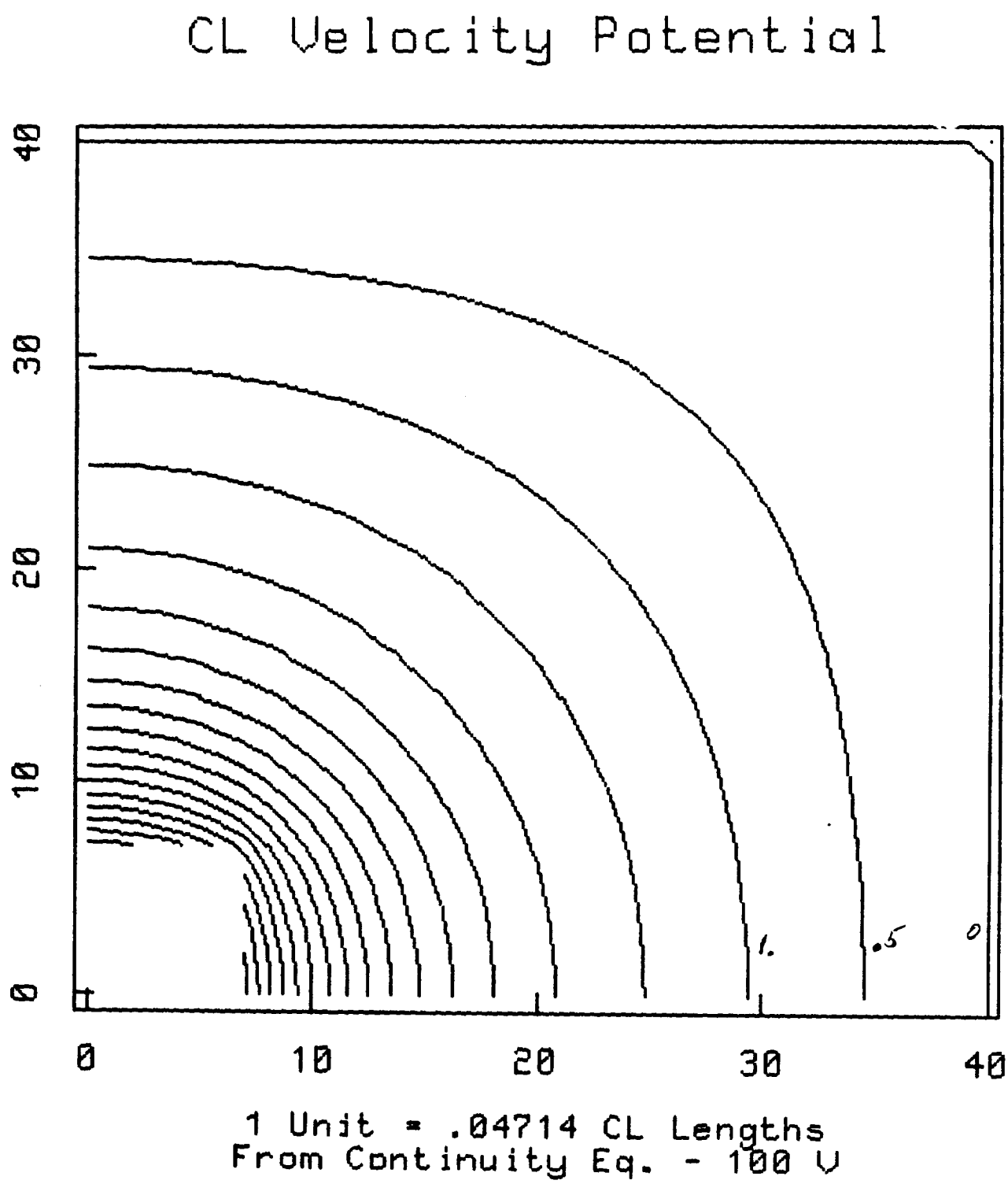
CL Velocity Potential
40
30
20
10
0
0
10
20
30
40
1.
.5
0
1 Unit = .04714 CL Lengths
From Continuity Eq. - 100 V

Fig.62

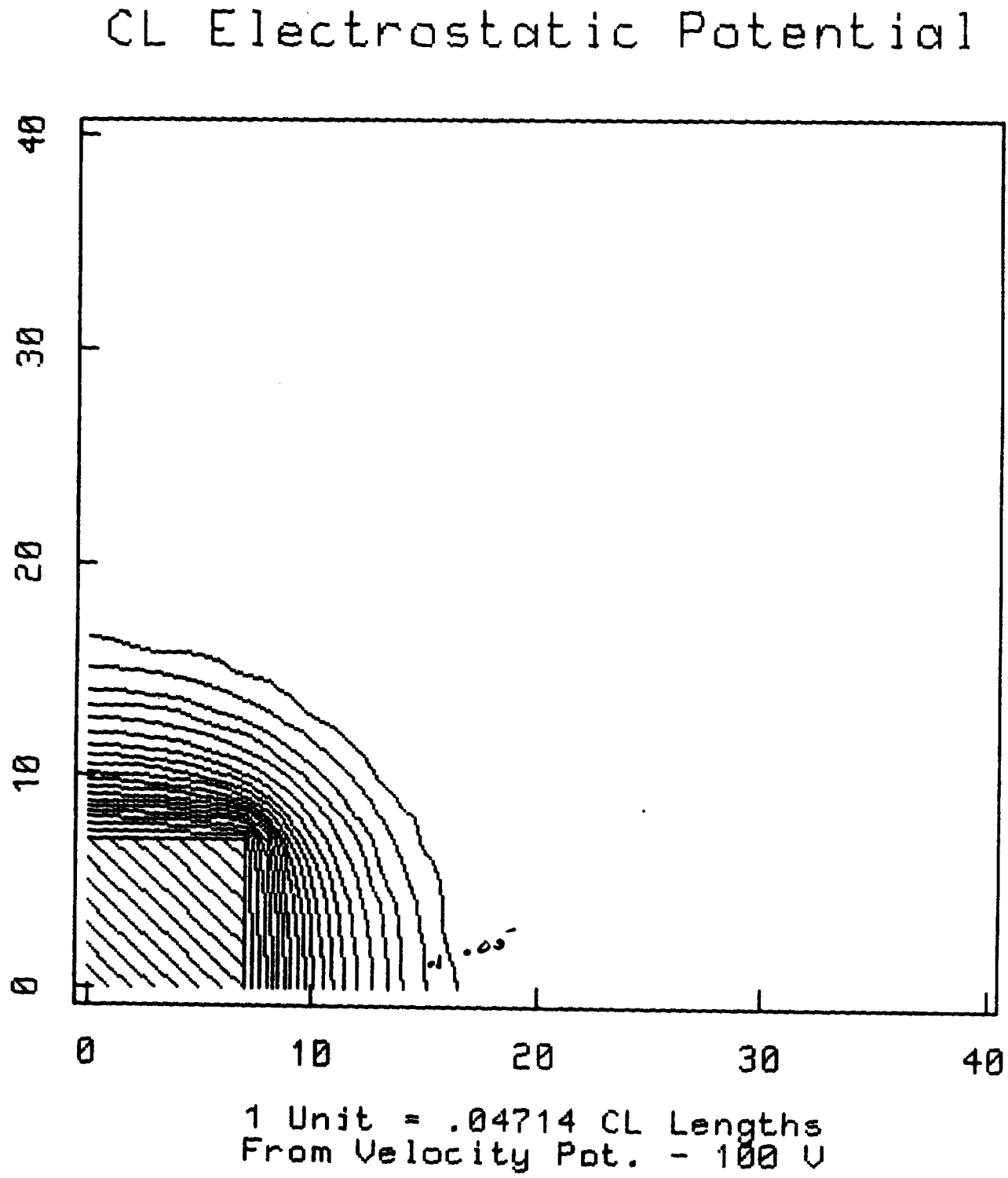
CL Electrostatic Potential
40
30
20
10
0
0
10
20
30
40
.05
1 Unit = .04714 CL Lengths
From Velocity Pot. - 100 V

Fig.63